Plasma diagnostics

(Focus on magnetic confinement fusion)

Prof. Dr. Mathias Groth
Aalto University
School of Science, Department of Applied Physics

Aalto University
School of Science

Outline

- **Concepts, measurement principles and ranges of diagnostics in fusion research ⇒ diagnostics in Magnetic Confinement Fusion (MCF)**
- **Common MCF diagnostic systems ⇒ primary focus on JET**
  - Not exclusive! Smaller devices have often better diagnostic systems than JET because of lower neutron yields, no tritium
- **Diagnostic challenges for ITER (selected examples)**
- **Set of 20 lectures on diagnostics used in Inertial Confinement Fusion (ICF) exist, outside scope of one lecture**

A diagnostic is an instrument / system of instruments to measure or infer plasma and many other parameters

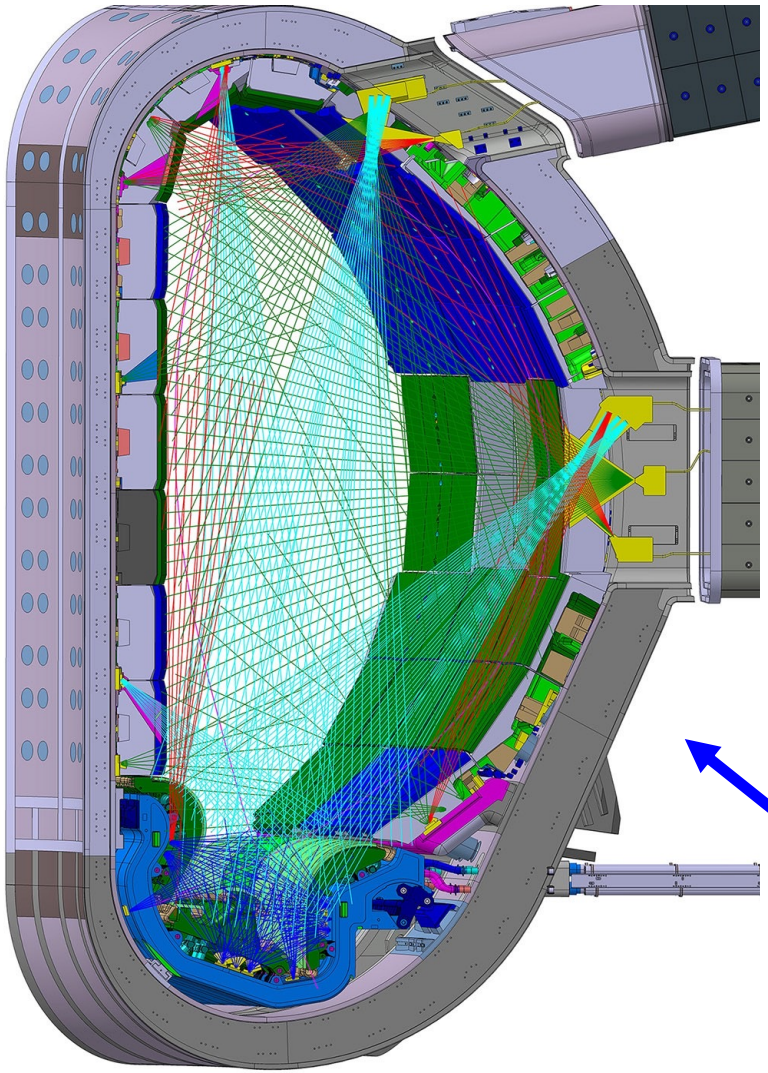

https://www.iter.org/

- **Plasma position and wall heat loads**
- **Plasma temperatures and densities**
- **Magnetic and plasma-kinetic energy**
- **Neutron yields and γ radiation**
- **Impurity content**
- **Plasma radiation**: bolometer
- …

The primary purpose of diagnostics are machine protection and plasma control

- **Basic control ⇒ advanced control**
  - Plasma position and wall heat load ⇒ heating systems for safety factor profile/MHD
  - ITER has four levels of measurements: machine protection (1.a1), basic control (1.a2), advanced control (1.b), evaluation and physics studies (2)
- **Performance evaluation and physics:**
  - Fusion products and neutron production
  - Plasma stability and MHD
  - Energy and particle confinement times
  - Development of auxiliary heating methods
  - …

Diagnostics may be classified into four basic groups

Category	Parameter	Method
Magnetics	Plasma current Loop voltage (Ohmic power, T_e) Diamagnetic energy Plasma position/equilibrium	Rogowski coil Voltage loops Diamagnetic loop Poloidal field coils
Passive radiation	Total radiation and surface heating power, electron temperature and densities, Bremsstrahlung, line radiation (including impurities → impurity influxes)	Bolometry, thermography electron cyclotron emission, VUV and visible spectroscopy, soft x-rays
Active radiation	Electron density and temperature, current profile, ion temperature	Thomson scattering interferometry, reflectometry, polarimetry, charge exchange, Li or He beams, heavy ion probe
Particle diagnostics	Plasma particle fluxes, neutron and γ yields	Langmuir probes, fission chambers, neutron cameras, neutron spectrometers

Matching of physics principles with plasma parameters

	f_e	f_i	n_e	n_i	n_Z	T_e	T_i	p	E	B
Magnetics						×		×		×
Particle flux	×	×	×	×		×	×		×	
Refractive index			×							×
Cyclotron emission	×					×				
Bremsstrahlung			×		×	×				
Line radiation					×		×		×	×
Scattering	×		×			×		×		
Charge exchange		×			×		×			
Nuclear reaction		(×)		×			×			

Diagnostics in fusion research cover the entire electromagnetic emission spectrum

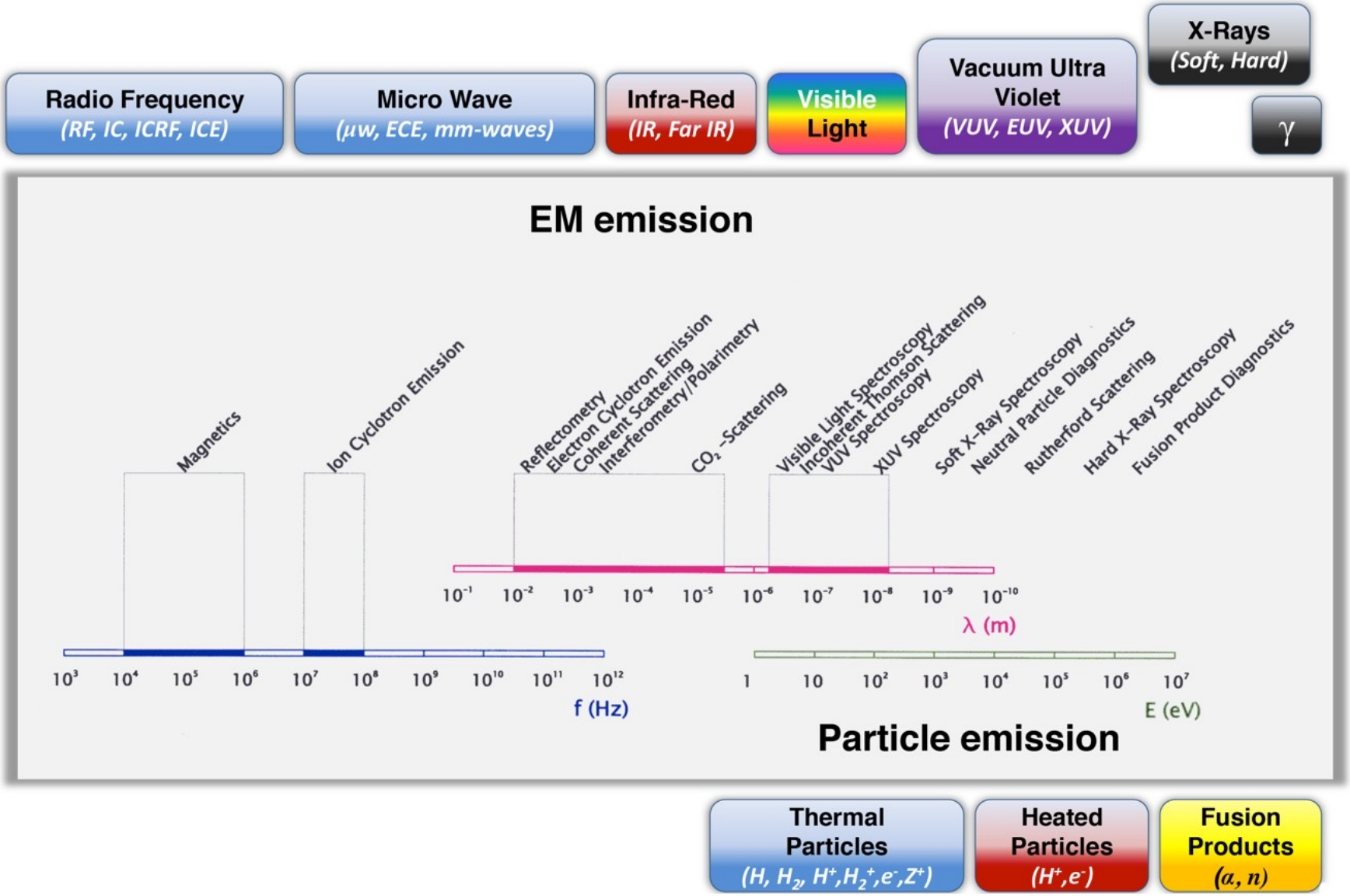

Alignment, spatial and temporal resolution, and channel redundancy are key issues when developing diagnostics

Line-integrated, single LOS

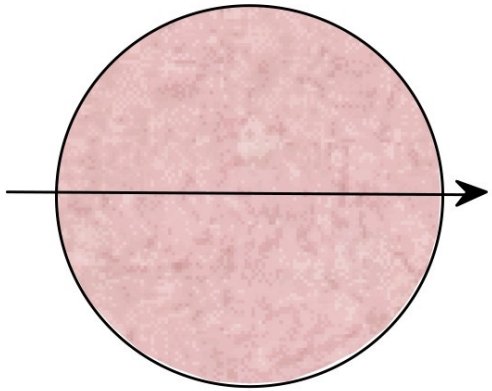

Spectroscopy, NPA

Line-integrated, multiple LOS ⇒ Abel inversion

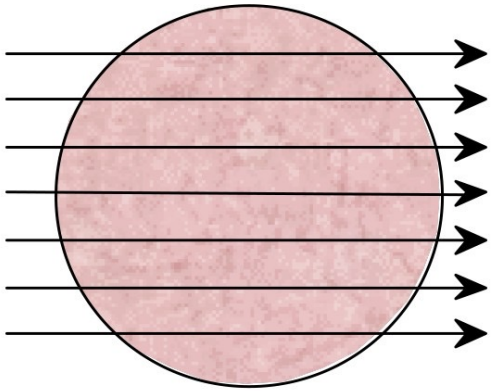

Interferometry, polarimetry

Crossed-views

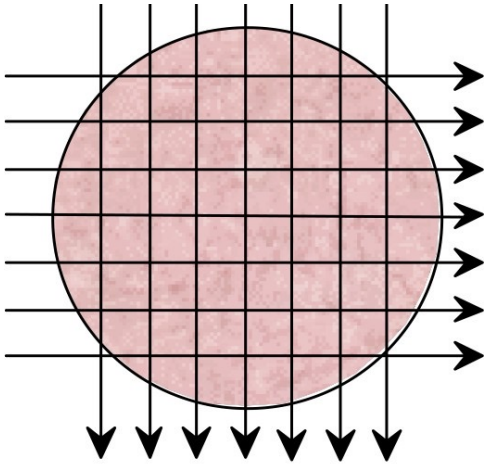

Tomography

Localized by active beams

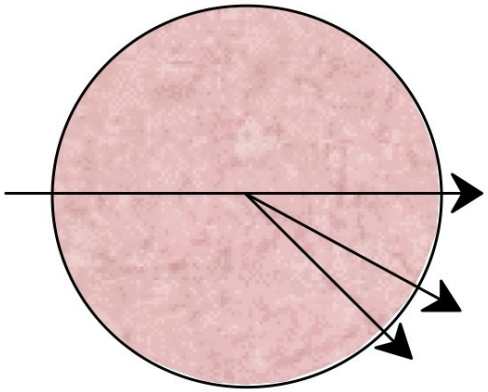

Scattering, LIF

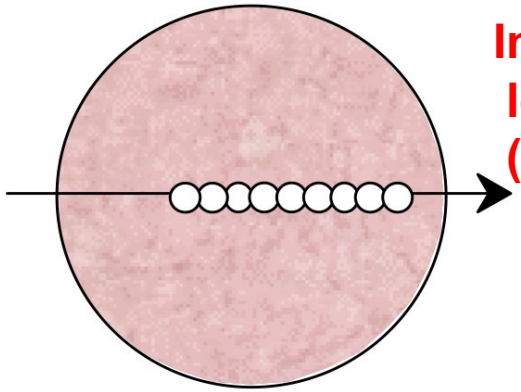

ECE, Reflectometry

Inherently localized (B field)

Diagnostics are externally installed on tokamaks, with access to the plasma via ports

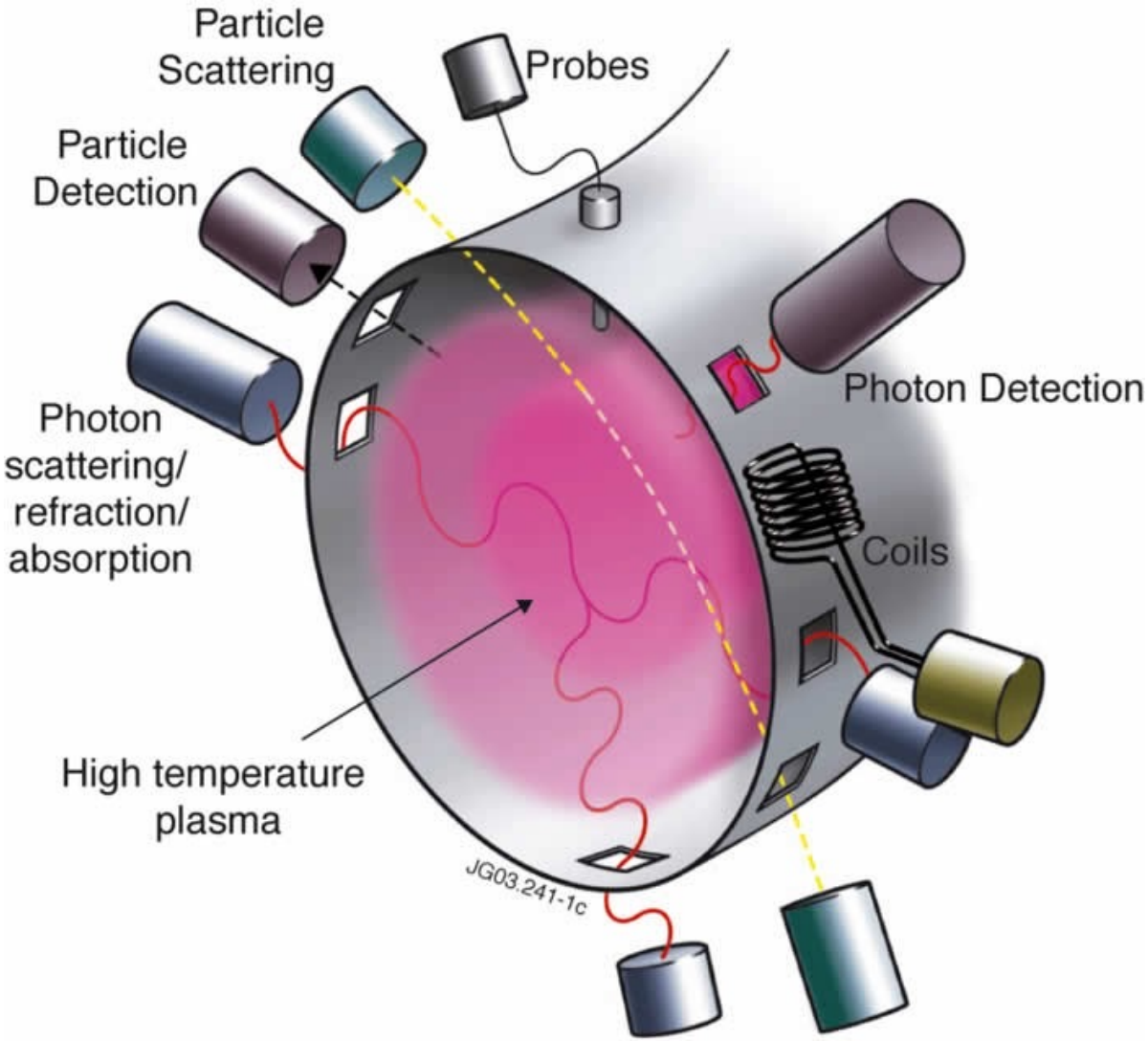

- **Passive and active diagnostics**

⇒ **Active-beam diagnostics require ports for beam and detector lines-of-sight**

- **Intrusive diagnostics (e.g., reciprocating Langmuir probe)**

Over 100 diagnostics are installed (and operated) on JET; similar or even higher number on other tokamaks

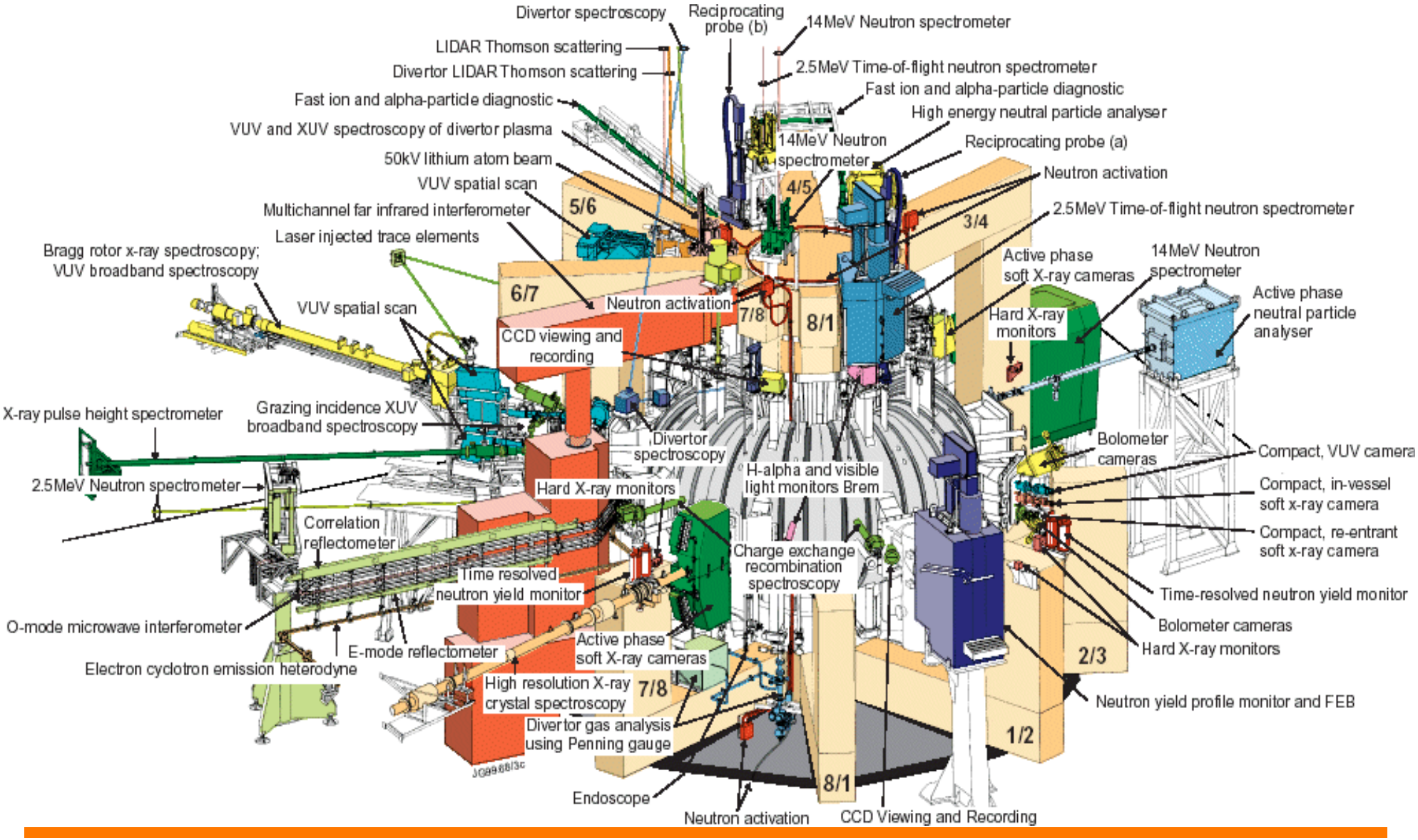

Architecture of Feedback on JET

Parameters to control equilibrium
profiles T_e, T_i, q, V_{rot}
neutrons, n_D, n_T

Actuators
PF coils & saddles coils, DMV, SPI; Heating: LHCD, ICRH, NBI; Fuelling

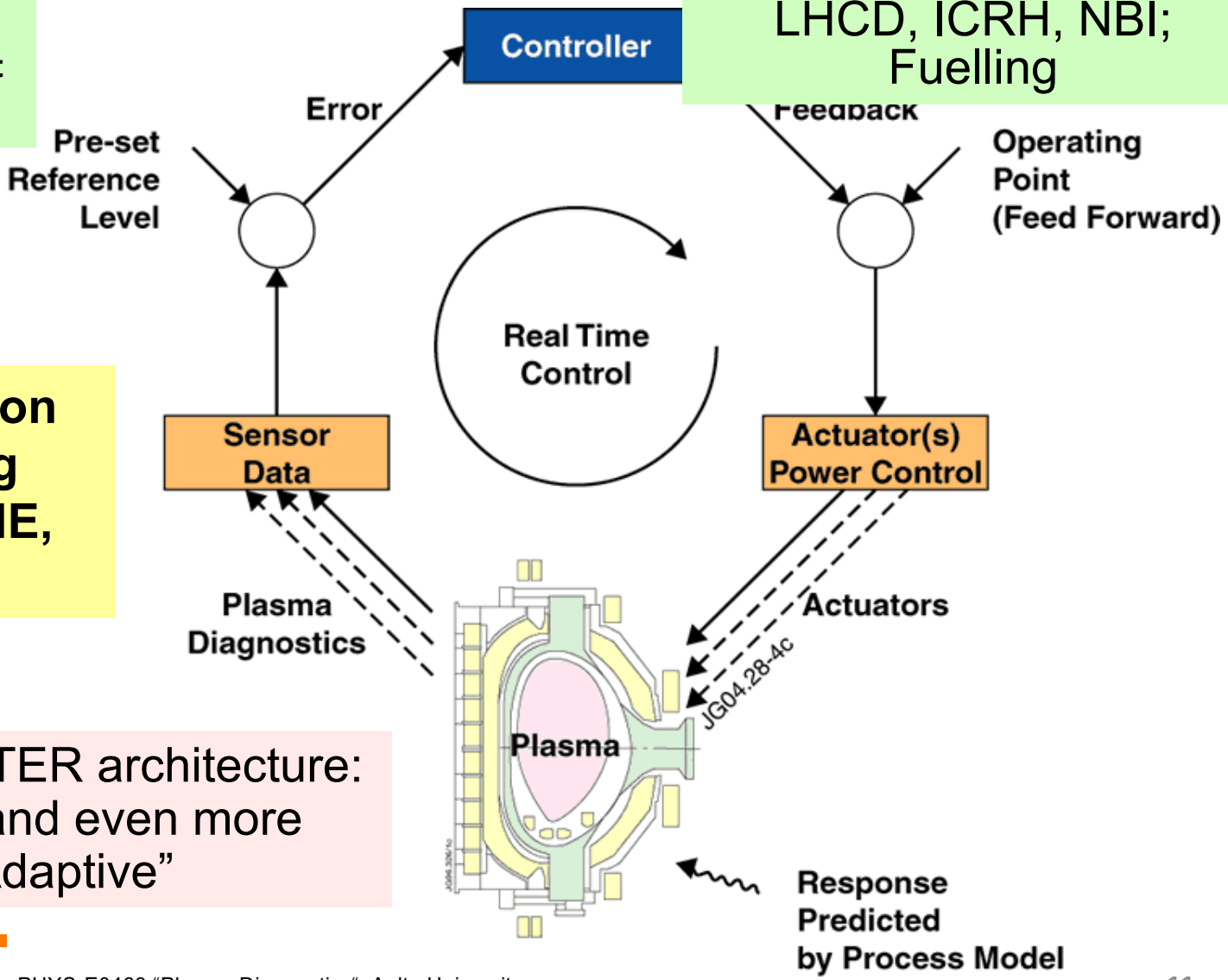

Distributed system on parallel computing multi-platforms (VME, PCI, cloud, etc.)

Good candidate for ITER architecture: flexible, efficient and even more important “Adaptive”

Presemo quiz #1

https://presemo.aalto.fi/fet/

Magnetic measurements

Diagnostics may be classified into four basic groups

Category	Parameter	Method
Magnetics	Plasma current Loop voltage (Ohmic power, T_e) Diamagnetic energy Plasma position/equilibrium	Rogowski coil Voltage loops Diamagnetic loop Poloidal field coils

Magnetic coils installed at the wall are used to determine the equilibrium and plasma stored energy

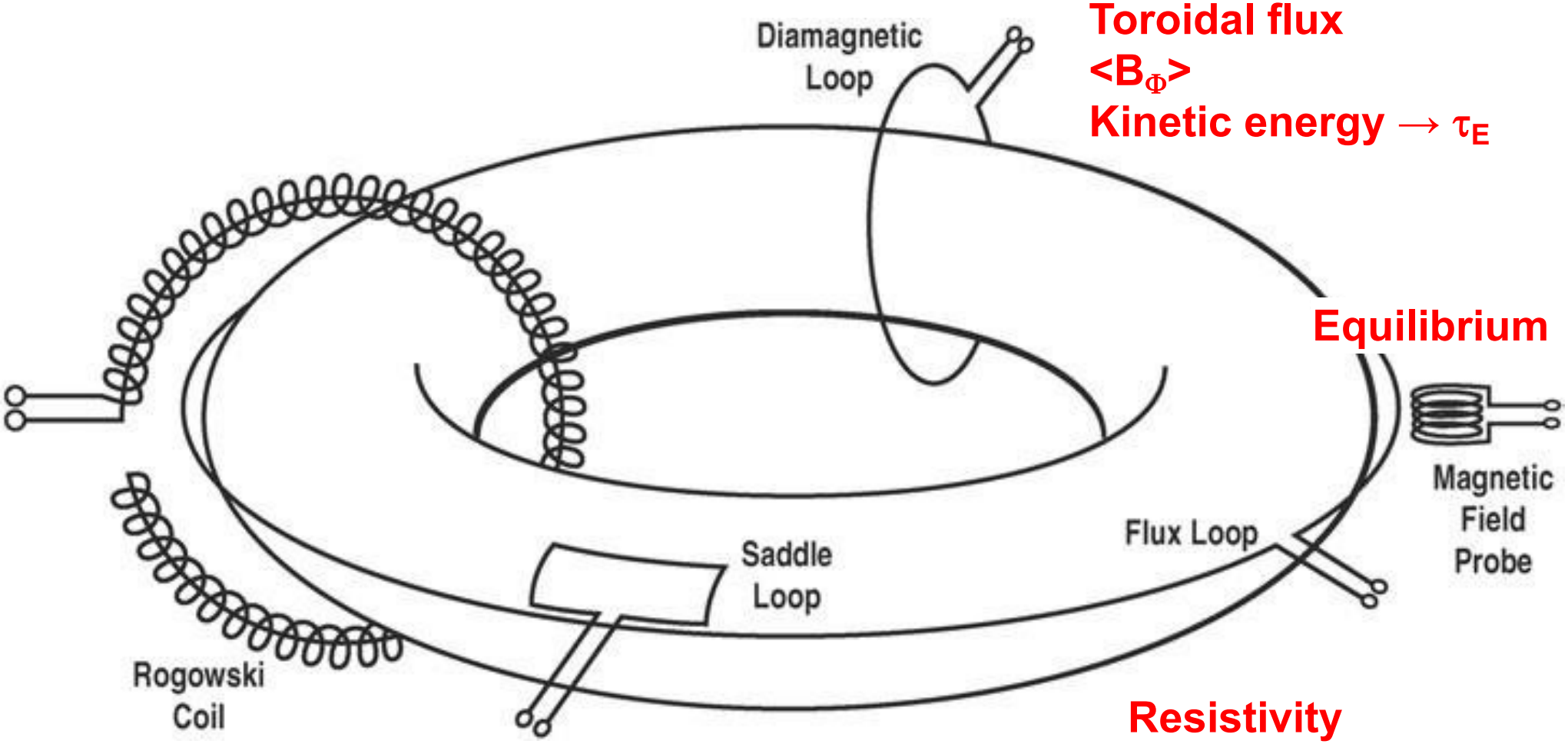

Magnetic pick-up coils are installed behind the plasma-facing tiles protecting the coils

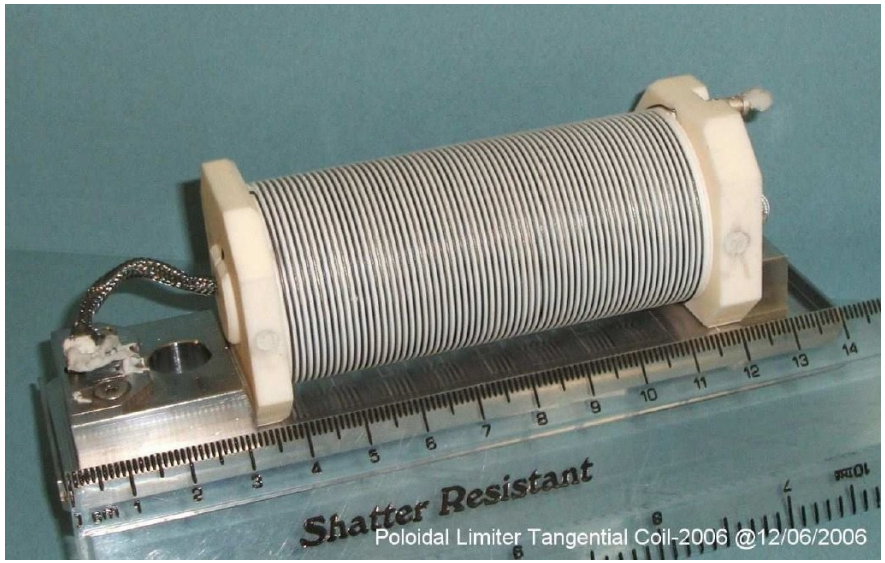

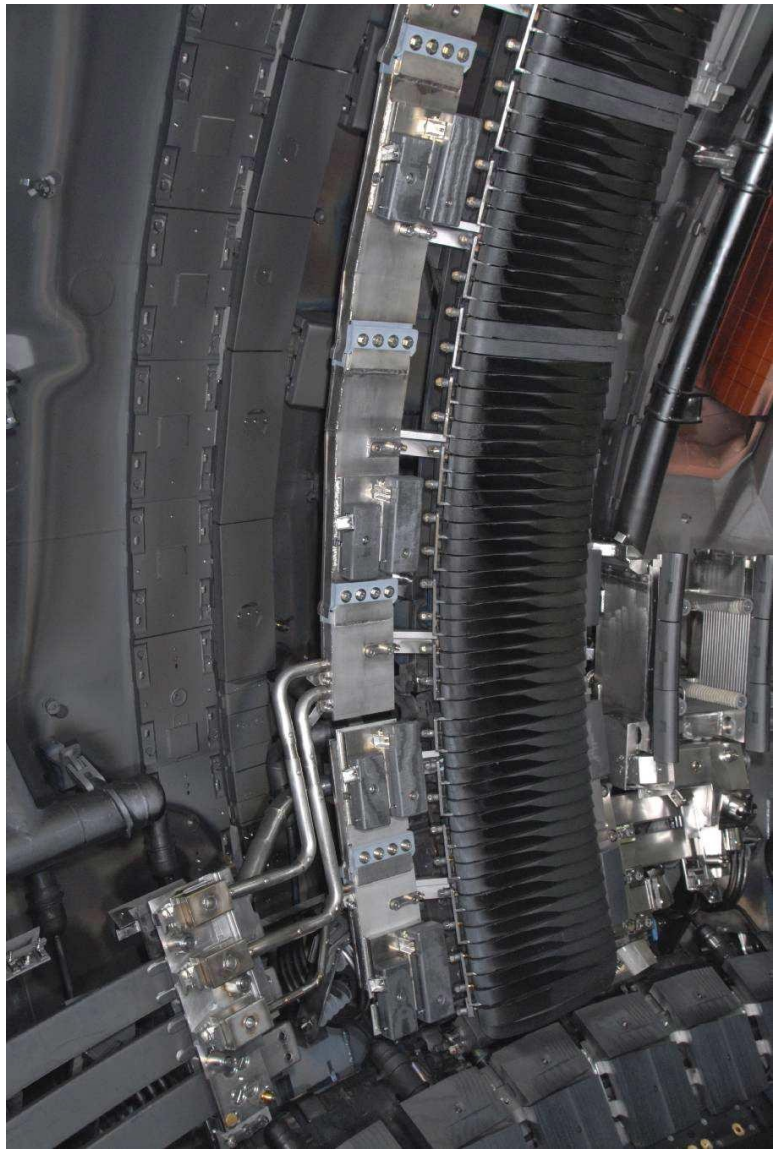

Magnetic pick-up coils are installed behind the plasma-facing tiles protecting the coils

There are several sets of magnetic coils installed around JET poloidally and toroidally

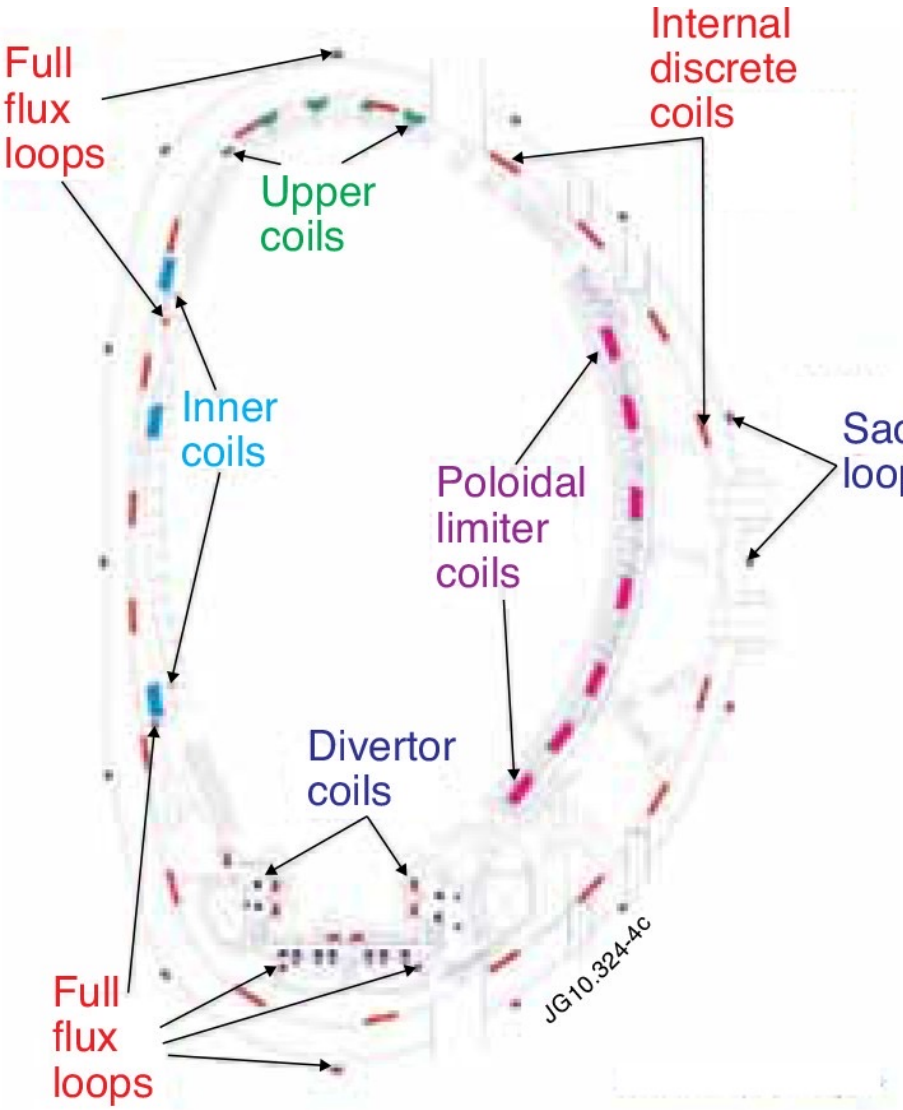

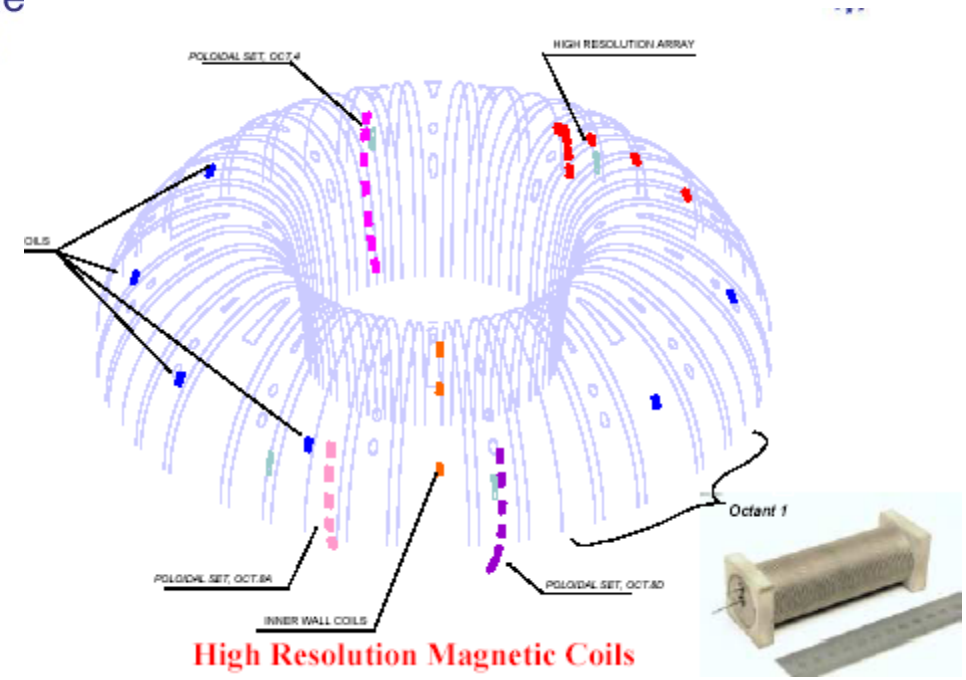

Using the magnetic probe data, a 2-D magnetic equilibrium is reconstructed

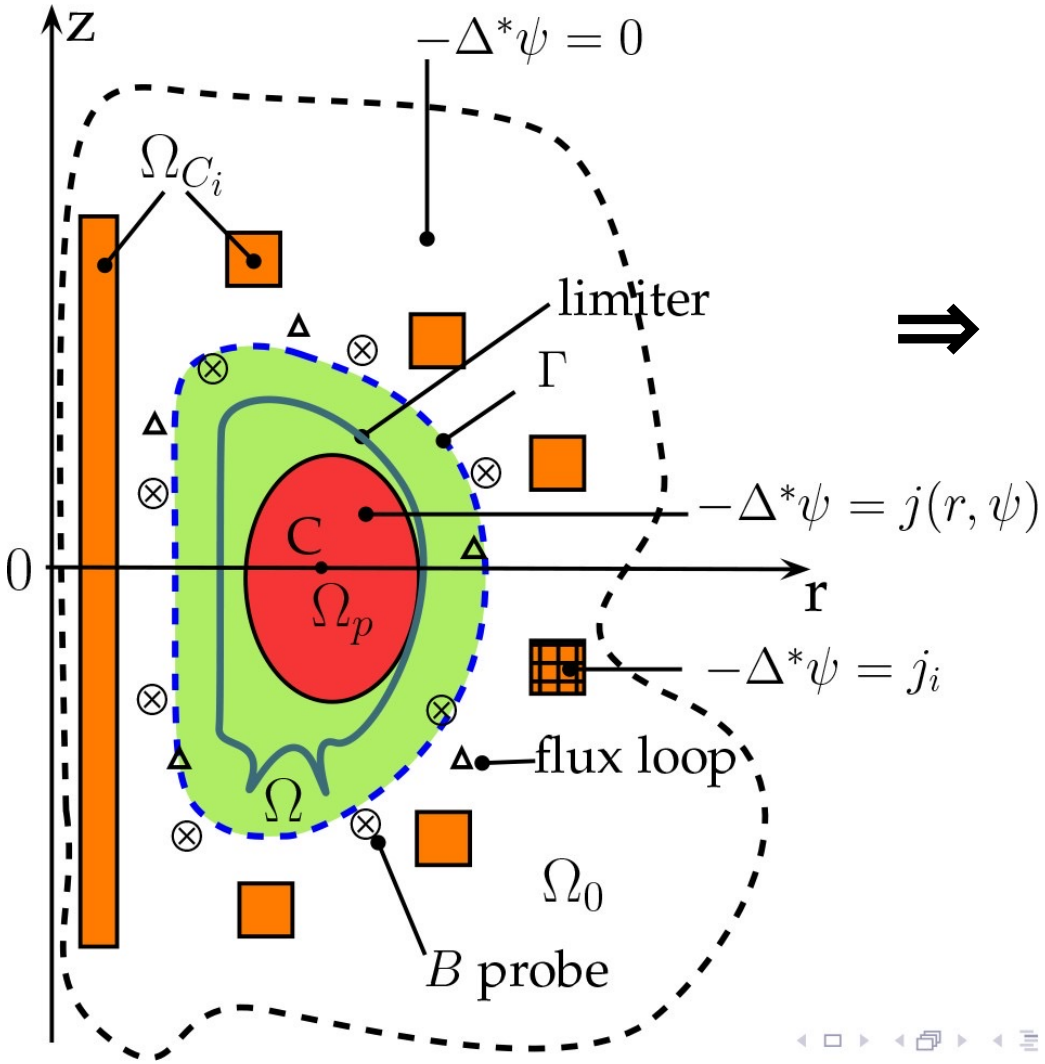

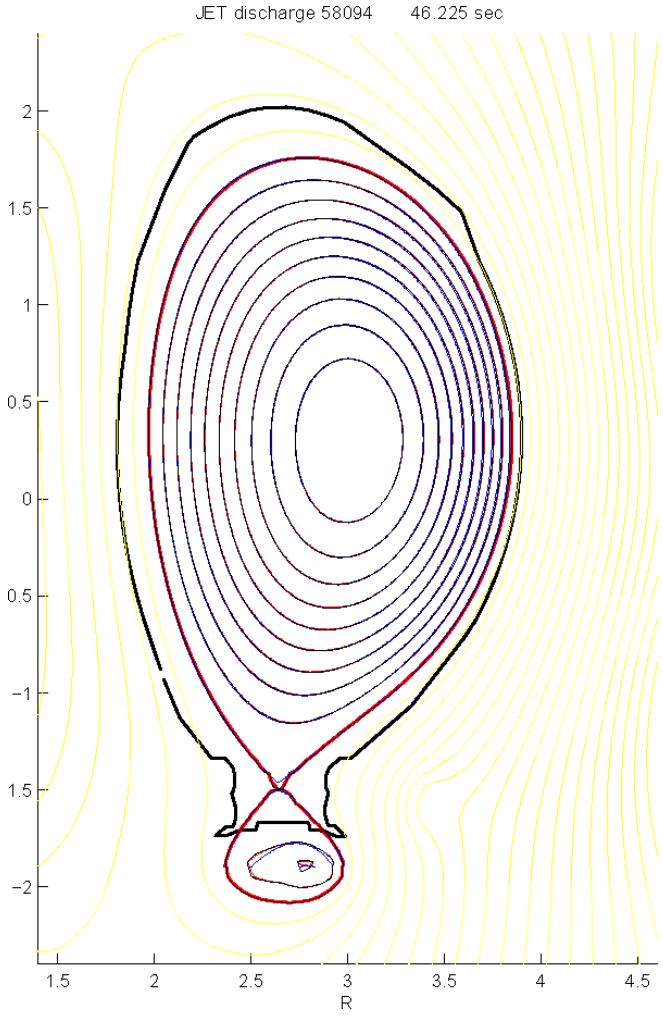

Passive radiation measurements

Diagnostics may be classified into four basic groups

Category	Parameter	Method
Passive radiation	Total radiation and surface heating power, electron temperature and densities, Bremsstrahlung, line radiation (including impurities → impurity influxes)	Bolometry, thermography electron cyclotron emission, VUV and visible spectroscopy, soft x-rays

The total radiated power from the plasma is measured by foil (or semiconductor) bolometers

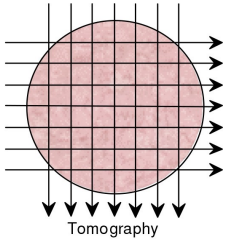

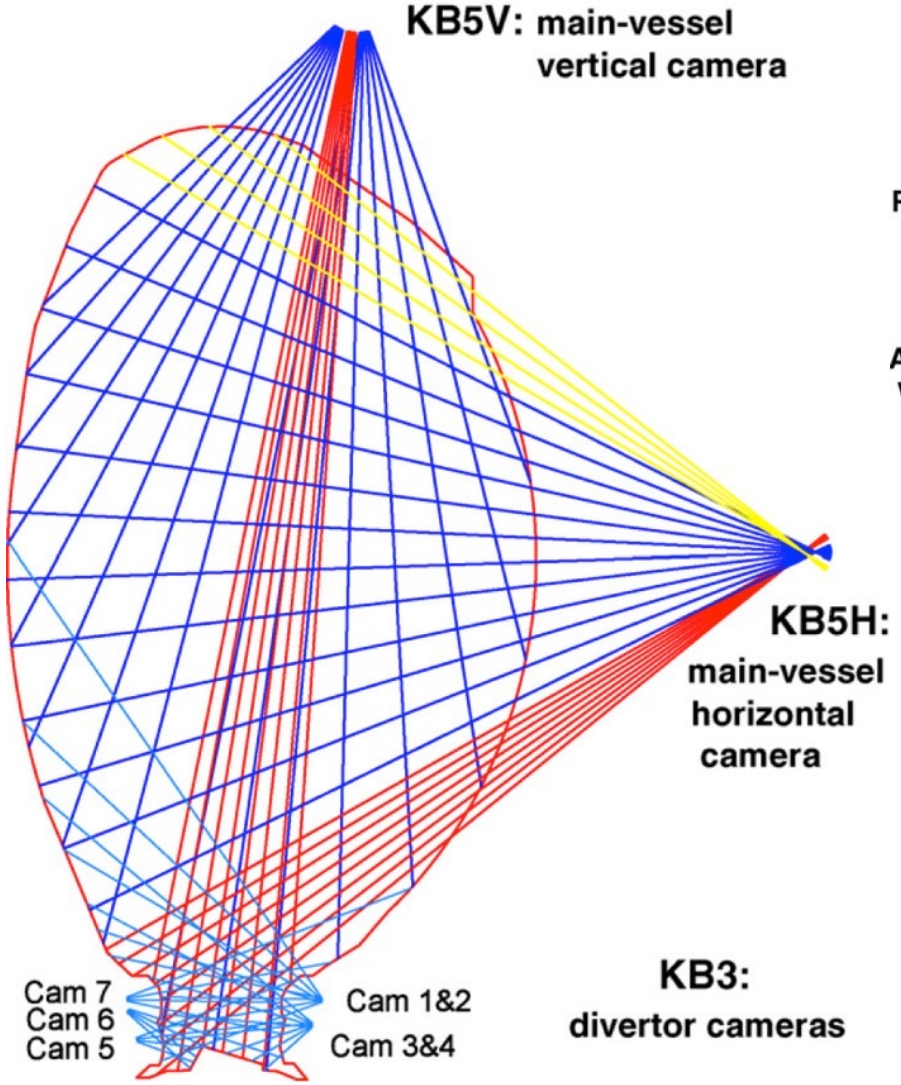

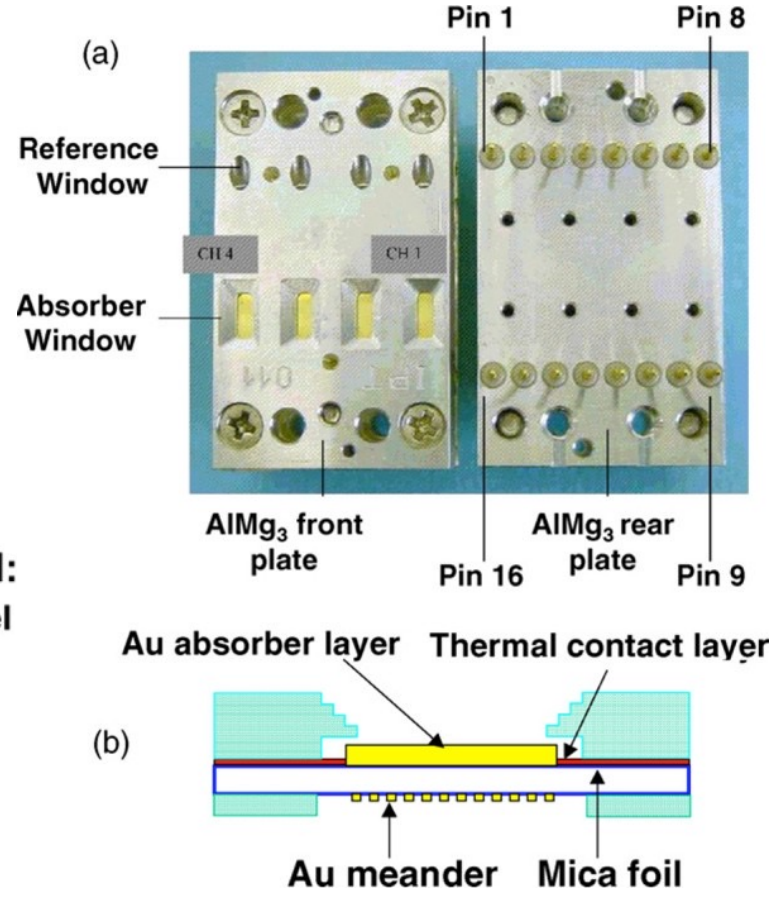

Huber et al. FED 2007

2-D radiation profiles can be derived from multi-chord system using tomographic reconstruction

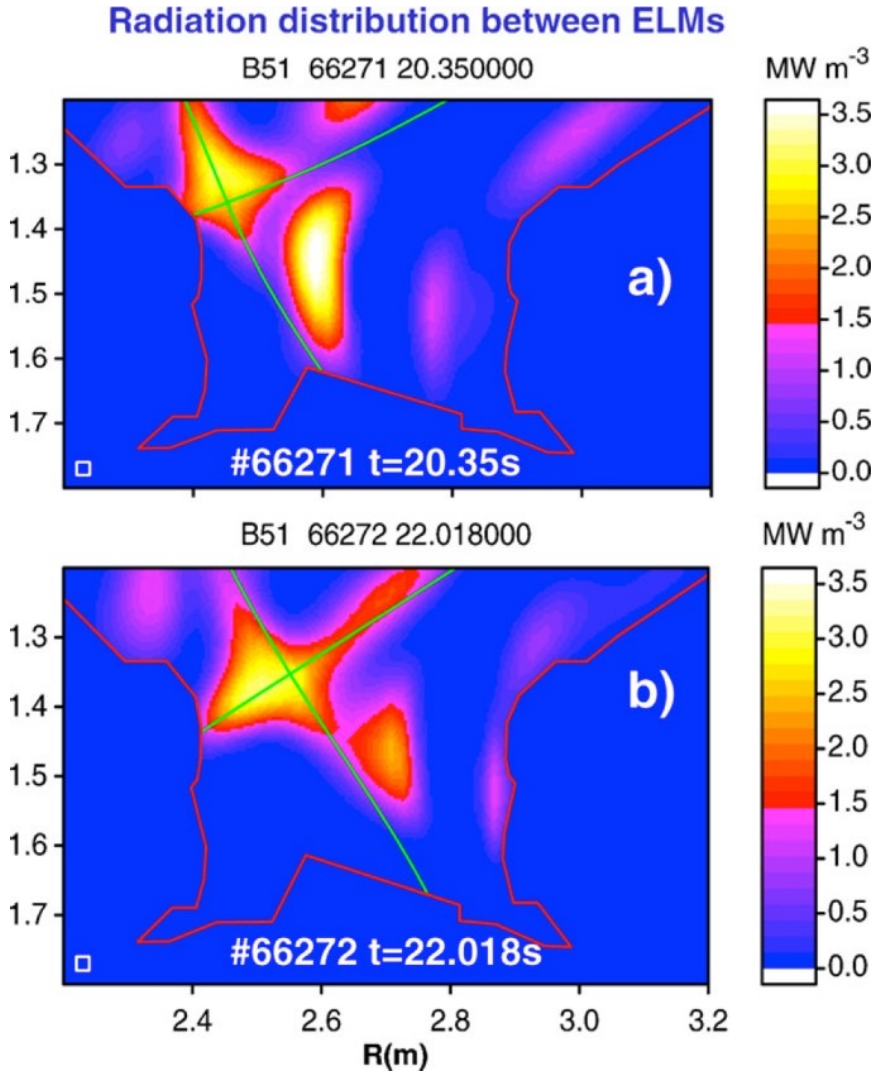

- **Zero-dimensional total power balance (P_{rad})**
- **Radiation distribution**
  - Dominant radiation occurs outside the core plasma
  - Bremsstrahlung and heavy-ion (e.g., W) line emission
- **Radiation distribution tracks magnetic configuration**

Huber et al. FED 2007

The local electron temperature is determined from electron cyclotron emission (free electrons)

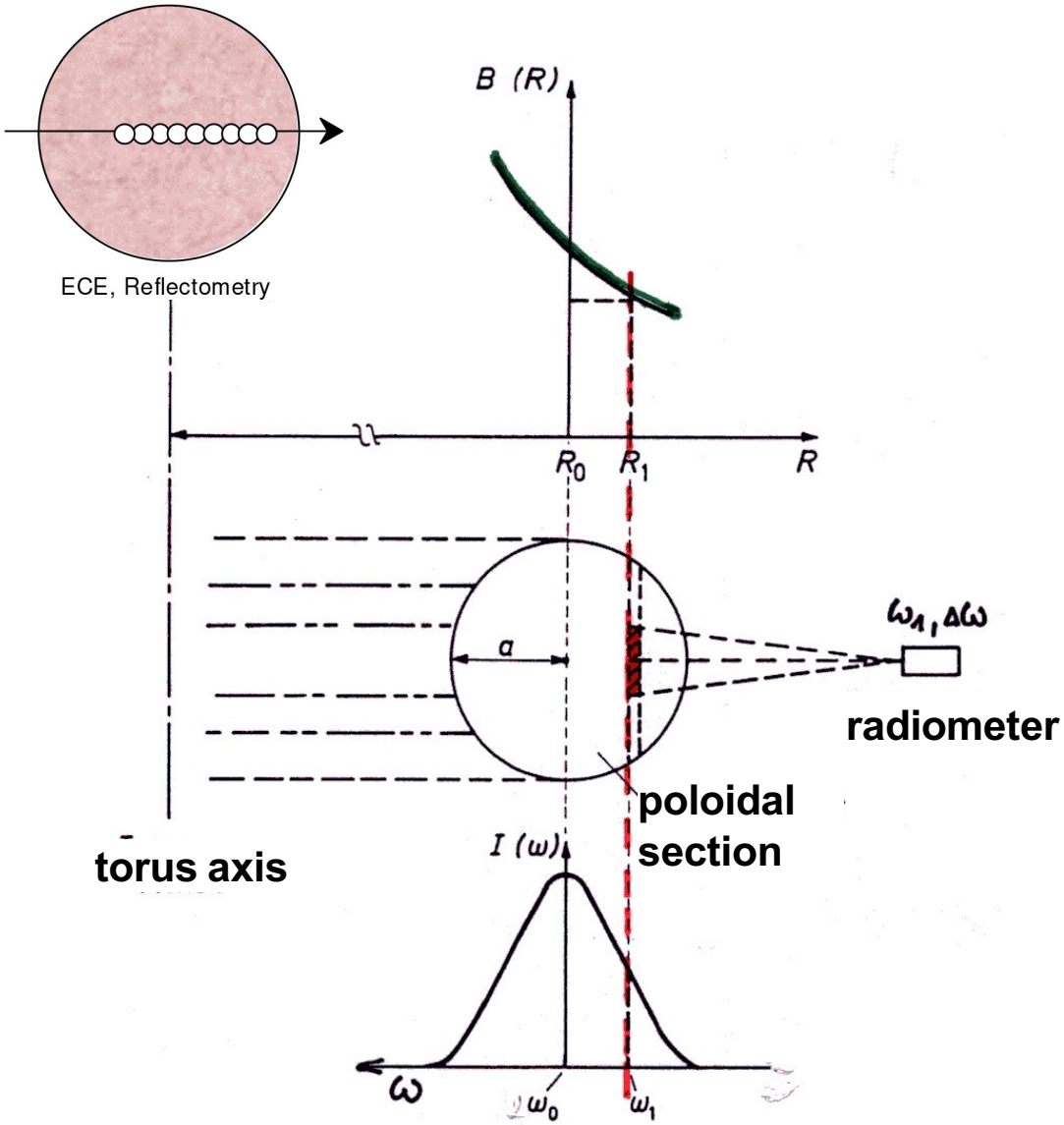

- **In tokamaks, B(R) ∝ 1/R**

⇒ **Electron cyclotron frequency:**

$$\omega_e = \frac{n\, e\, B}{m_e}$$

⇒ 2nd harmonic (n=2): ~ 110 GHz

- **ω localized to flux surface**

$$I(\omega) = \frac{\omega^2}{8\pi^3 c^2} T_e (1 - e^{-\tau})$$

for optical thickness τ assuming blackbody radiation

1-D radial and even 2-D distributions of the electron temperatures can be measured with ECE

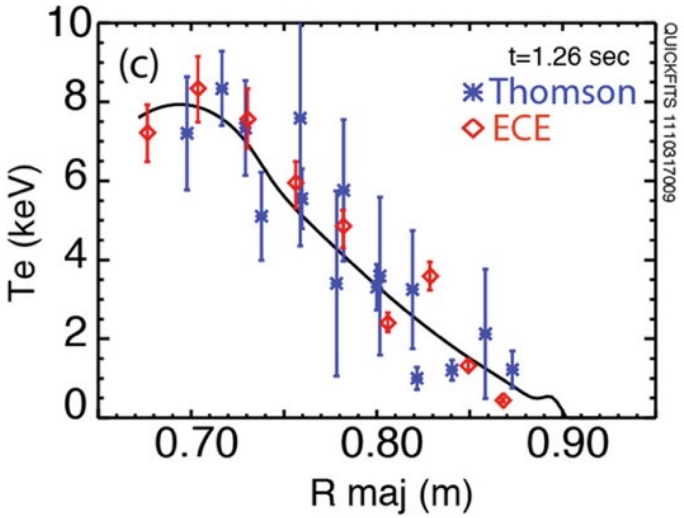

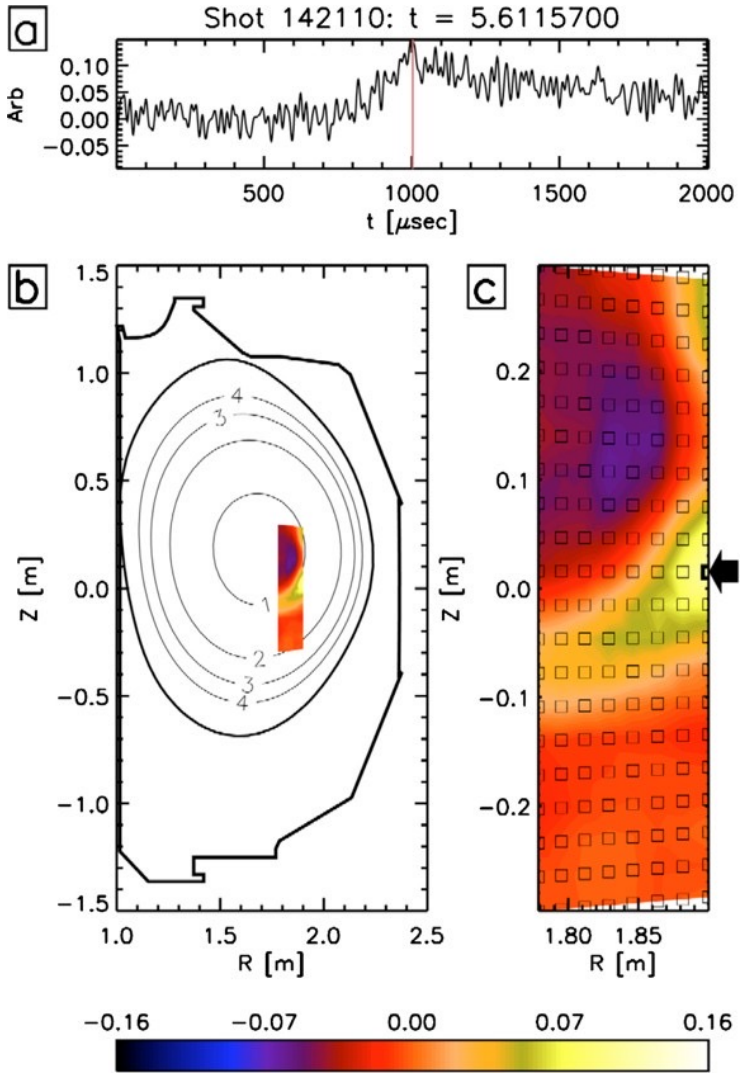

White et al. NF 2012

Tobias et al. RSI 2010

Spectroscopy covers the wavelength range from near-infrared to soft x-ray

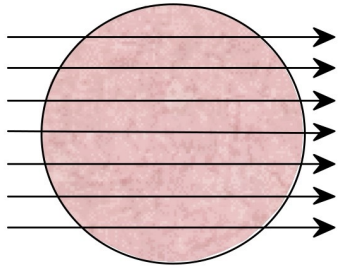

- **Bremsstrahlung (radiation from free (unbound) electrons in the field of ions)**
  - Electron temperature from intensity distribution: $I = I(\lambda)$
  - Effective charge state of the plasma (Z_{eff})

- **Line radiation from bound electrons at distinct wavelength specific to atom or ion**
  - Identification of elements in the plasma
  - Impurity influx from walls
  - Total impurity concentration

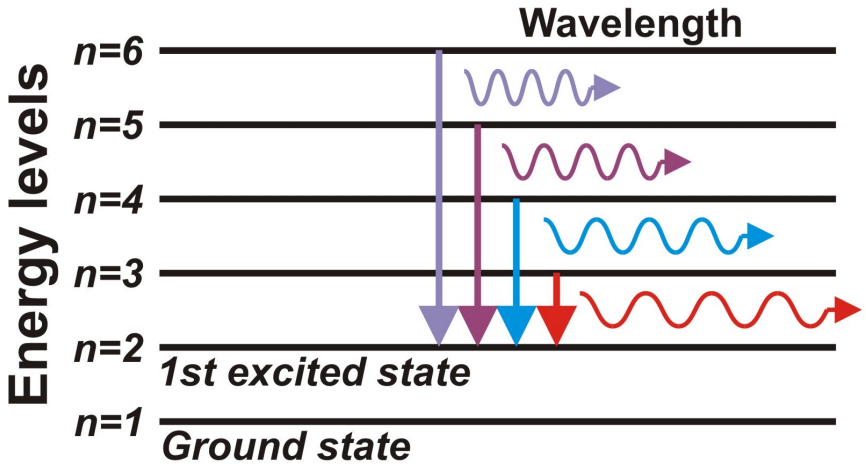

Radiated power in the DIII-D divertor includes emissions throughout the visible wavelength range

Hydrogen

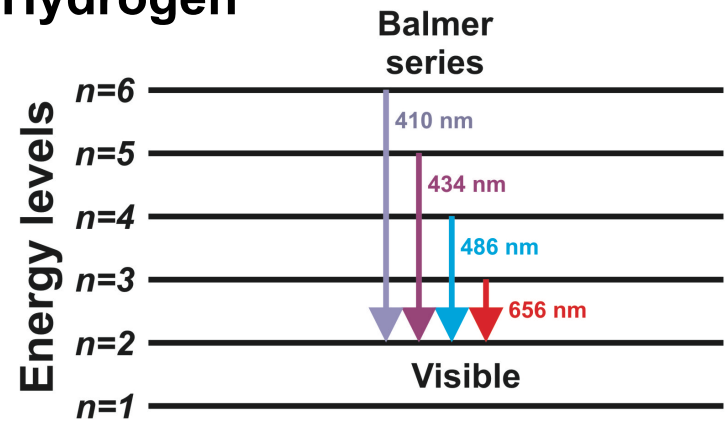

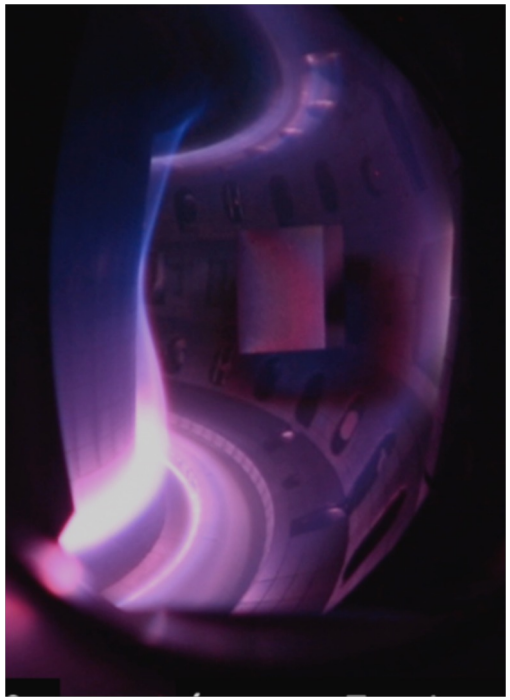

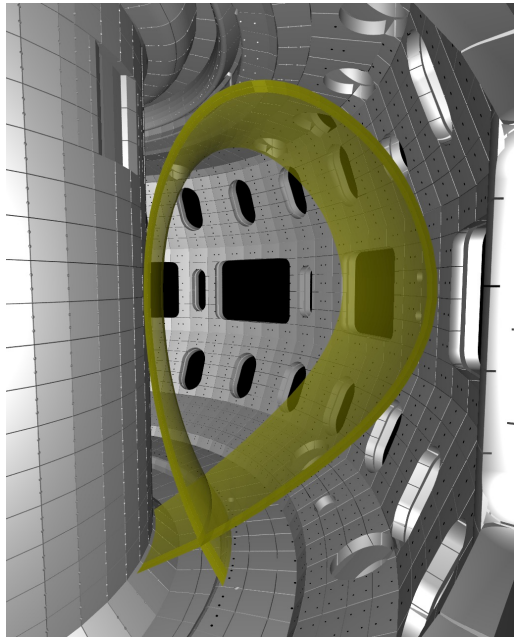

M.G. McLean et al., APS-DPP 2018

Radiated power in the DIII-D divertor includes emissions throughout the visible wavelength range

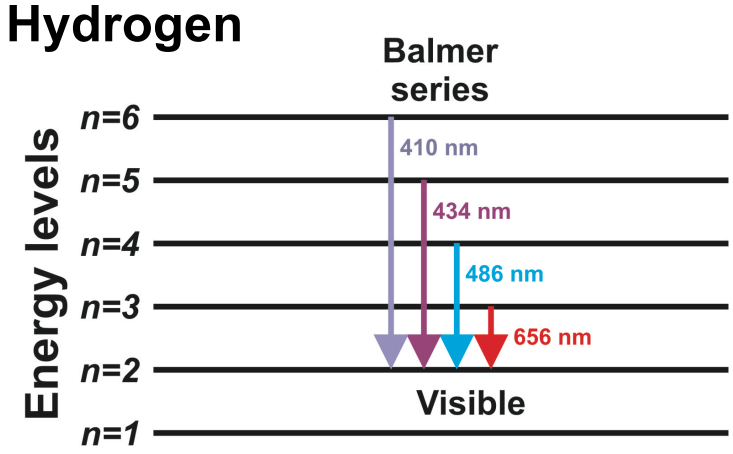

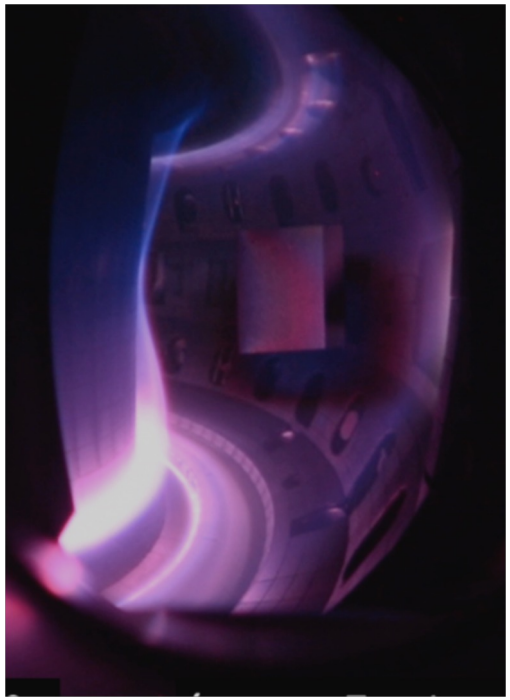

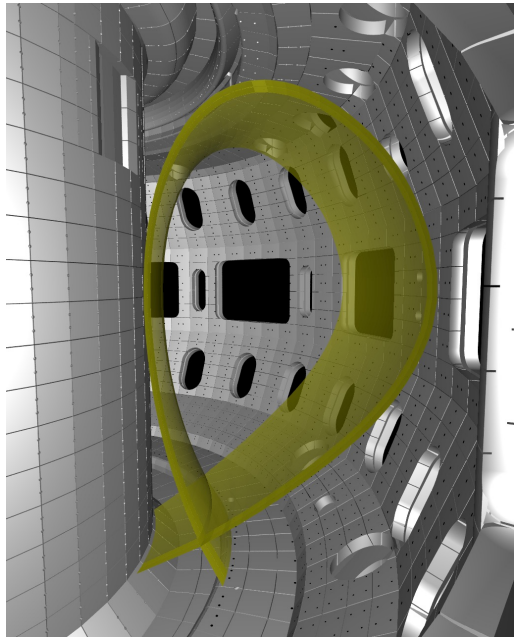

- **Visible spectroscopy is relatively straight-forward compared to other wavelength regions/bands**
  - Availability of efficient optics, filters, fibers, detectors, calib. sources
- **Only *visible* emission is from the plasma edge**
  - Core contains fully stripped ions, optically ‘thin’

M.G. McLean et al., APS-DPP 2018

Dominant / most energic line emission is in the Ultra-Violet (UV) wavelength range

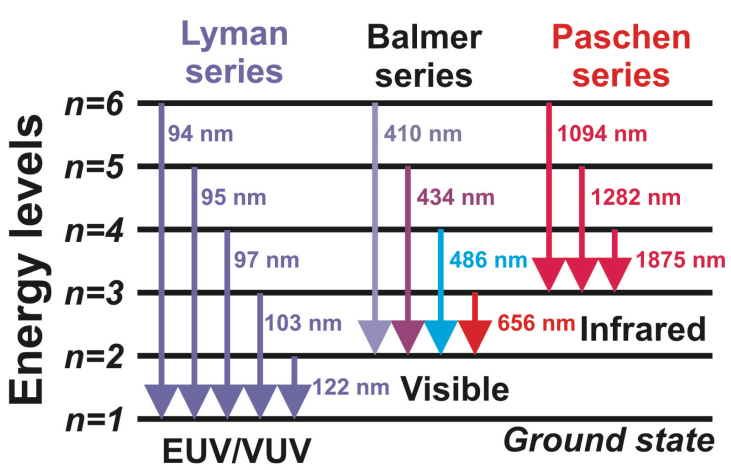

Hydrogen

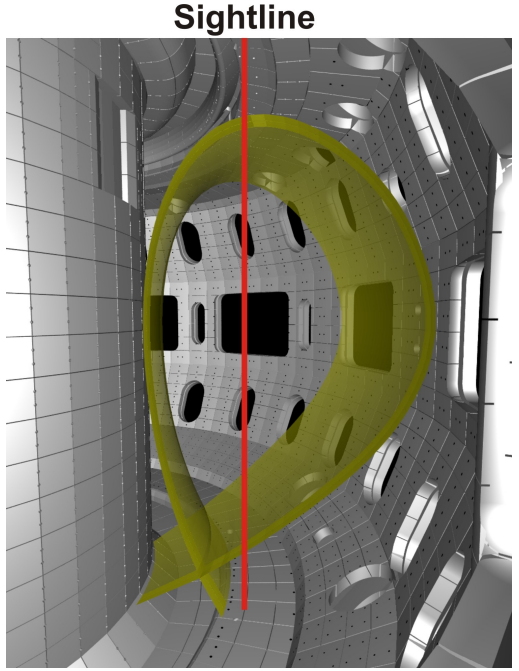

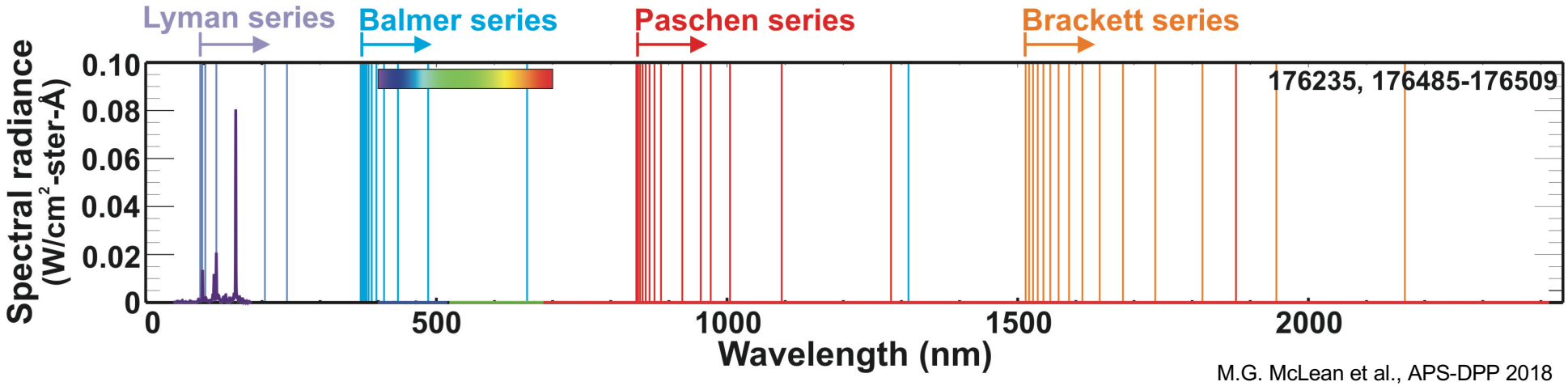

M.G. McLean et al., APS-DPP 2018

Dominant / most energic line emission is in the Ultra-Violet (UV) wavelength range

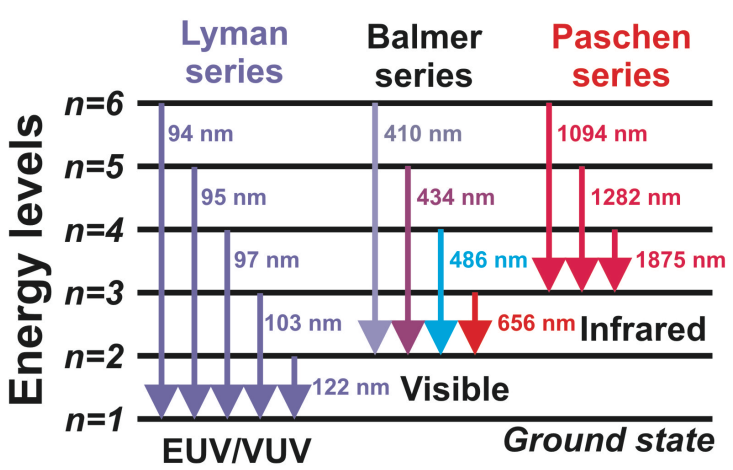

Hydrogen

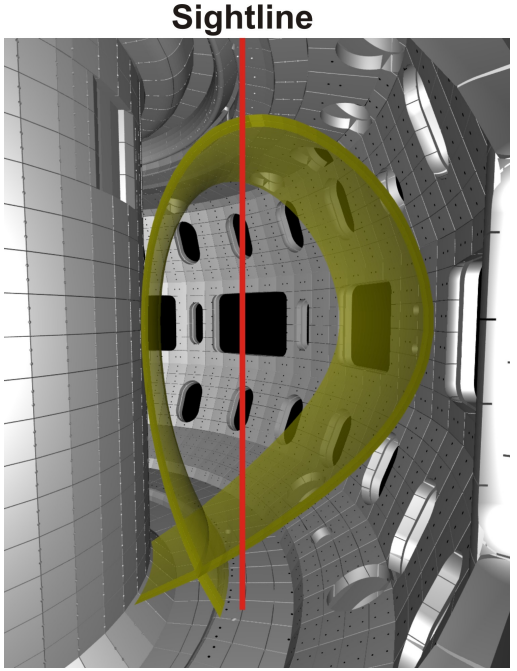

Linear

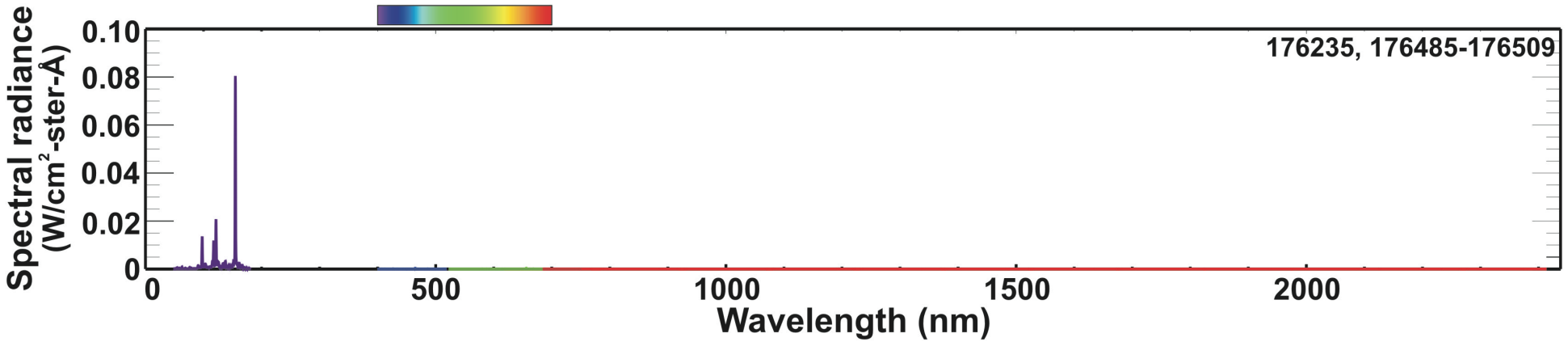

M.G. McLean et al., APS-DPP 2018

Dominant / most energic line emission is in the Ultra-Violet (UV) wavelength range

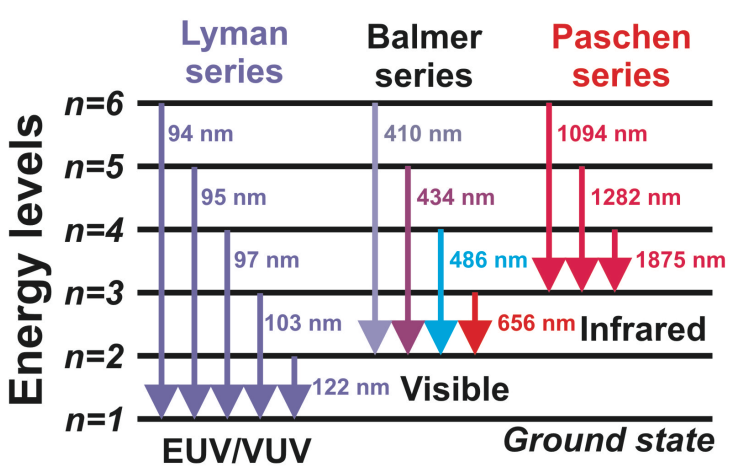

Hydrogen

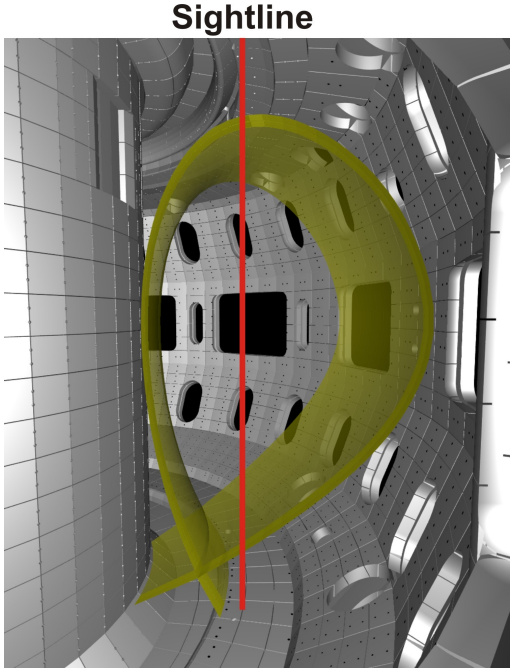

Log

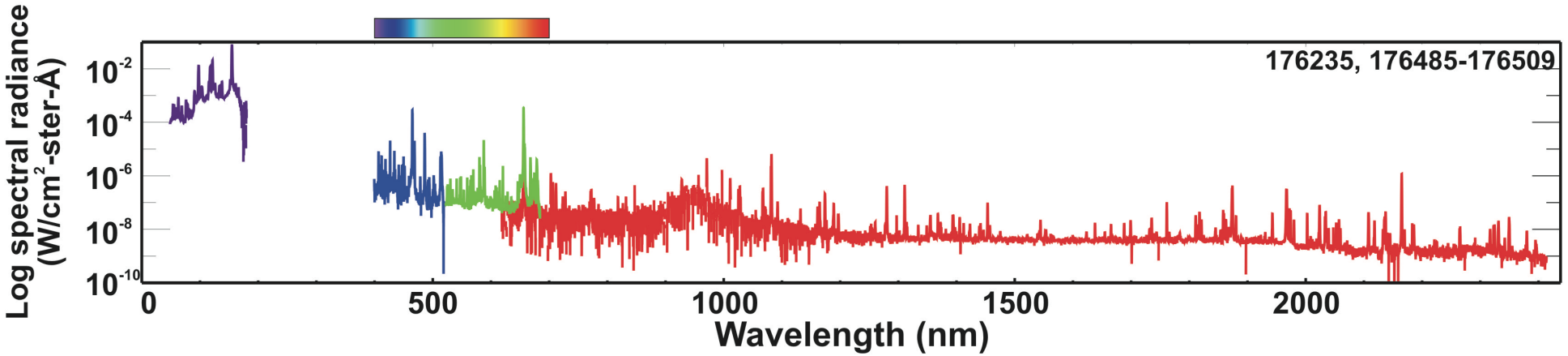

M.G. McLean et al., APS-DPP 2018

Dominant / most energic line emission is in the Ultra-Violet (UV) wavelength range

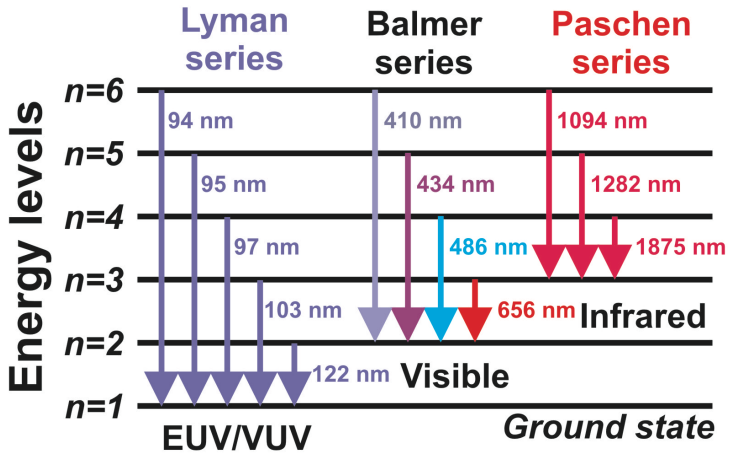

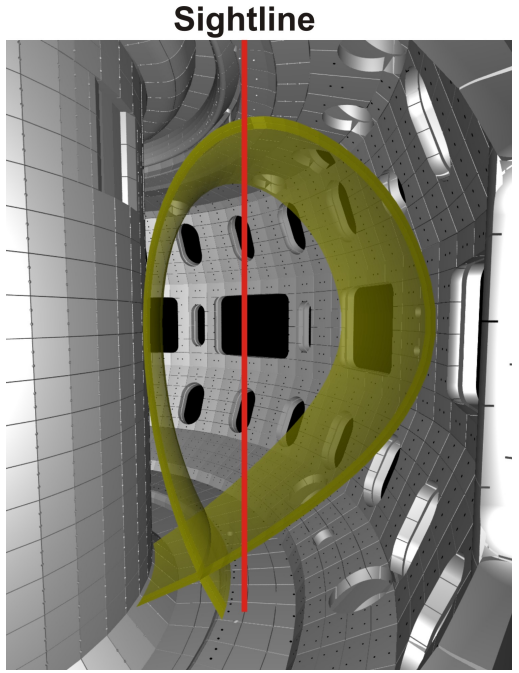

Log

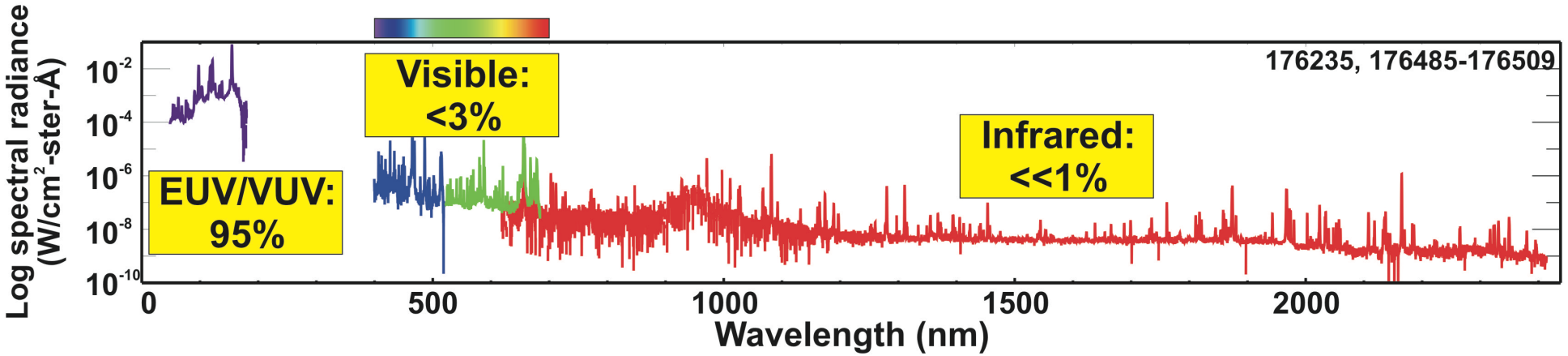

M.G. McLean et al., APS-DPP 2018

Spectroscopy covers the wavelength range from near-infrared to soft x-ray

- **Line radiation from bound electrons at distinct wavelength specific to atom or ion**
  - Electron and temperature density from line broadening and line ratios
  - Atomic and molecular hydrogenic distribution from atomic line emission and molecular bands ⇒ recycling and fueling
  - Multiple charge state spectroscopy of single elements ⇒ ion transport
- **Doppler spectroscopy for T_i in the center (x-ray) and flow velocity**

Active radiation measurements

Diagnostics may be classified into four basic groups

Category	Parameter	Method
Active radiation	Electron density and temperature, current profile, ion temperature,	Thomson scattering interferometry, reflectometry, polarimetry, charge exchange, Li or He beams, heavy ion probe

Interferometry measures the electron density along a laser beam through the plasma

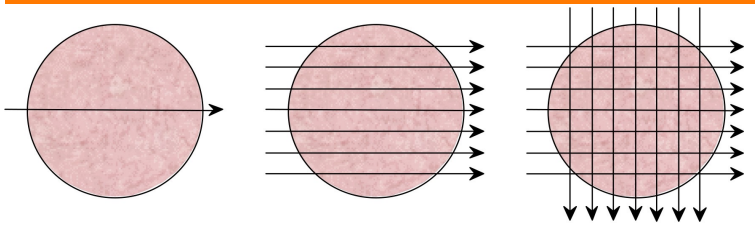

- **Infra-red CO_2 laser at 119 μm, 200 mW**
- **Phase shift between the probe and reference laser beam:**

$$\Delta\phi = r_e \lambda \int_L n_e dl$$

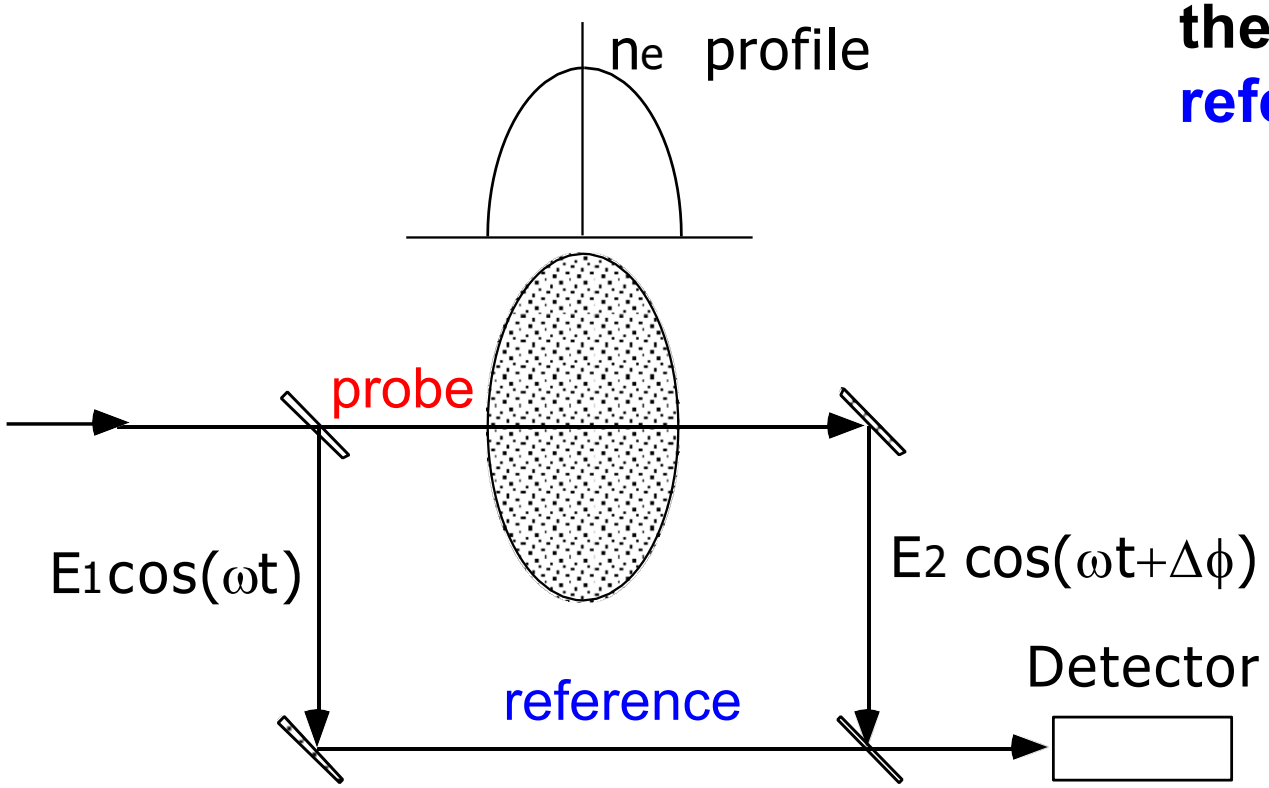

The JET interferometry/polarimetry is a 2x4 channel system viewing vertically and horizontally

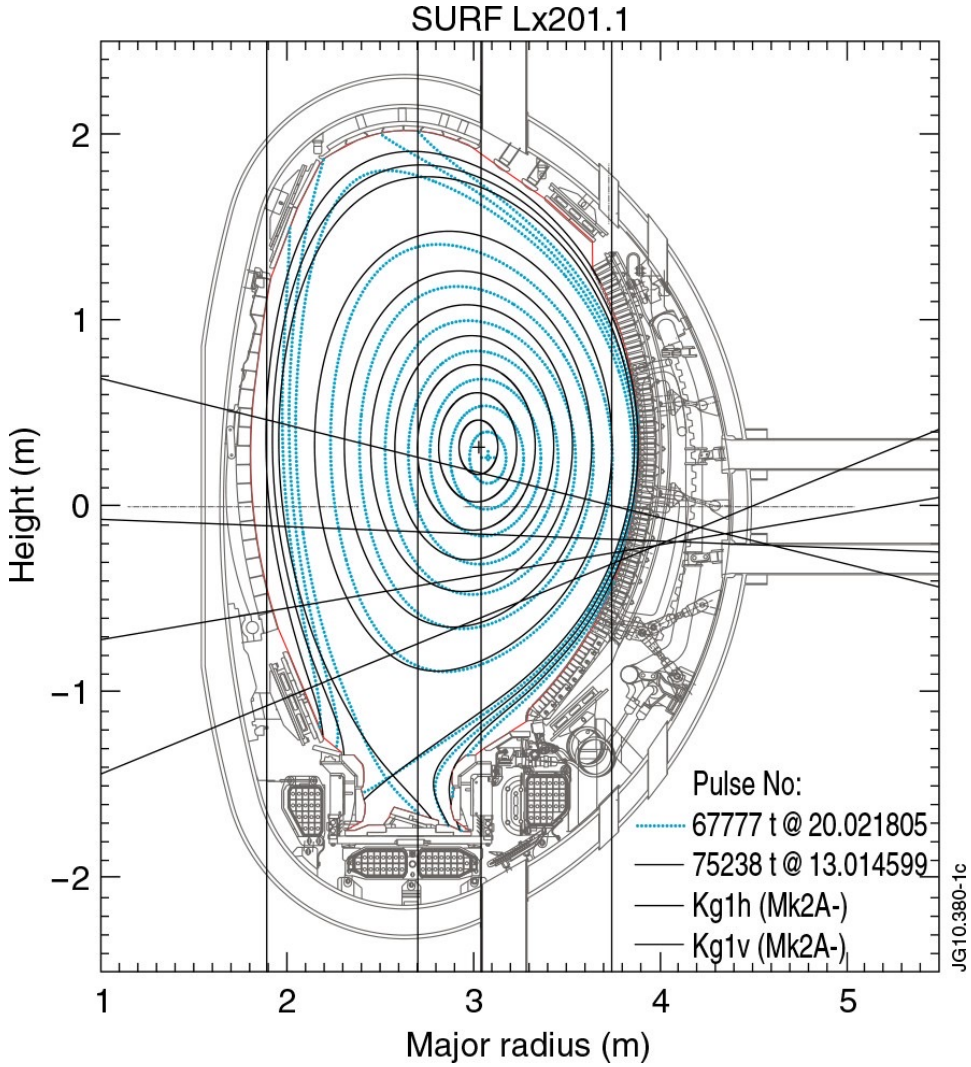

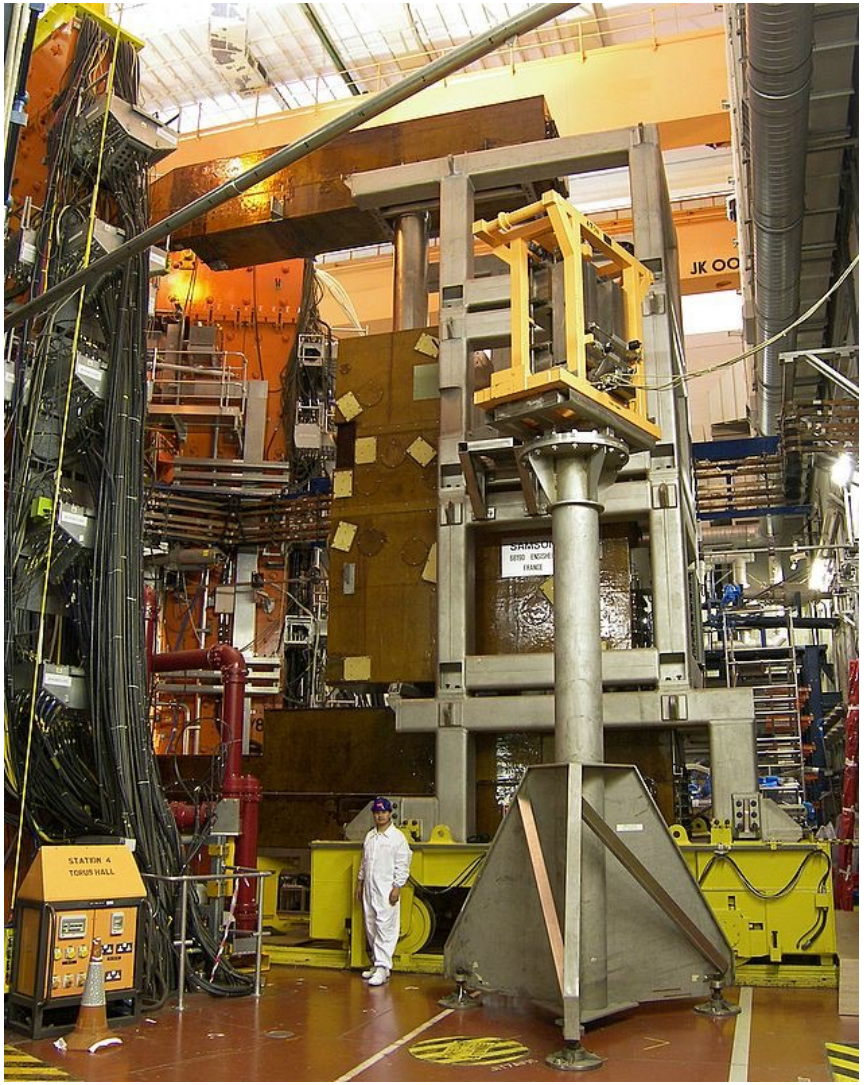

There are several other laser and beam-aided diagnostic systems on JET

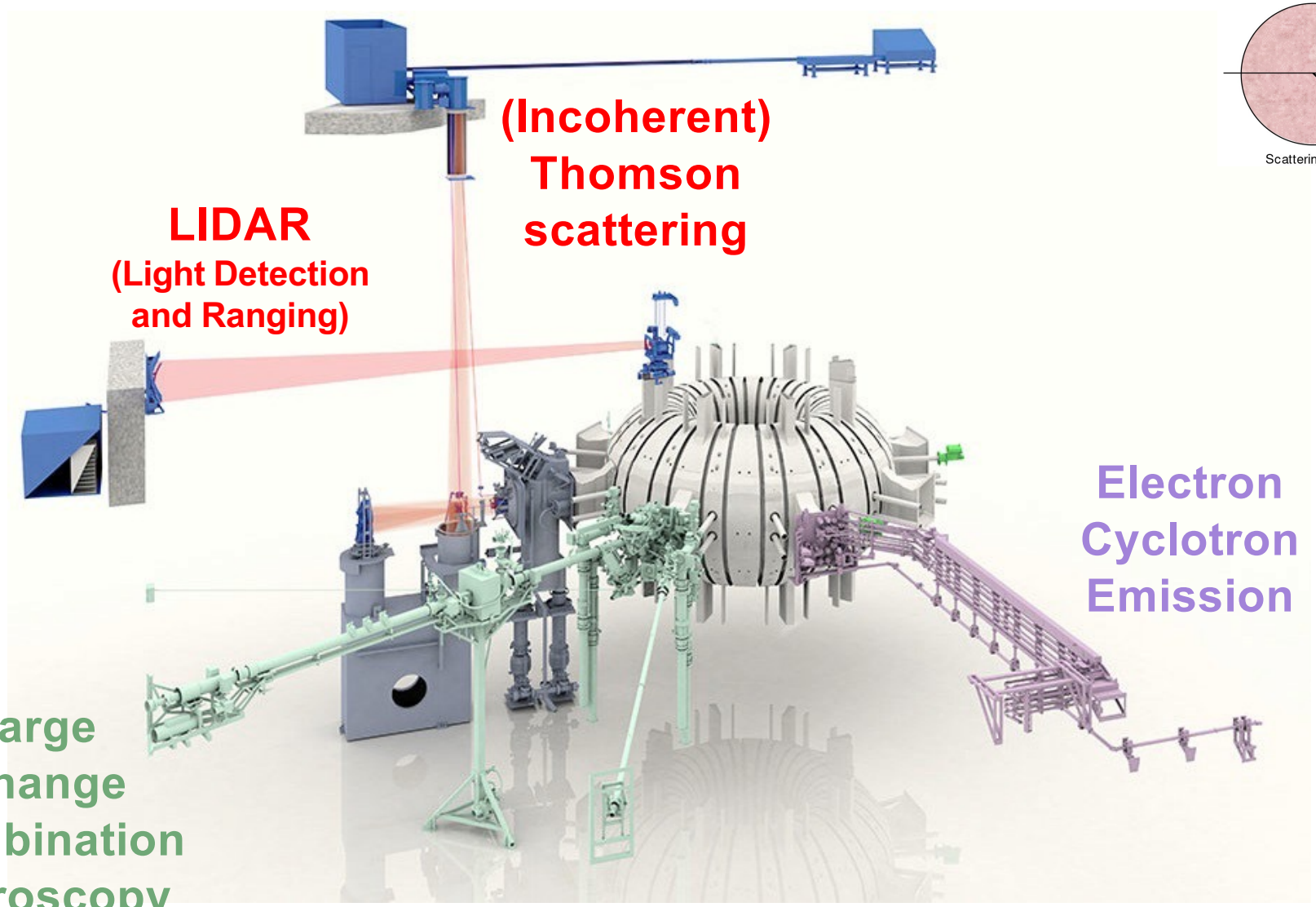

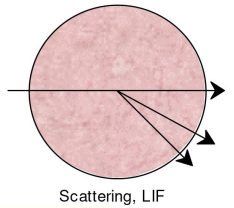

Imaging a laser beam path and spectrally resolving the scattered light yields the electron temperature and density

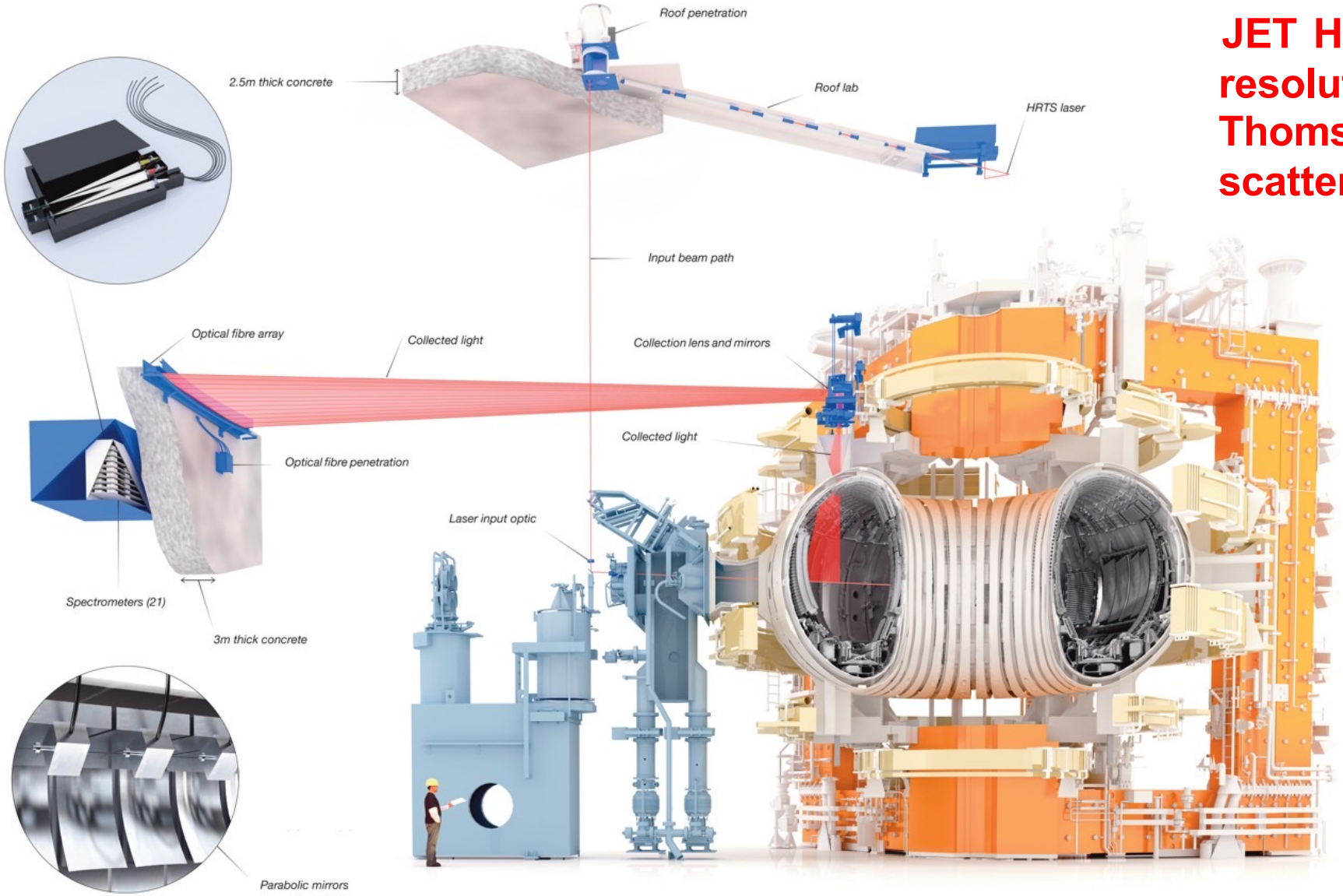

JET High-resolution Thomson scattering

Photon scattering on electrons leads to broadening and wavelength shift wrt. the original laser spectrum

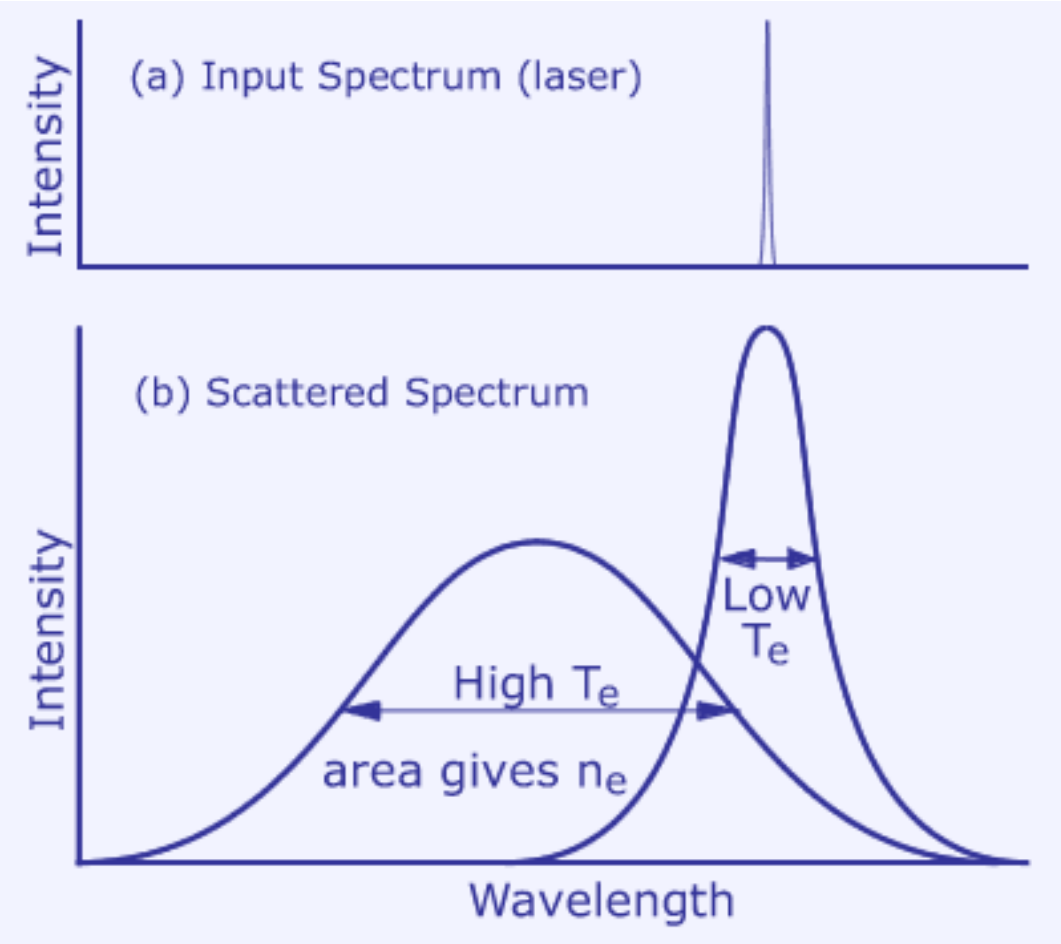

- **Electrons oscillate in light's electric field ⇒ emit photon of same wavelength**

Interaction of a keV-fast neutral beam with plasma impurities leads to charge exchange emission

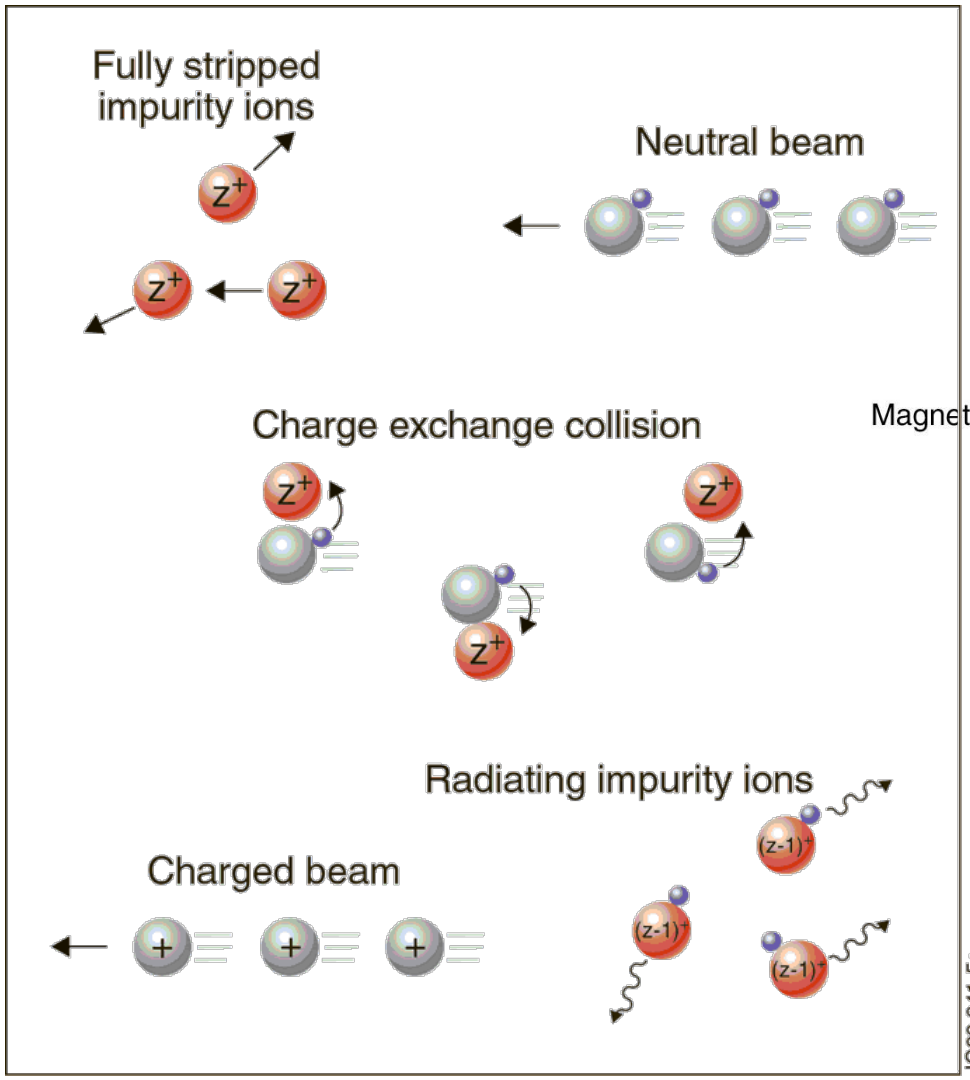

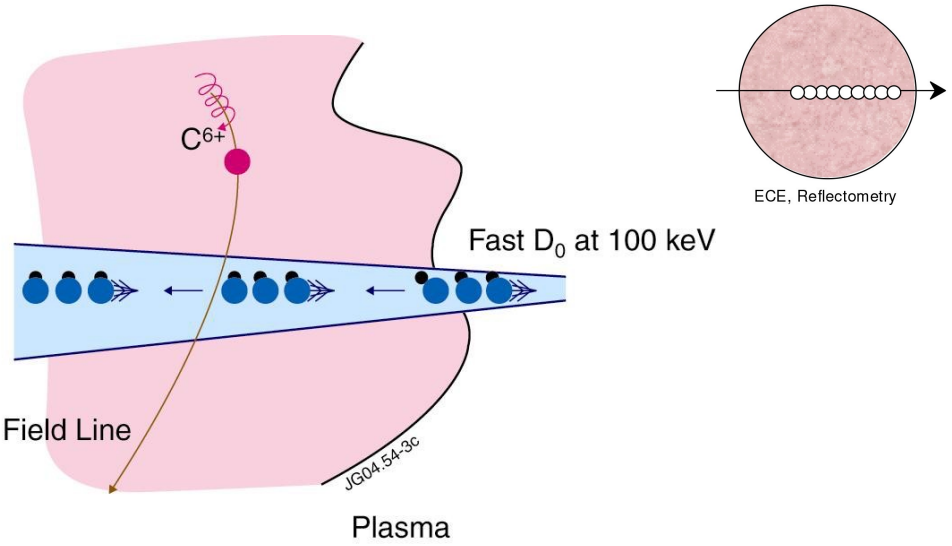

- **Doppler shift and broadening provide velocity and temperature; absolute calibration the impurity density**

At JET, Charge Exchange Recombination spectroscopy utilizes the two heating beam

- **Highly resolved measurements of T_i, v_{tor} and v_{pol}, and n_{imp} covering the entire plasma cross-section**

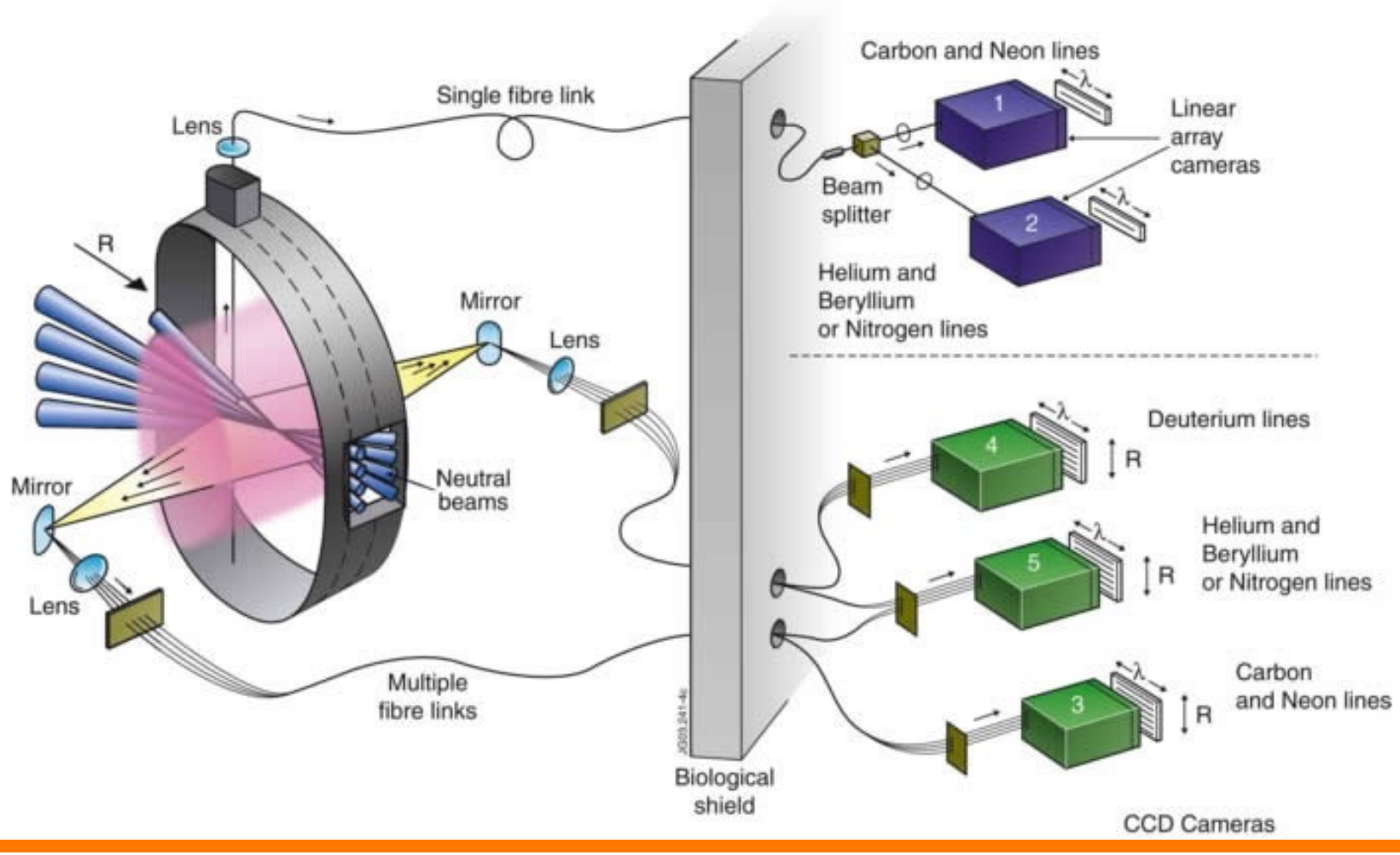

At ASDEX Upgrade, lithium and helium beam emission spectroscopy is used for ne and CXRS measurements

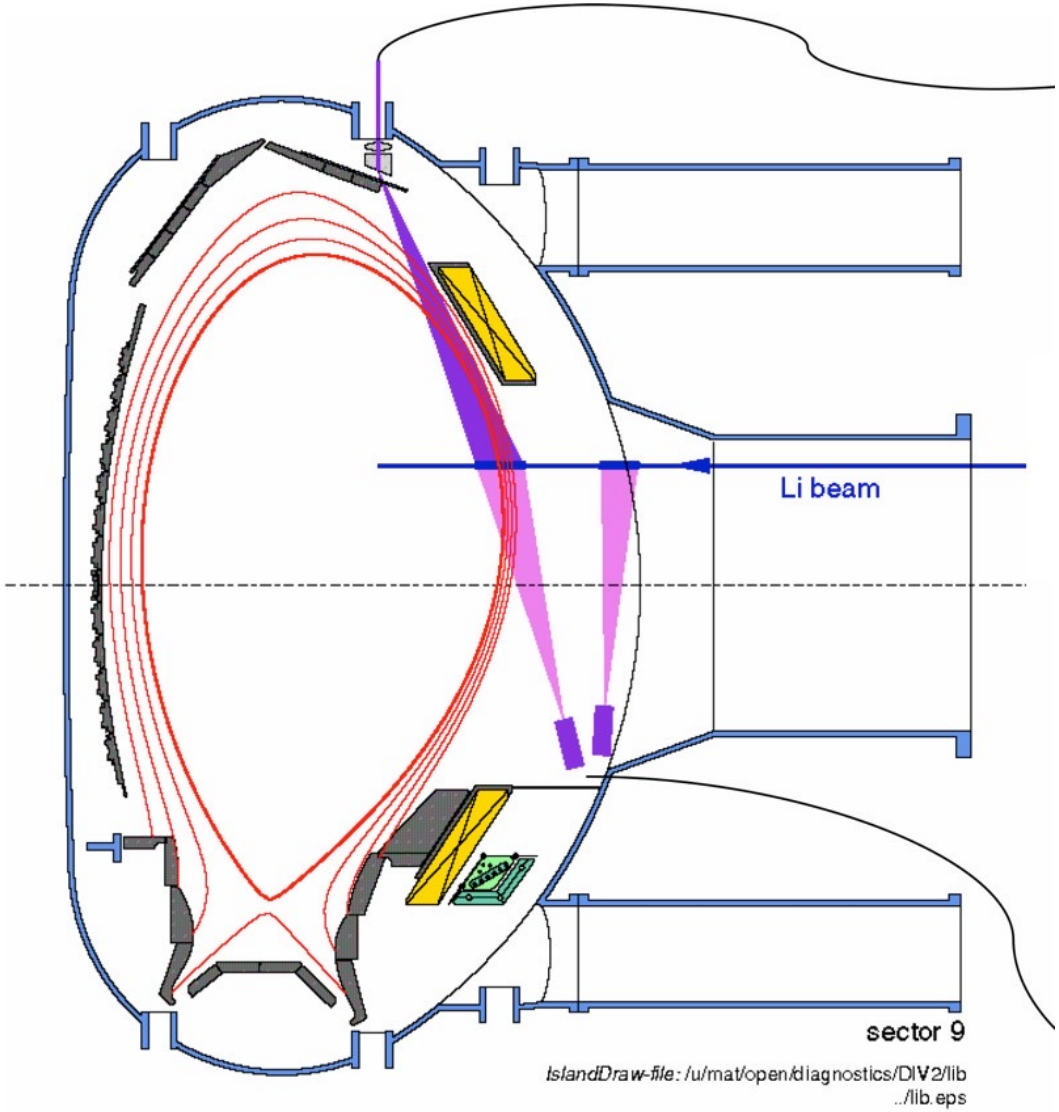

Wolfrum et al. ADAS WS 2007

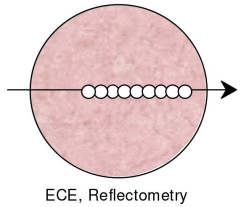

- **Horizontal Li beam 30-80 keV, 2-4 mA, 1.2 cm in diameter**
- **Vertical lines of sight**
  - Down view for electron density (6708 Å)
  - Up view for T_i and n_{imp} from CX

Particle measurements

Diagnostics may be classified into four basic groups

Category	Parameter	Method
Particle diagnostics	Plasma particle fluxes, neutron and γ yields	Langmuir probes, fission chambers, neutron cameras, neutron spectrometers

Langmuir probes are the simplest diagnostic to measure particle (ion) fluxes to material surfaces

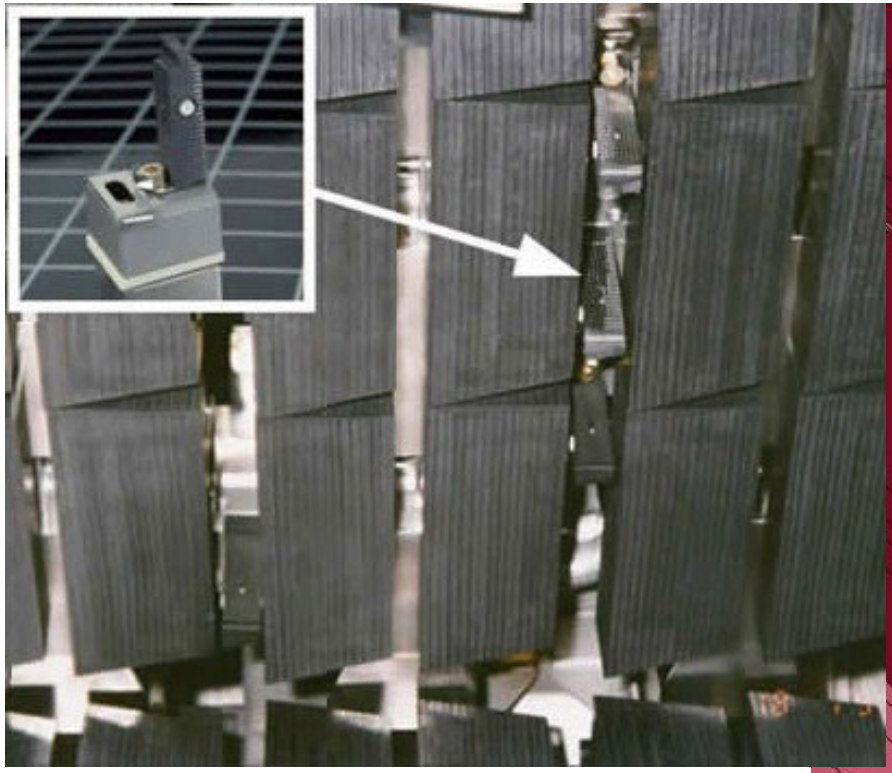

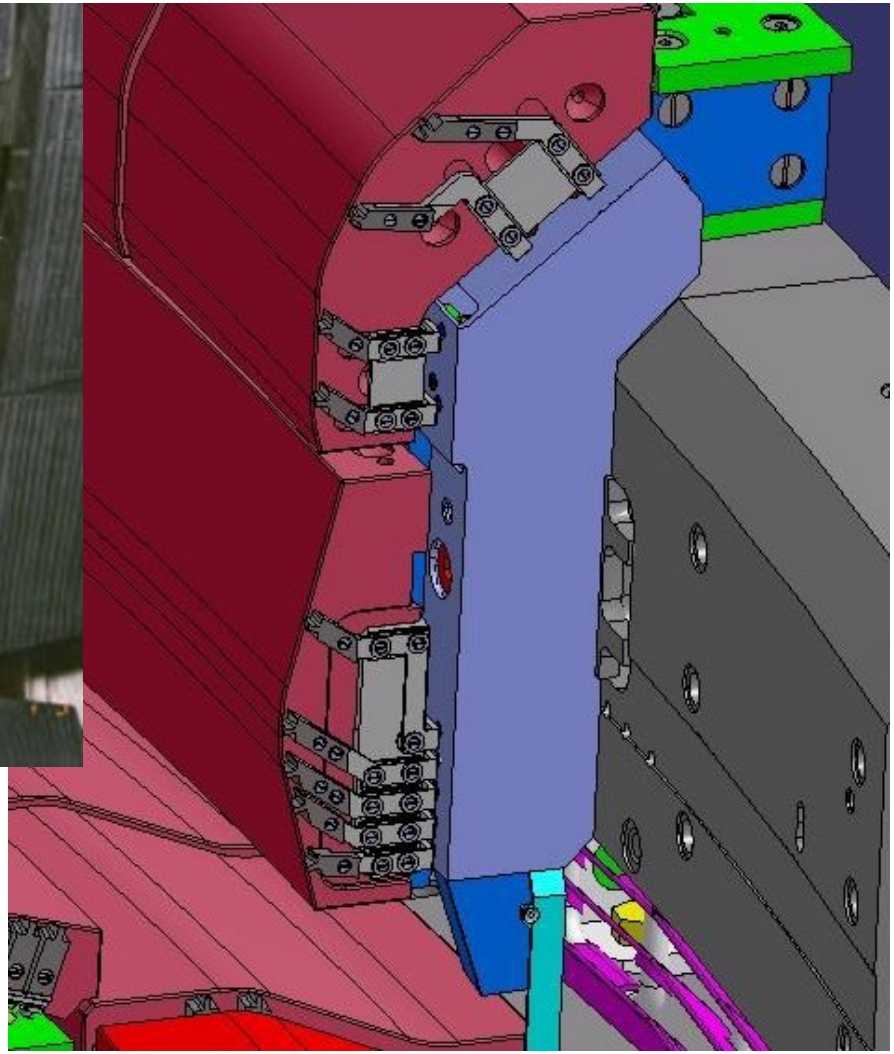

- **Probes are typically mounted between tiles**
- **Bias voltage swept to measure fluxes, T_e, and n_e**

Reciprocating Langmuir probe system have same design … and are plunged into plasma

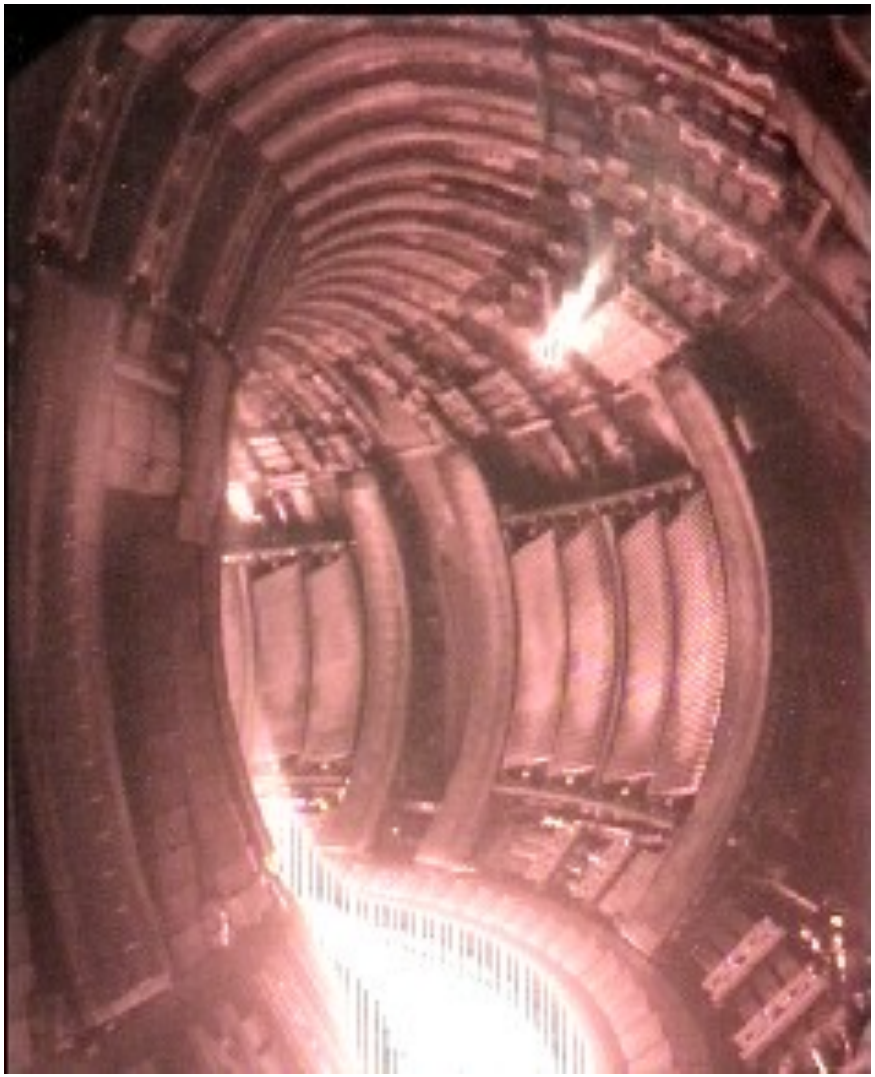

Neutrons are measured via fission chambers utilizing neutron - U^{235} and U^{238} reactions

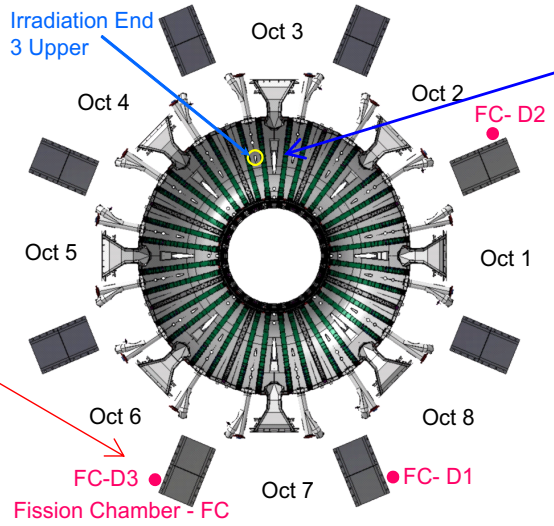

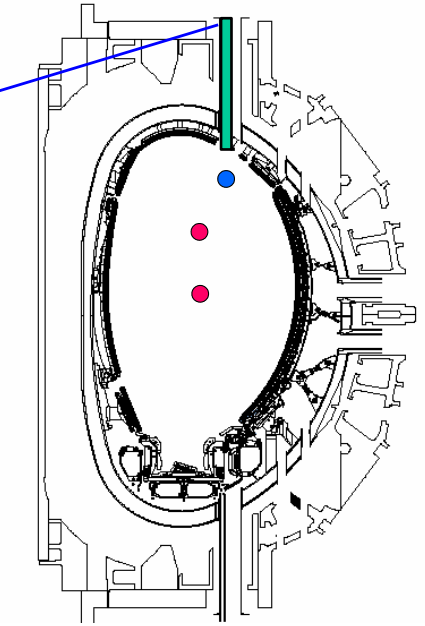

- **Usable for neutron emissions from 10^{10} to 10^{20} n/s**
- **Relatively insensitive to the neutron energy**
- **Absolutely calibrated, uncertainty < 10% ⇒ extensive neutron calibrations in 2013 (2.2 MeV) and 2017 (14 MeV)**

The JET neutron cameras yield 2-D distribution profiles of 2.5 MeV and 14 MeV neutrons

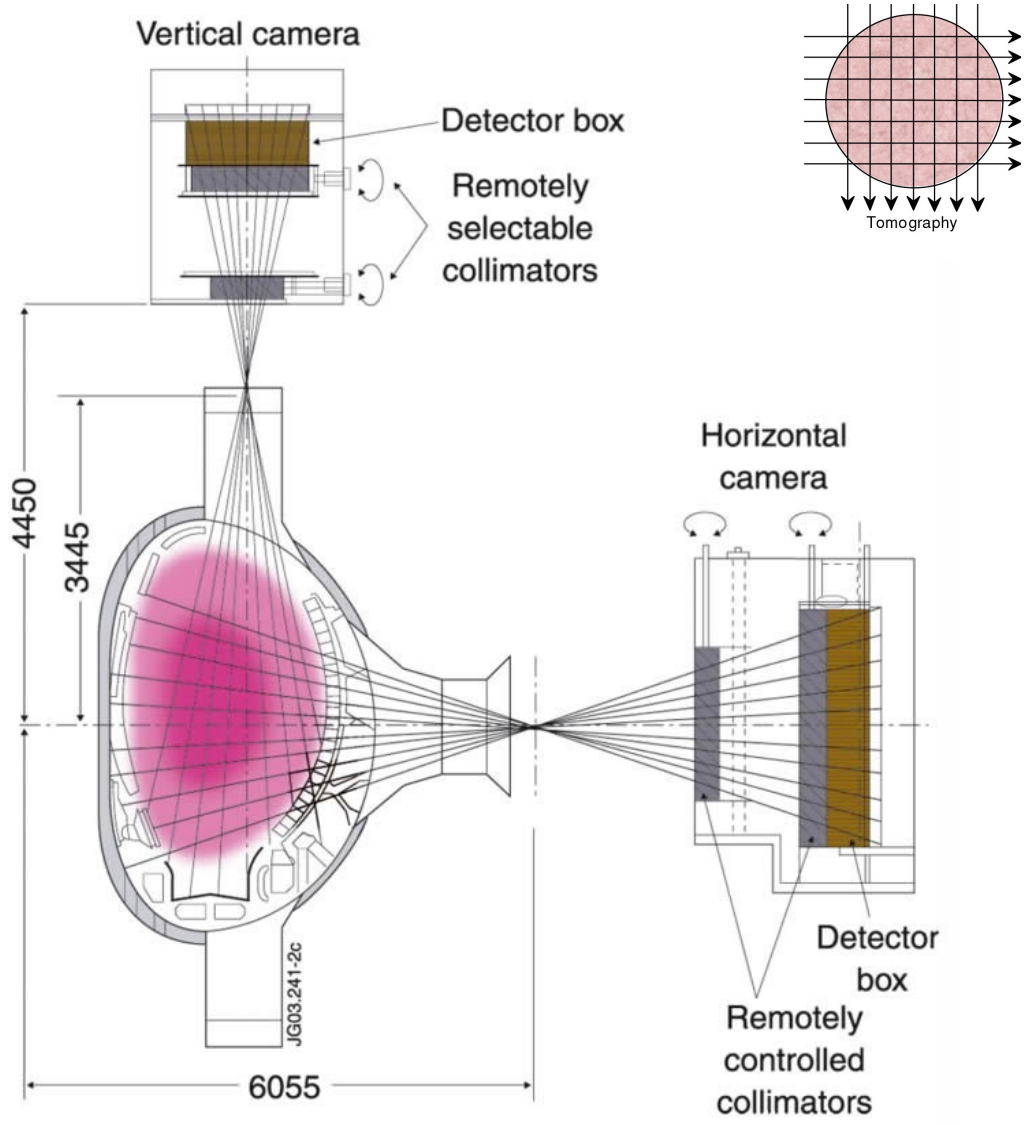

- **Crossed views from a vertical (9 channels) and horizontal (10) collimated lines of sight**
- **Neutron detectors:**
  - Liquid scintillators NE213 for 2.5 MeV and 14 MeV
  - Plastic Bicron 418 for 14 MeV
- **19 CsI(Tl) solid state photodiodes for γ-rays**

The neutron spectrum is spatially resolved for 3.1 MeV and 4.4 MeV γ-rays

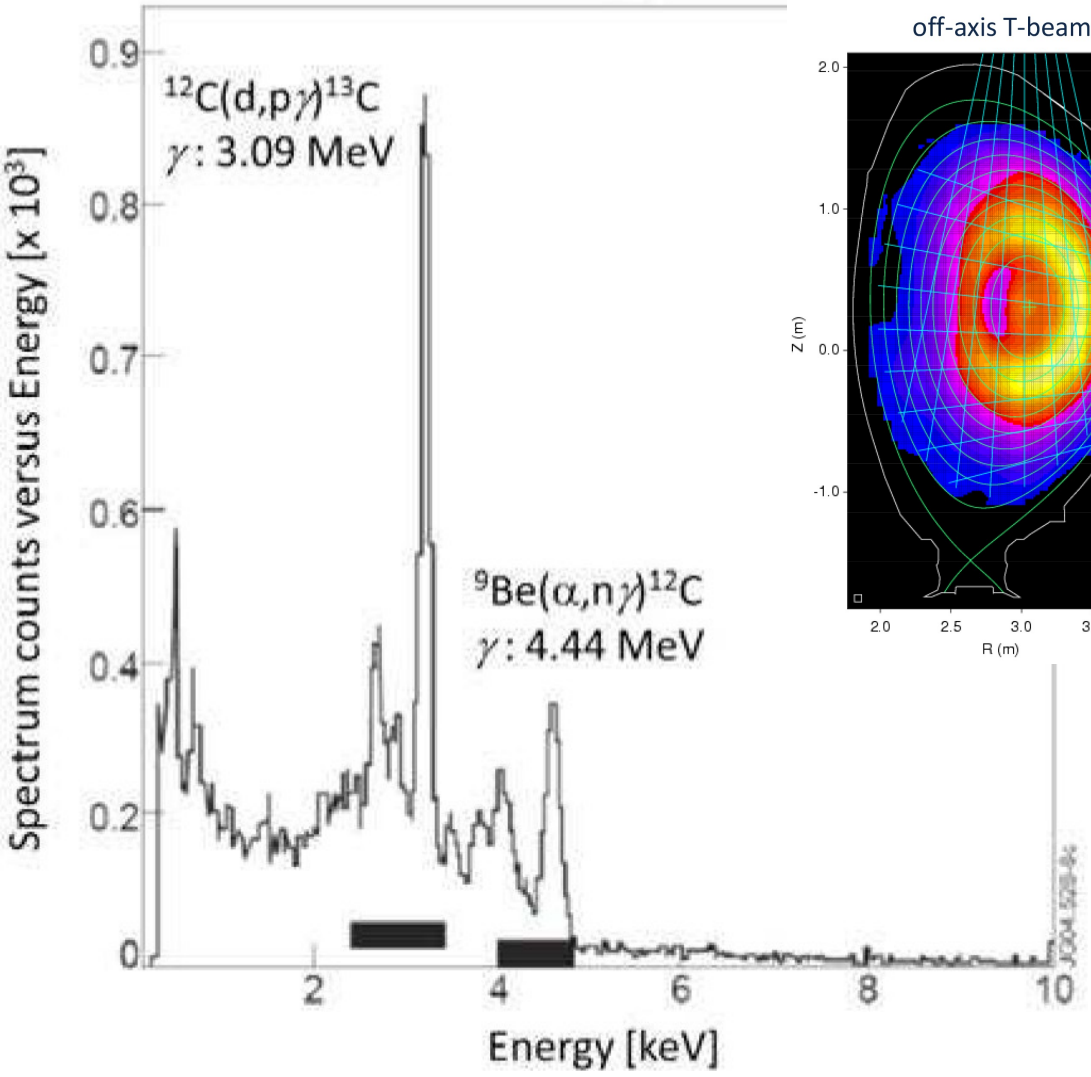

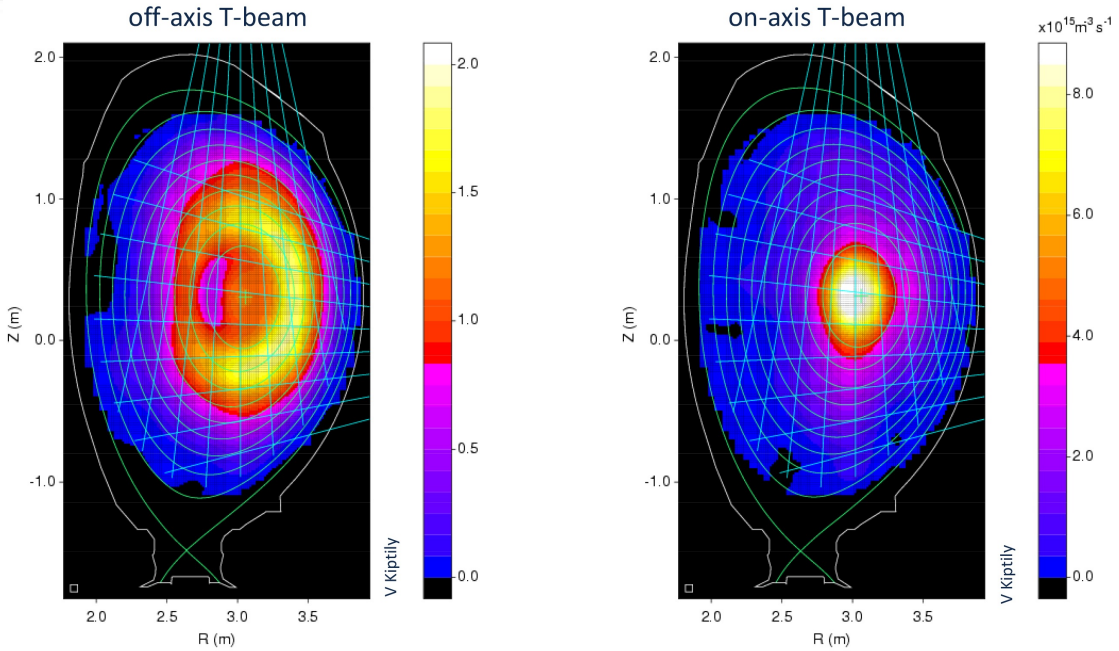

- **Indirect measurements of neutrons through γ rays**
- **Test for measurement of fusion-born α-particles at 3.5 MeV**

First measurements of fusion-born neutrons were carried out in the 2021 JET deuterium-tritium campaign

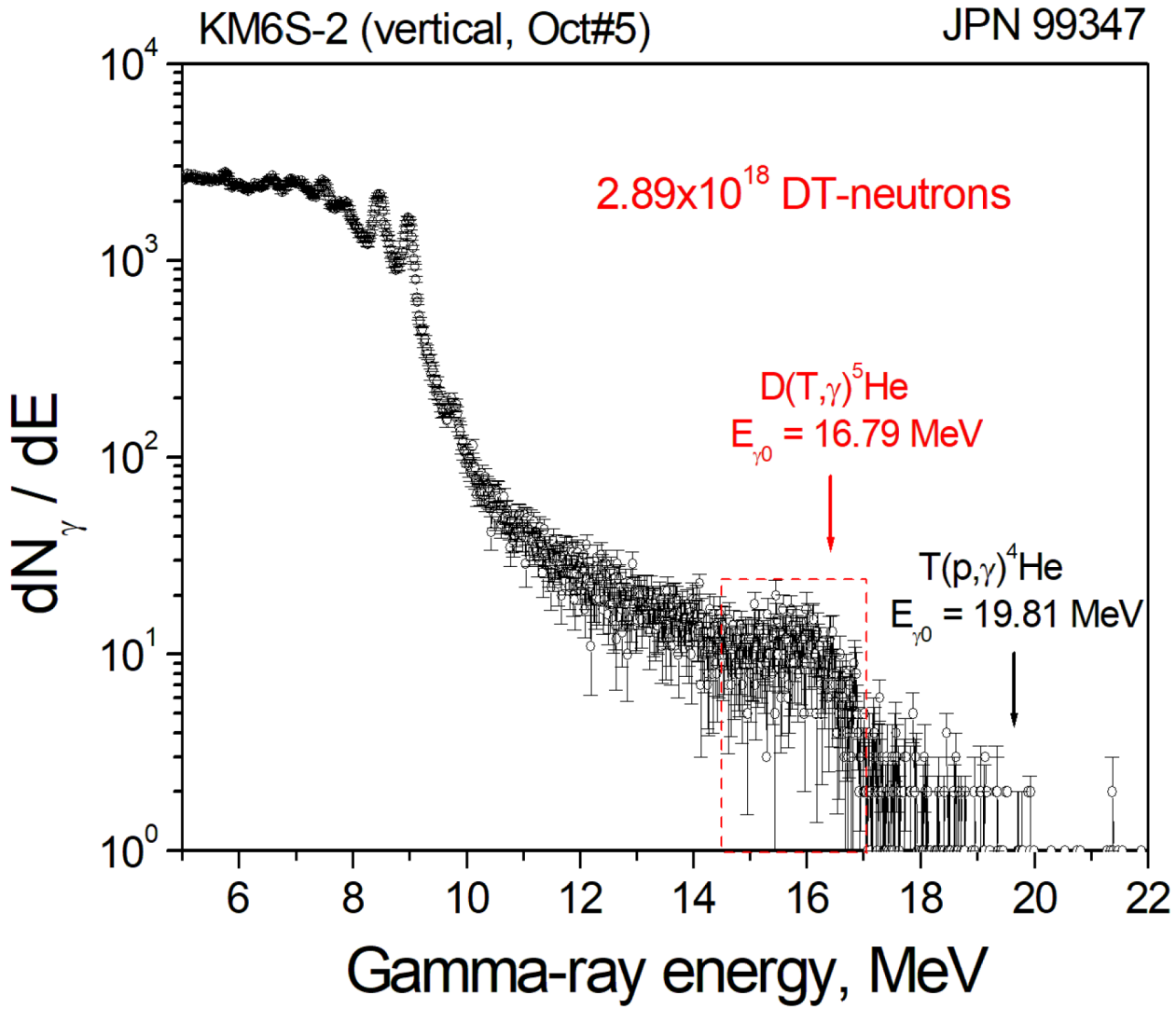

- **Challenging measurement of 14 MeV neutrons due to low yields and other reactions**

A magnetic proton recoil spectrometer is used to measure neutron spectrum at high (energy) resolution

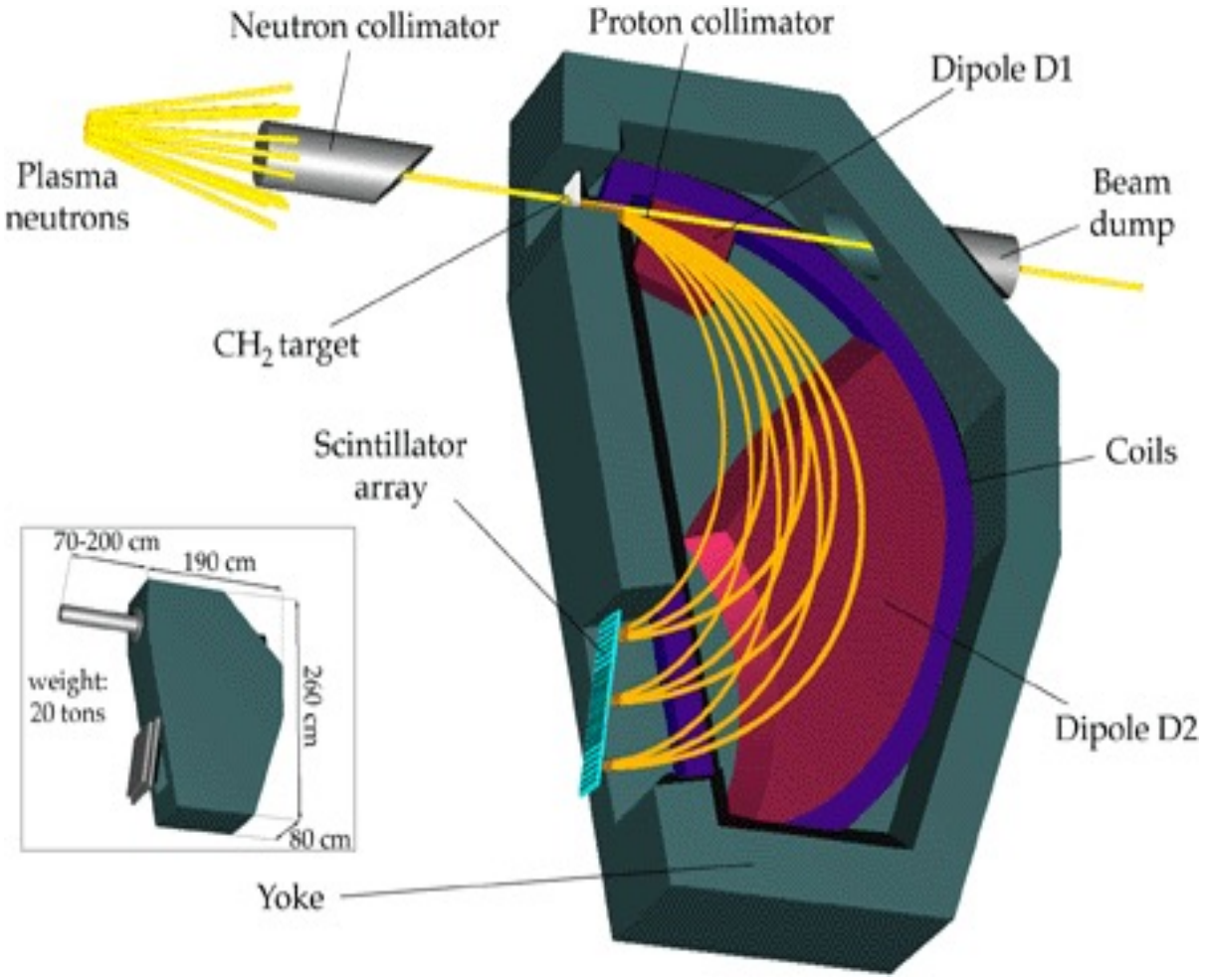

- **Conversion of neutrons into protons**

⇒ **Mass spectrometer and imaging onto a scintillator array**

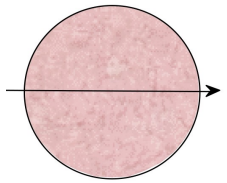

The proton recoil spectrometer is a significant installation outside the tokamak

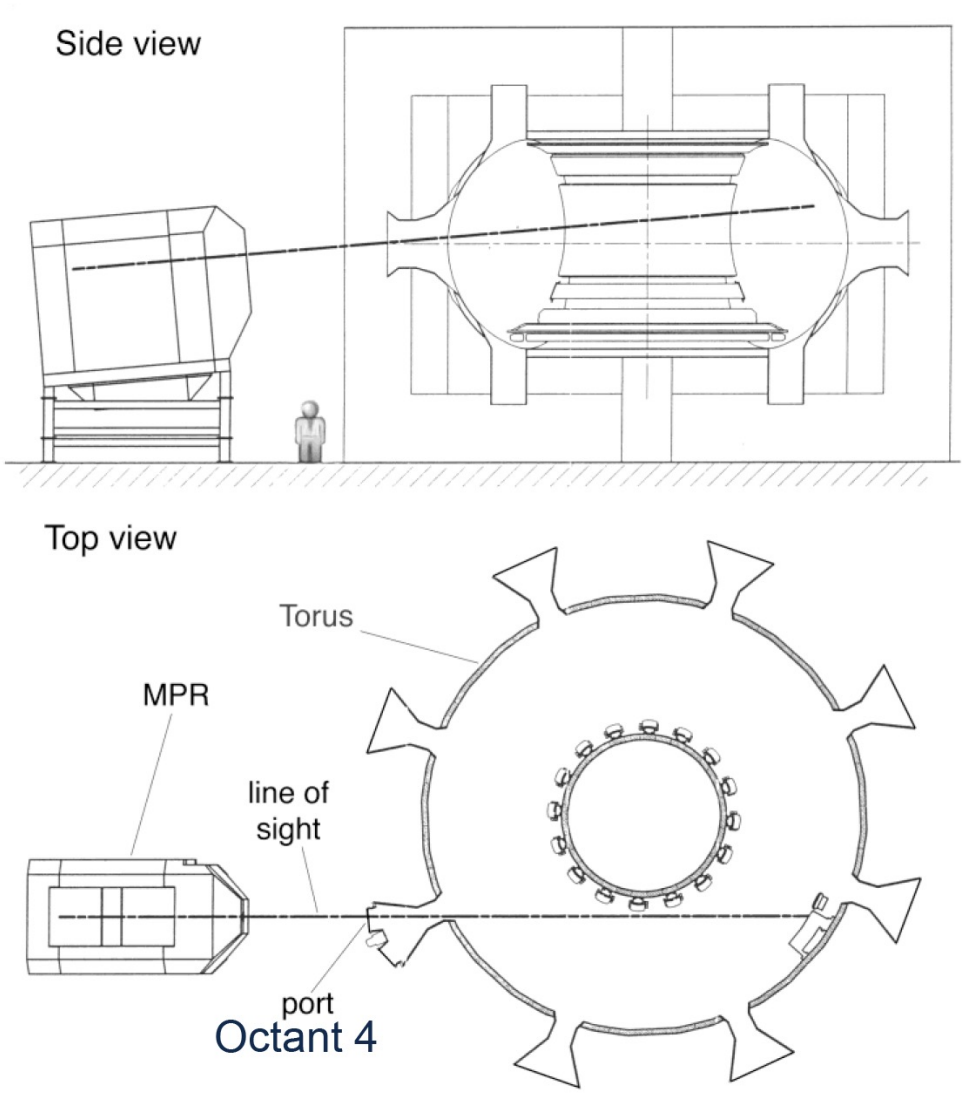

- **Single line of sight through the center of the plasmas**
- **Tangential view**

⇒ **Line-averaged measurement only, needs to be combined and interpreted with other diagnostics**

- **Total weight = 20 tons!**

Crossed-view neutron cameras will also provide 2-D neutron (fusion) information in ITER

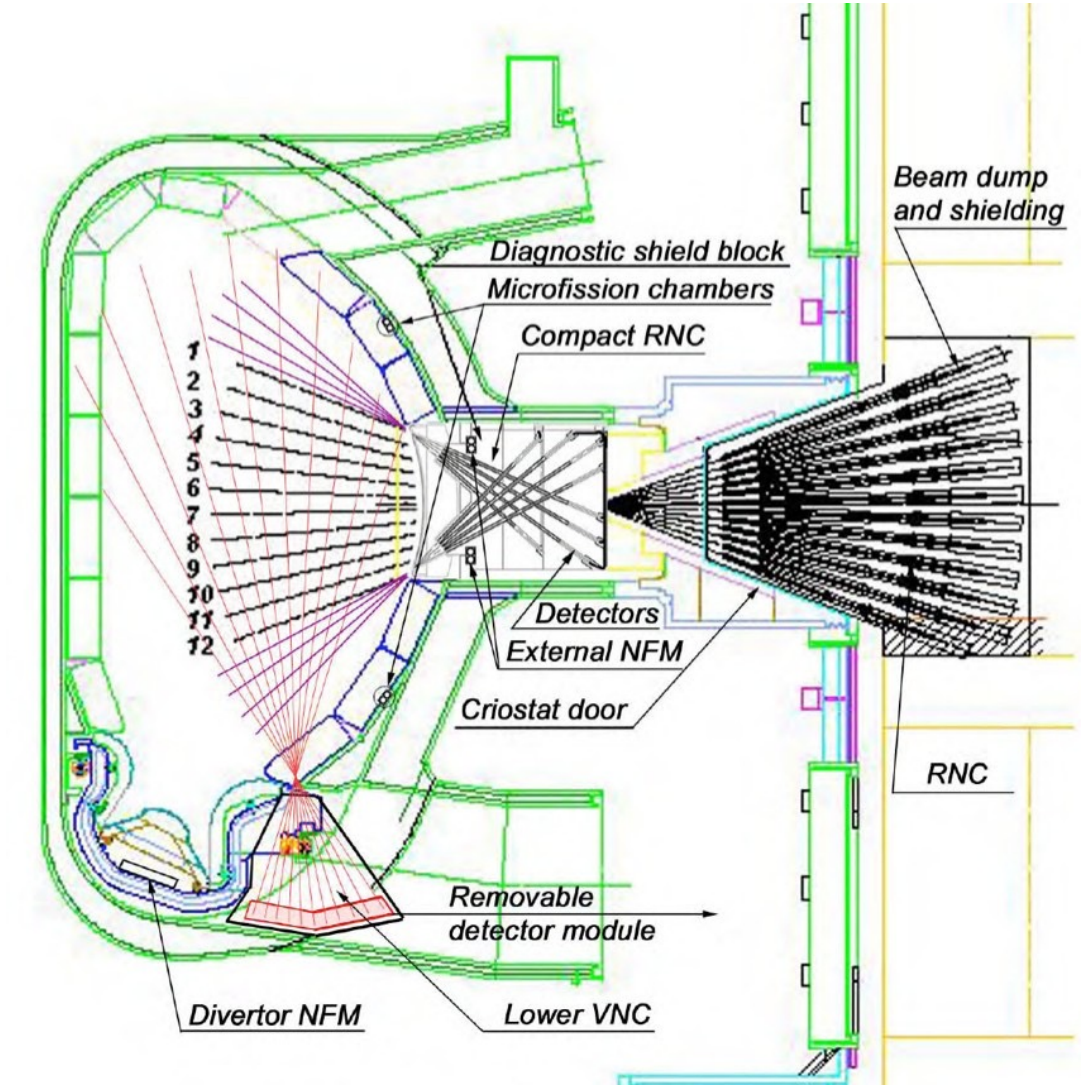

- **Horizontal system**
- **Lower vertical systems from divertor**
- **Other neutron diagnostics:**
  - Micro-fission chambers
  - Neutron spectrometers
- **In-situ calibration system**

Krasilnikov et al. NF 2005

Incident neutrons and fast particles produce radiation defects changing properties of materials

- **Mechanical properties**
  - Radiative swelling, relaxation and creep, amorphization of crystalline materials, transmutation, irradiation hardening and embrittlement
- **Electrical properties**
  - Radiation-induced electromagnetic forces, electrical degradation, and conductivity
- **Optical properties**
  - Radioluminescence, induced absorption
  - Effects on polymers for optical transmission
  - (Coating of mirror and other optical components)

Neutron and fast-particles are expected to significantly affect the performance of ITER diagnostics

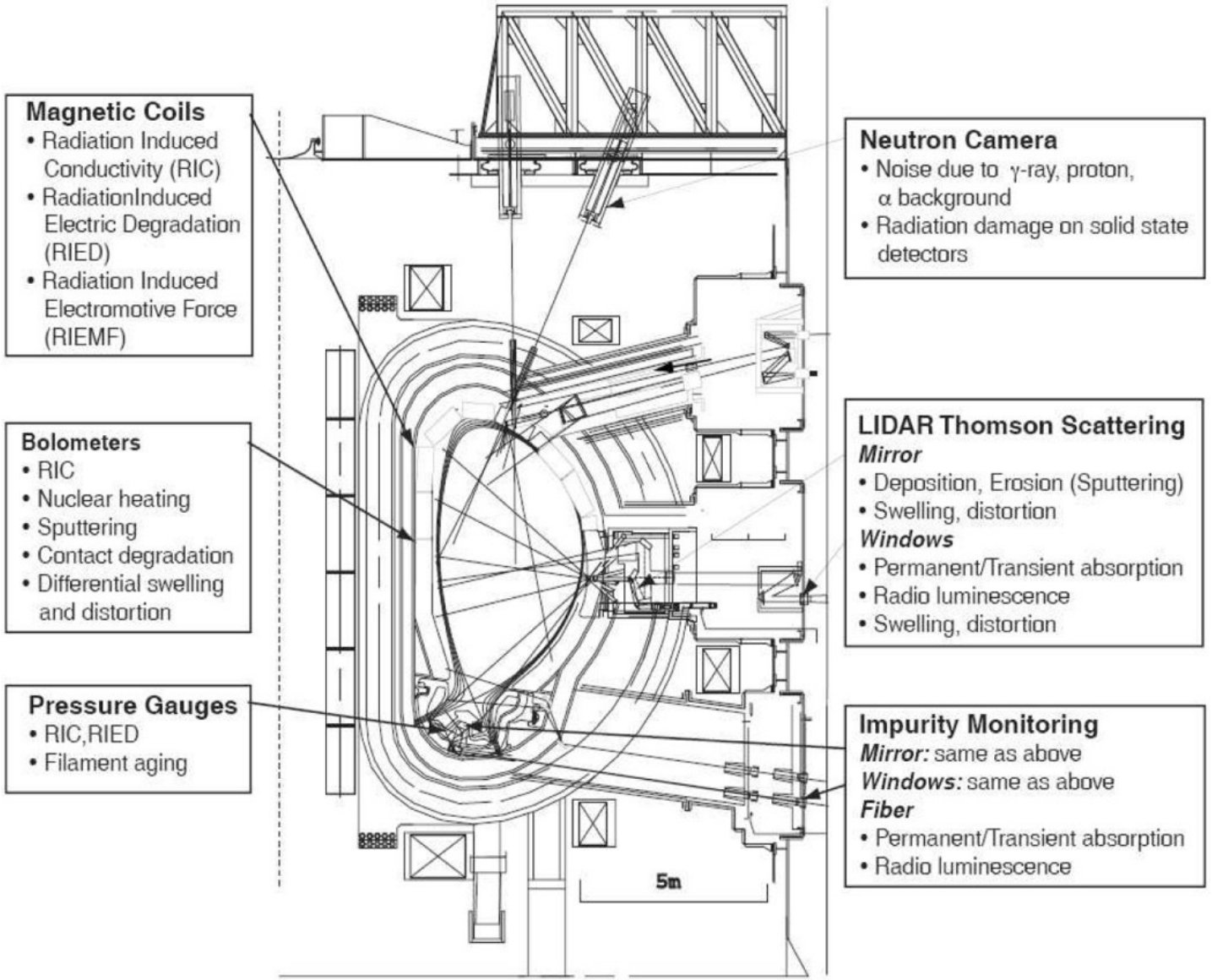

Hierarchy and staging of ITER diagnostics for detachment control

Group	Measurement	Role	Diagnostic	Available
Plasma position, shape	Divertor leg location	BC	55.A0	FP
	Gaps and δr_{sep}	BC	55.A0	FP
	Total SOL current (shunt)	?	55.AM	PFPO1
Radiated power (profile)	$P_{rad,div}$	BC	55.D1	PFPO1
	$P_{rad,x\text{-}point}$	AC	55.D1	PFPO1
Impurity species monitoring	Ne, Ar, Kr influx	BC	55.E2	FP
	Divertor impurity and D,T influx	BC	55.EG	FP
Divertor parameters	Gas composition	BC	55.G4	PFPO1
	Gas pressure	BC	55.G3	FP
	Surface temperature	MP	55.G1/G6/GA	FP
	Ionization front	BC	55.E4	PFPO1
Target plasma parameters	N_e, T_e	AC	55.G7	PFPO1
Divertor heat load	Power load, $T_{surface}$	AC	55.G1/G6/GA	FP
Divertor helium density	n_{He}	BC	55.G4	PFPO1

Ravensbergen, Piits ITPA-DSOL Jan 2022

55.EG VUV spectrometer

- **Measure impurity ion radiation (Be, W, C, O, Ne, N, Ar)**
- **Lyman-alpha (particularly relevant for detaching plasmas)**
- **10 ms time resolution**
- **Line-integrated measurement**

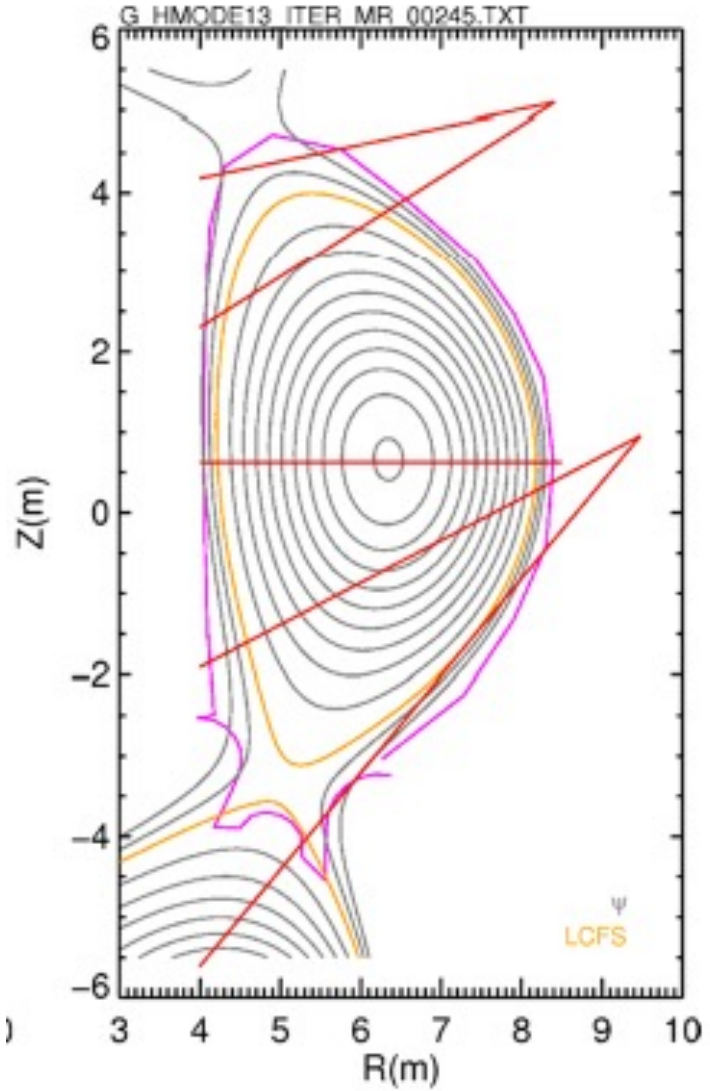

Ravensbergen, Piits ITPA-DSOL Jan 2022

Diagnostic output requires data management, including data processing and backup

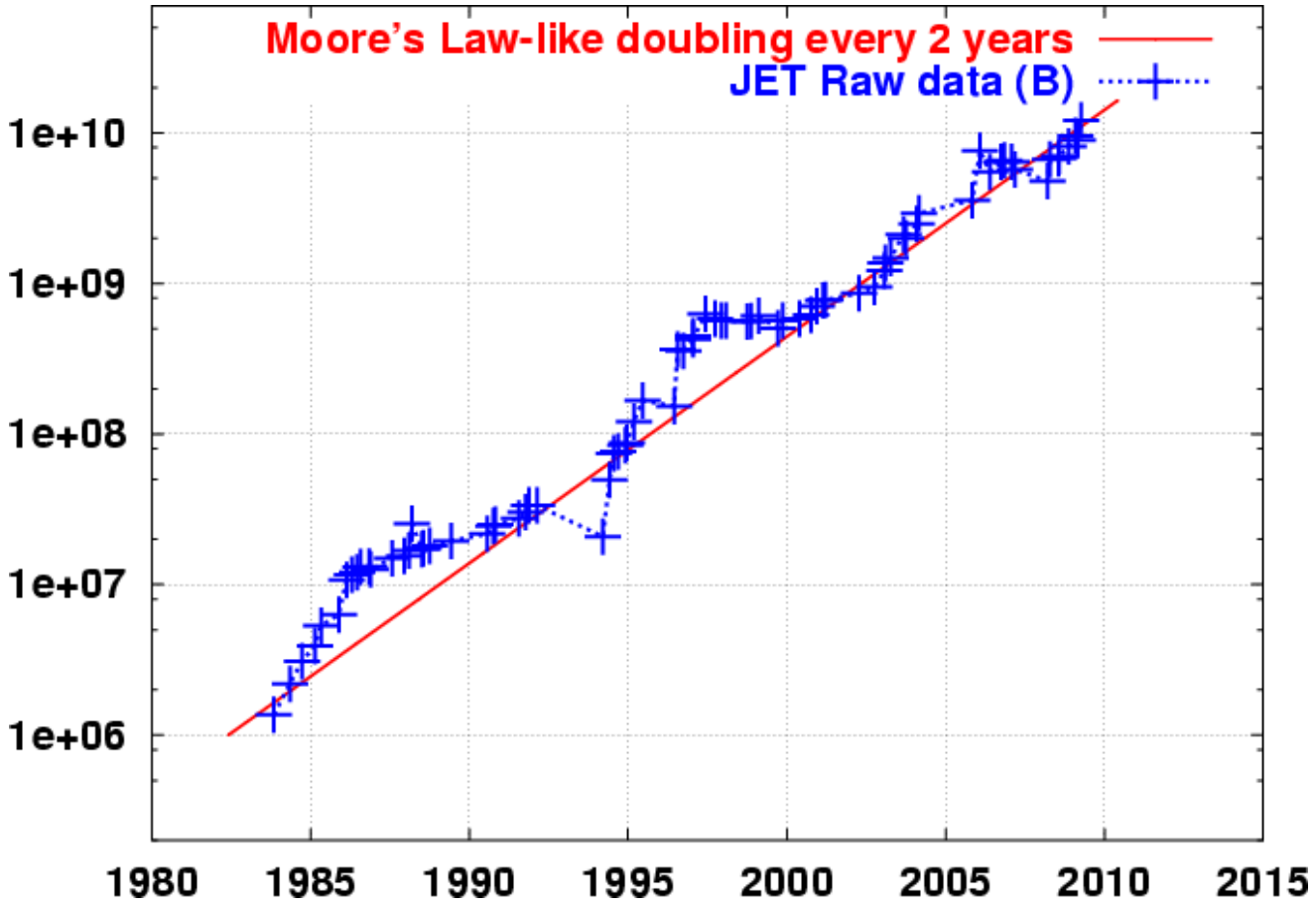

- Raw data output of JET roughly doubles every two years
- 2019: 55 GB per pulse, 1 TB per day
- Daily raw data output of ITER expected to be petabytes (10^{15} bytes)

Summary

- **Diagnostics are the primary tool to probe and understand fusion plasmas**

⇒ **In future reactors, they become the sensor to control plasma position, wall load and burn**

- **Diagnostics are as expensive as the tokamak facility ⇒ on JET there are currently over 100 diagnostic systems (measurements → analysis → interpretation)**
- **Instruments may be group into magnetic, passive and active radiation and particle diagnostics**
- **Diagnostics / measurement are complex and span the entire range of the electromagnetic radiation:** radio waves to γ rays

Presemo quiz #2

https://presemo.aalto.fi/fet/

Backup material

Wound-back Rogowski coils are used to measure the plasma current

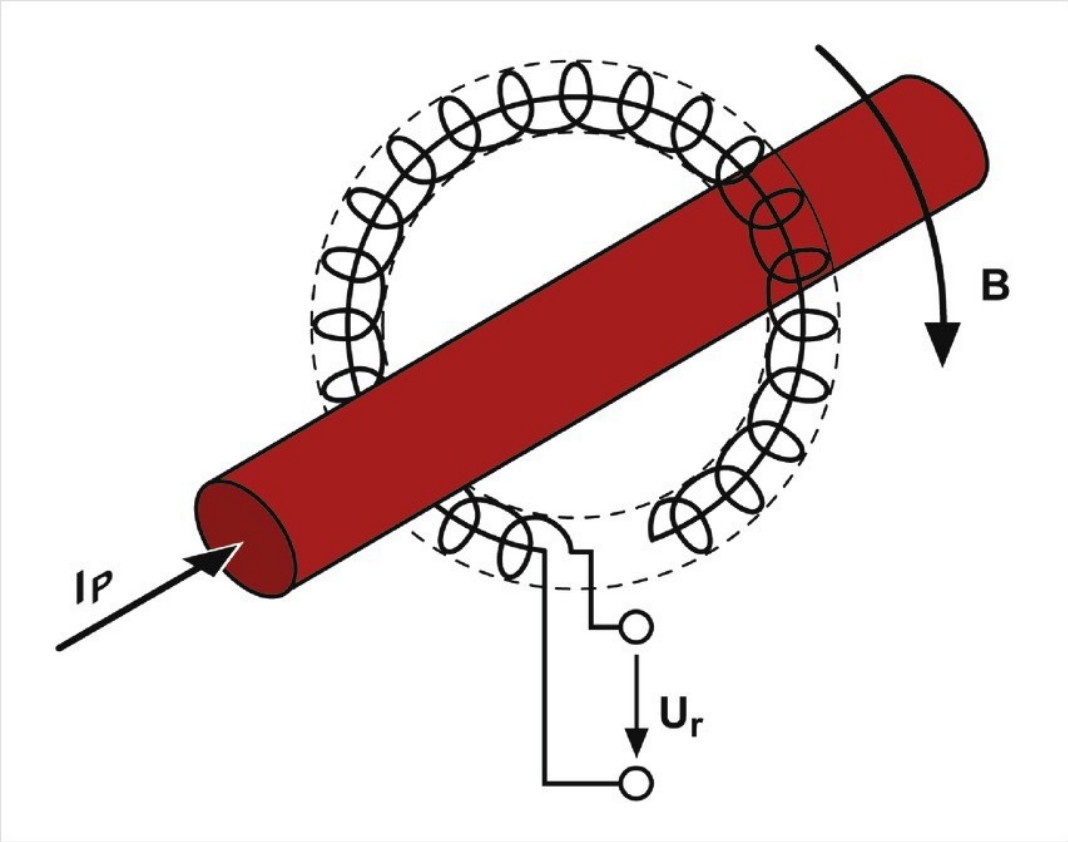

- **Set of discrete flux loops with their axis tangent to enclosed contour also serve as Rogowski coil**

- **Ampere's law:**

$$I = \int \vec{j} \cdot d\vec{A} = \frac{1}{\mu_0} \oint B_\varphi \, dl$$

- **Flux in Rogowski coil:**

$$\phi = n \int_S dS \oint_l B_\varphi dl = nS\mu_0 I$$

- l – length of coils
  S – coil surface area,
  n – # of turns per meter

- **Change in flux → voltage U**

$$U = -\frac{d\phi}{dt} \rightarrow I_P = \frac{2\pi a}{nS\mu_0} \int U dt$$

- a – minor radius

Diamagnetic loops are used to measure the toroidal flux ⇒ $\langle B_\Phi \rangle$ ⇒ plasma kinetic energy

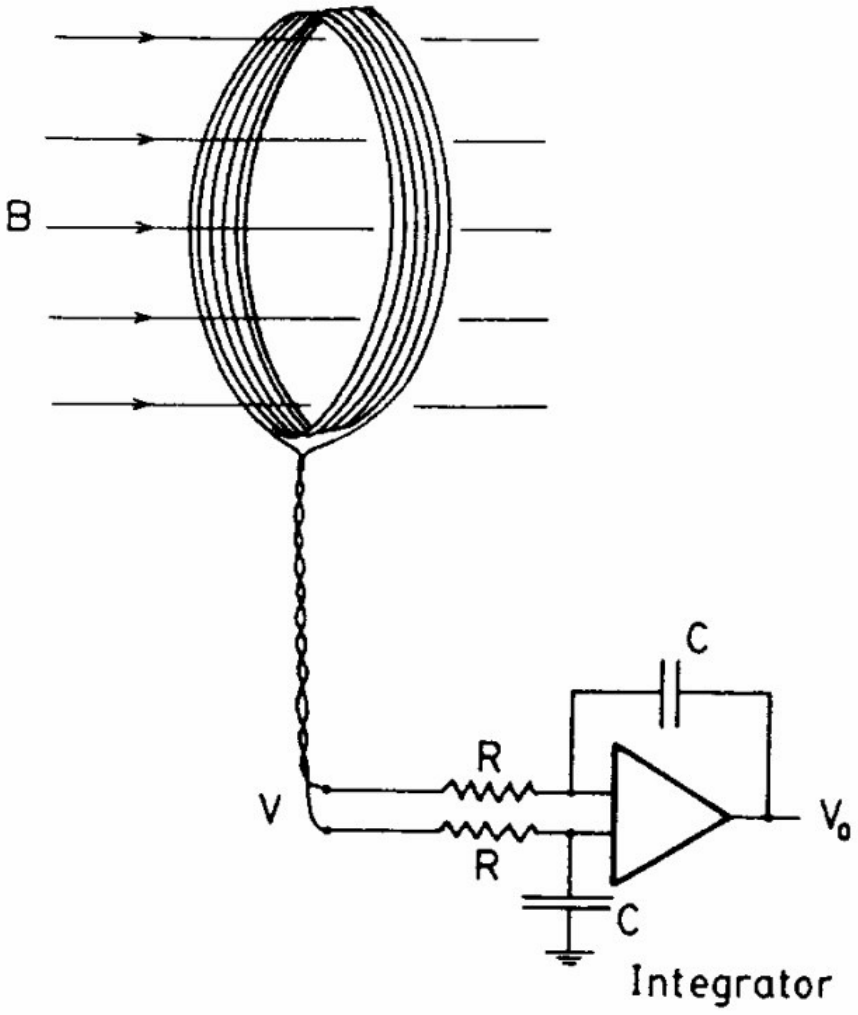

- **Poloidal beta:**

$$\beta_\theta = \int \vec{j} \cdot d\vec{A} = \frac{1}{\mu_0} \oint B_\varphi \, dl$$

- **Flux in Rogowski coil (**for $\beta \ll 1$**):**

$$\beta_\theta = \frac{2\mu_0 \langle p \rangle}{B_{\theta,a}^2} \approx 1 + \frac{2B_{\theta,a}\left(B_{\theta,a} - \langle B_\theta \rangle\right)}{B_{\theta,a}^2}$$

- **Energy confinement time τ_E:**

$$\tau_E = \frac{W}{I_P^2 R_P} = \frac{3}{8}\mu_0 \beta_\theta \left(\frac{R}{R_P}\right)$$

Single wire encircling torus in the toroidal direction measures the toroidal loop voltage, V_ϕ, induced by the transformer

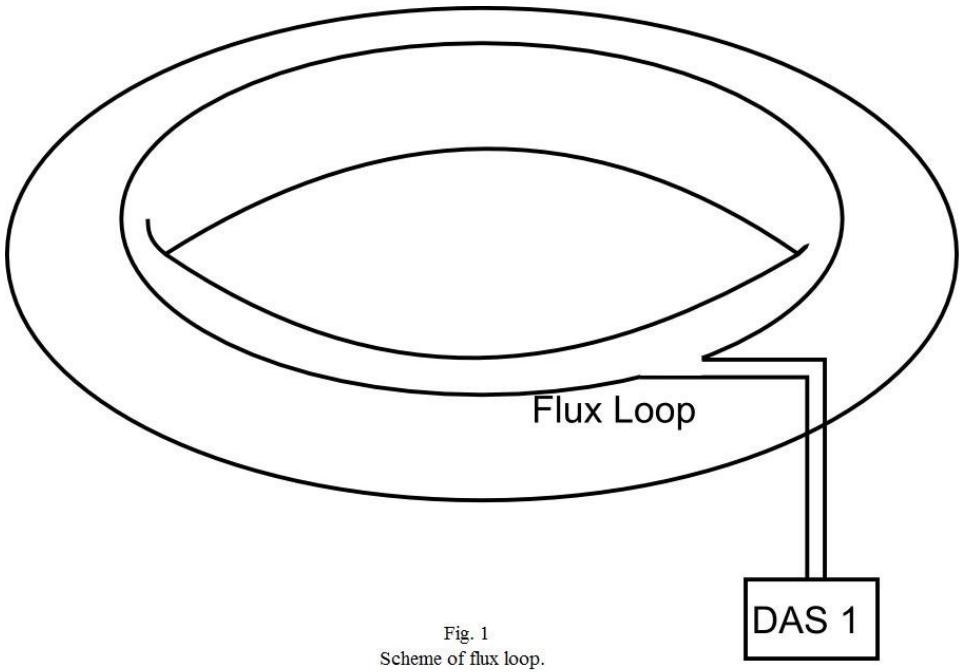

Fig. 1
Scheme of flux loop.

- **For $\frac{dI_P}{dt} = 0$:**
- **Plasma resistivity:** $R_P = \frac{V_\phi}{I_P}$
- **Ohmic heating power:**
  $P_{ohm} = \int_V \left(j_\phi^2/\sigma\right) dV = I_P^2 R_P$
- **Mean plasma conductivity:**
  $$\bar{\sigma} = \frac{2\pi R}{\pi a^2} \frac{1}{R_P}$$
- **Electron temperature:**
  $$\bar{\sigma} \propto \frac{T_e^{3/2}}{Z}$$
- R – major radius, a – minor radius

Magnetic coils installed at the wall are used to determine the equilibrium and plasma stored energy

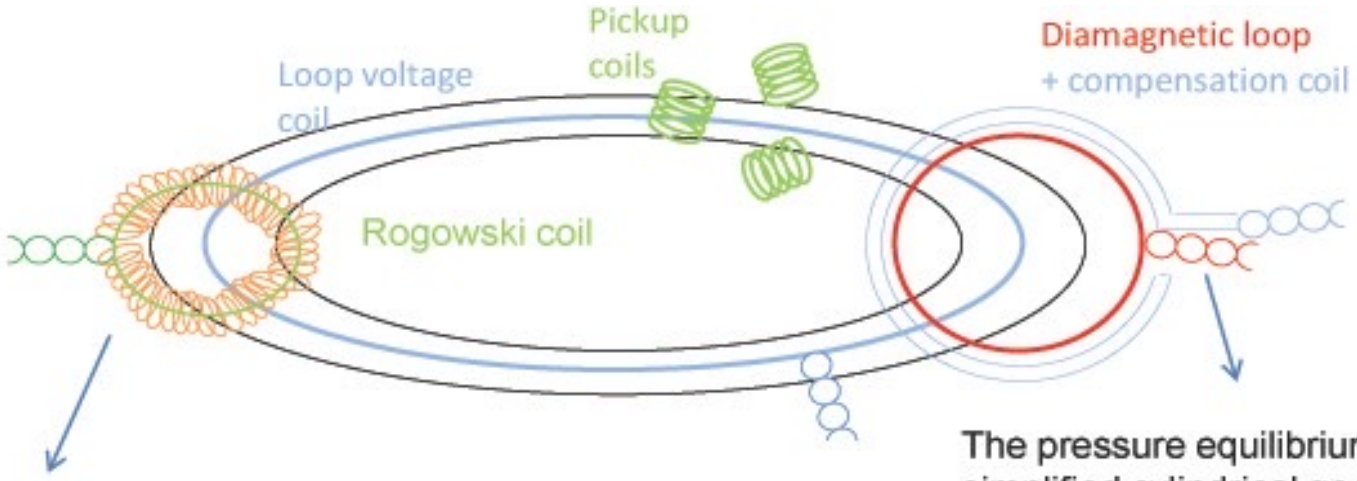

Ampères law provides the toroidal plasma current

$$I = \int \vec{j} \cdot d\vec{A} = \frac{1}{\mu_0} \oint B_\theta dl$$

$$\Rightarrow I_{plasma} = \frac{2\pi a}{NA\mu_0} \int U\, dt$$

The pressure equilibrium provides in simplified cylindrical geometry:

$$\nabla p = \vec{j} \times \vec{B}$$

$$\mu_0 \frac{dp}{dr} + \frac{d}{dr}\left(\frac{B_\phi^2}{2}\right) + \frac{B_\theta}{r}\frac{d}{dr}(rB_\theta) = 0$$

$$\Delta\Phi = -\frac{2\pi\mu_0}{B_0}\int_0^a pr\,dr + \frac{\mu_0^2 I_z^2(a)}{8\pi B_0} + \frac{\pi\mu_0}{B_0}\int_0^a j_z B_\phi r^2 dr$$

$$= -\frac{\mu_0 W}{3\pi R B_0} + \frac{\mu_0^2 I_{plasma}^2}{8\pi B_0} + \frac{\pi\mu_0 I_{vac}}{R}\int_0^a j_z r^3 dr$$

$$p_{plasma} = k(n_e T_e + n_i T_i) \Rightarrow W_{\text{kinetic}} = \int k(n_e T_e(\vec{r}) + n_i T_i(\vec{r}))\, d^3 r$$

Using the magnetic probe data, a 2-D magnetic equilibrium can be reconstructed

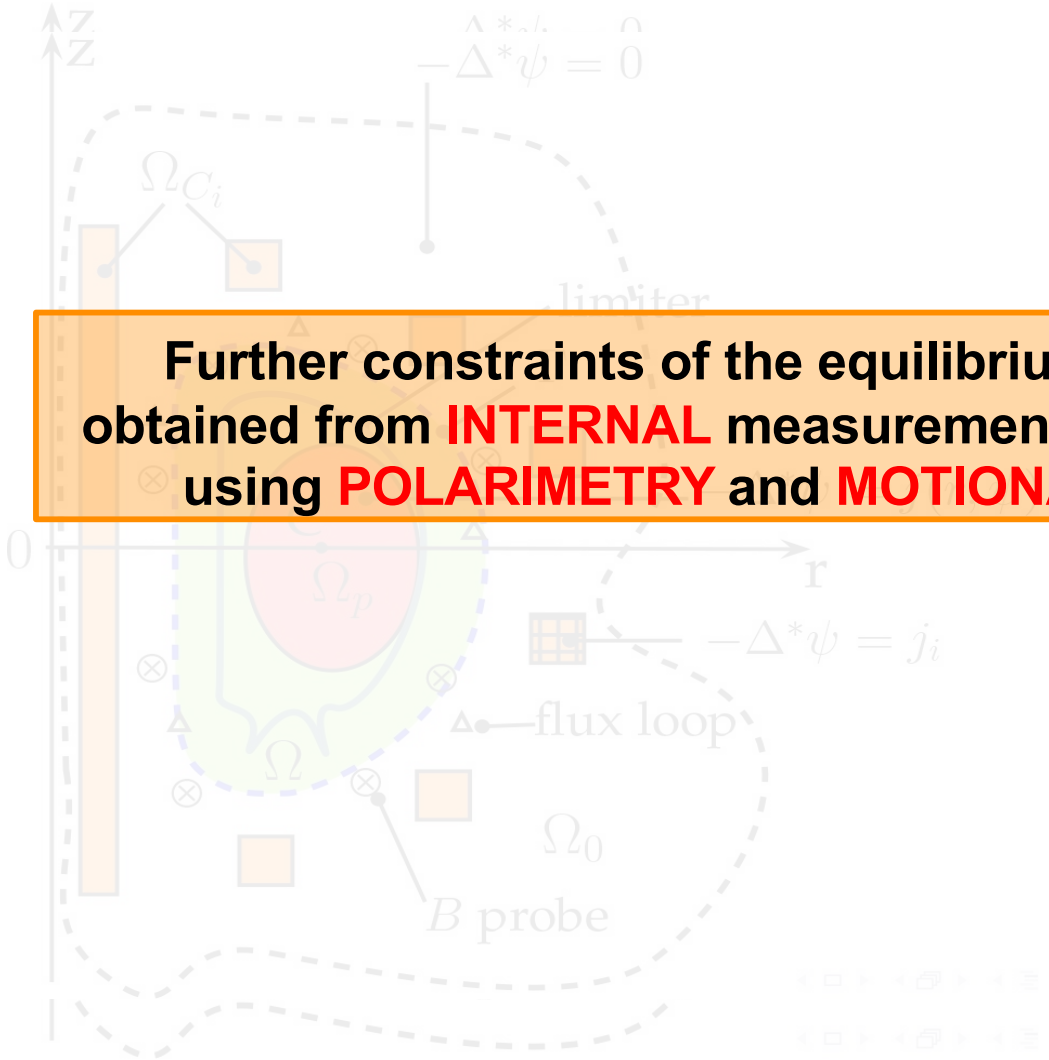

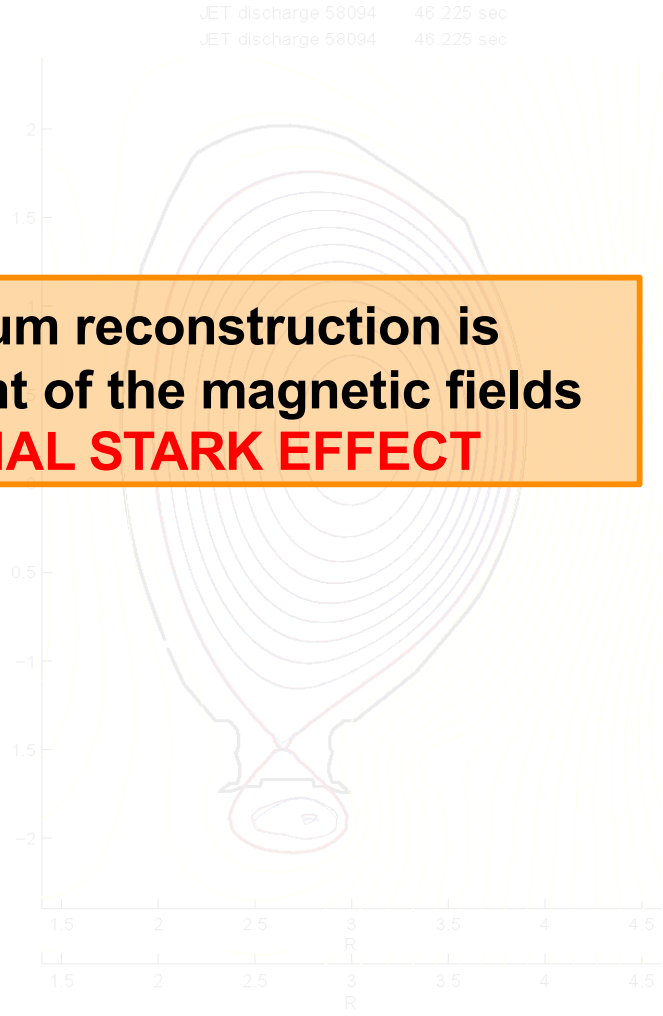

Further constraints of the equilibrium reconstruction is obtained from INTERNAL measurement of the magnetic fields using POLARIMETRY and MOTIONAL STARK EFFECT

Surface temperatures and heat flux densities are measured with infra-red cameras ⇒ $P_{divertor\ target}$

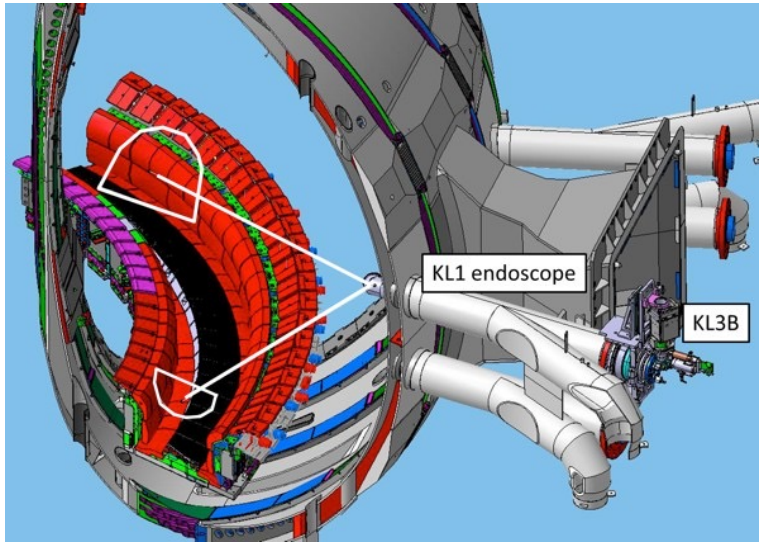

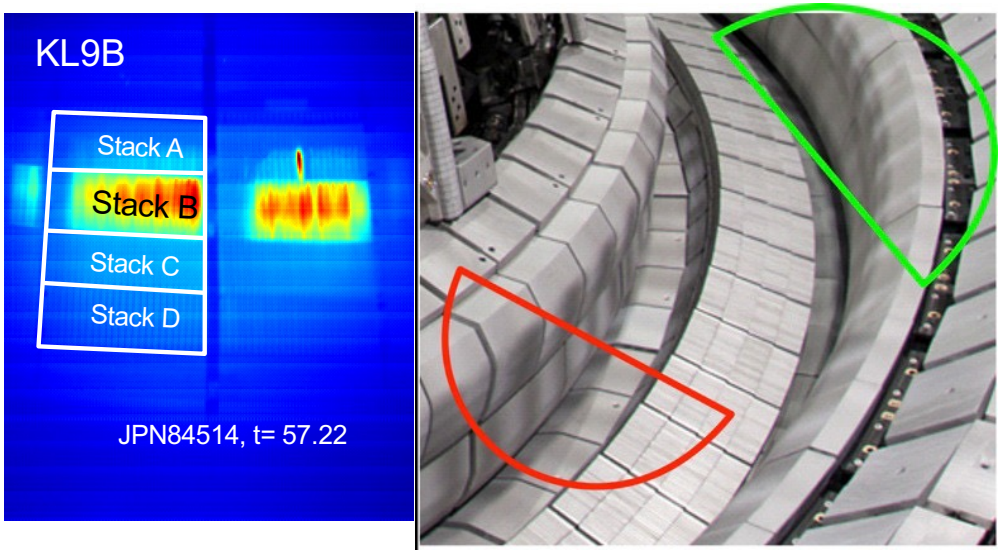

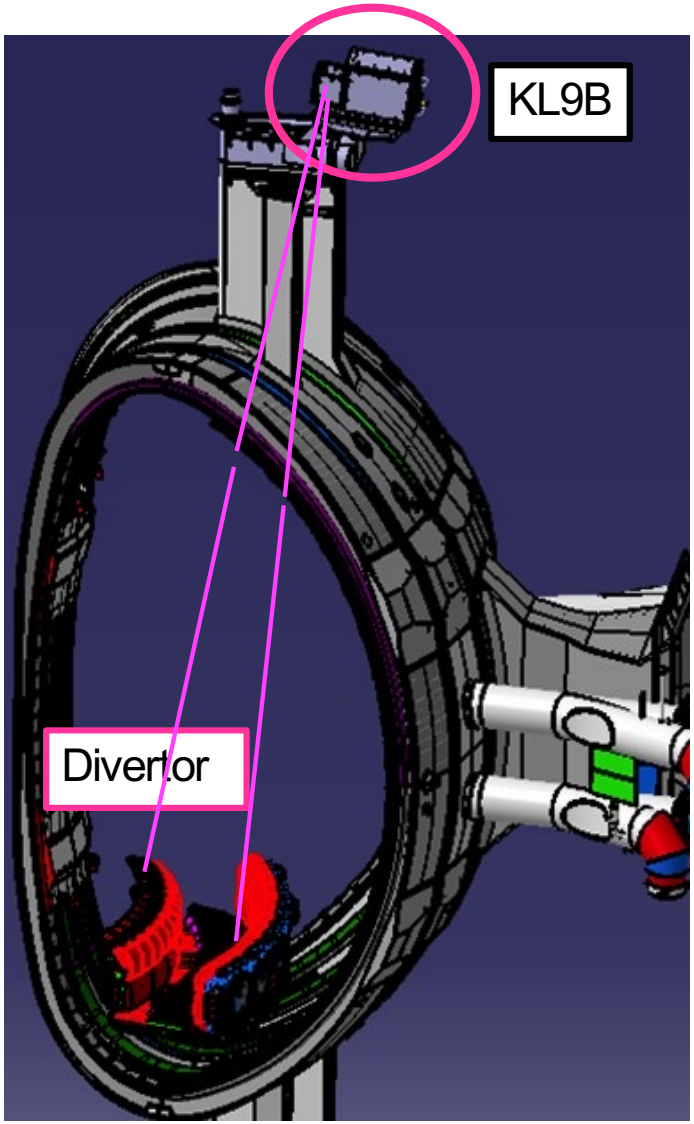

Balboa et al. JET 2013

At JET, spectroscopy is used to measure the (line-averaged) electron density in the divertor

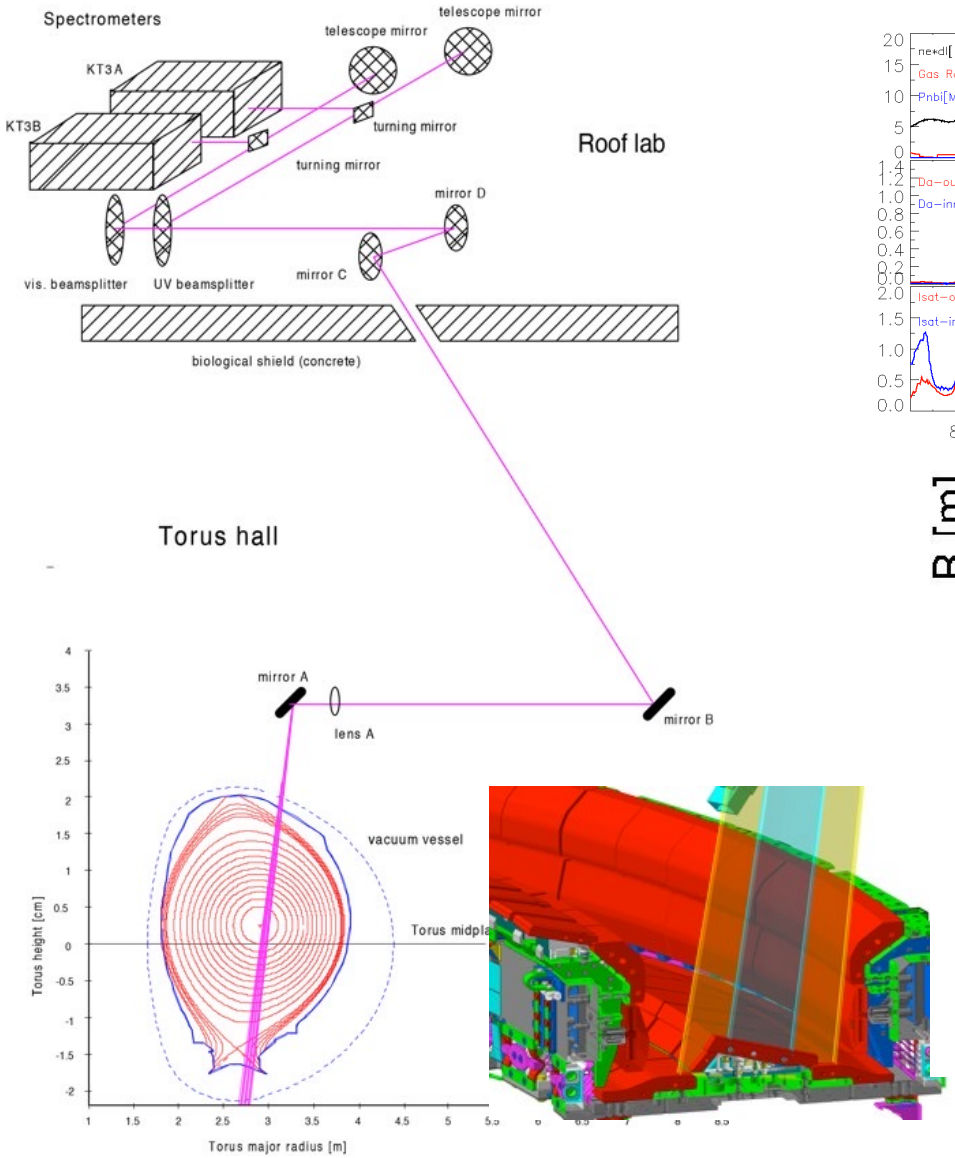

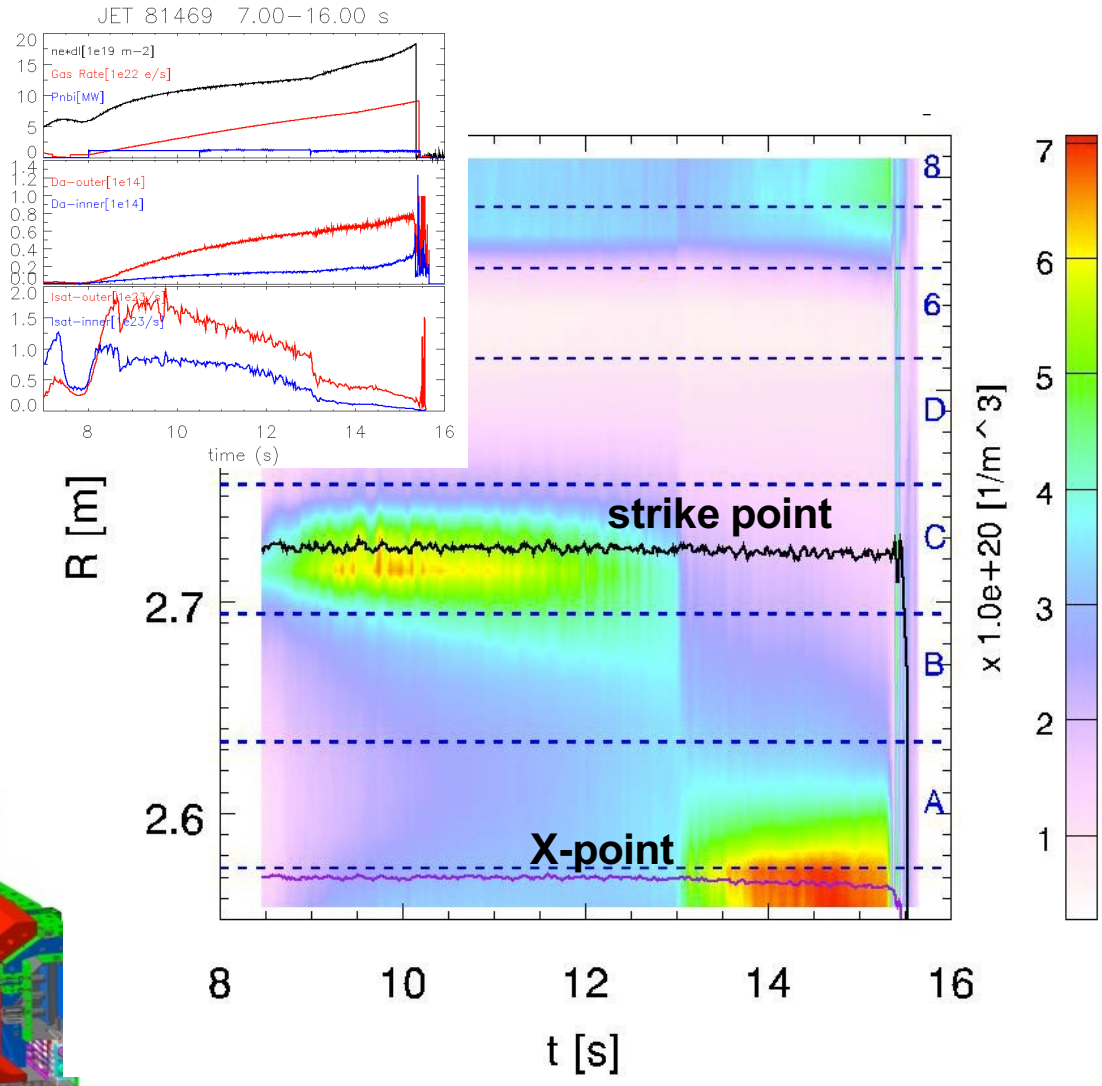

Meigs et al. JNM 2013

Utilizing polarized light, the magnetic field can be deduced (Faraday rotation, Cotton-Mouton effect)

Polarimeter

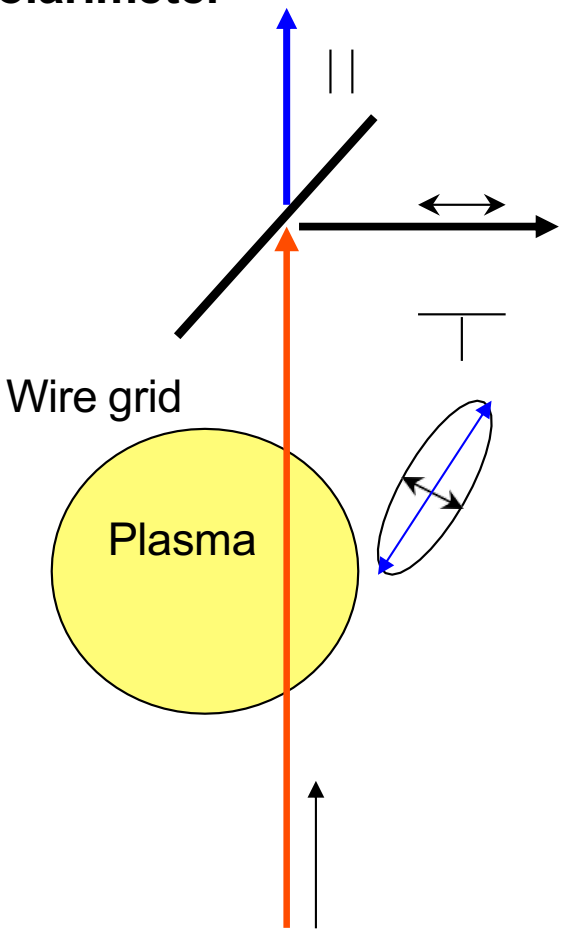

Linear polarization

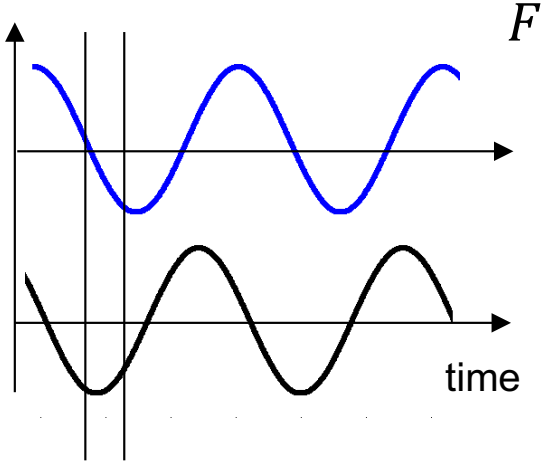

Faraday rotation angle

$$F = \frac{\varphi}{2\pi} = C\,\lambda \int_{z1}^{z2} n(z)dz$$

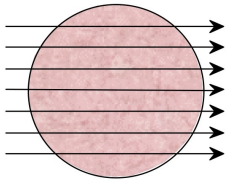

- **Rotated elliptical polarization due to anisotropy and optical activity of the medium ⇒ phase shift between two orthogonal polarization components**

Photon scattering on electrons leads to broadening and wavelength shift wrt. the original laser spectrum

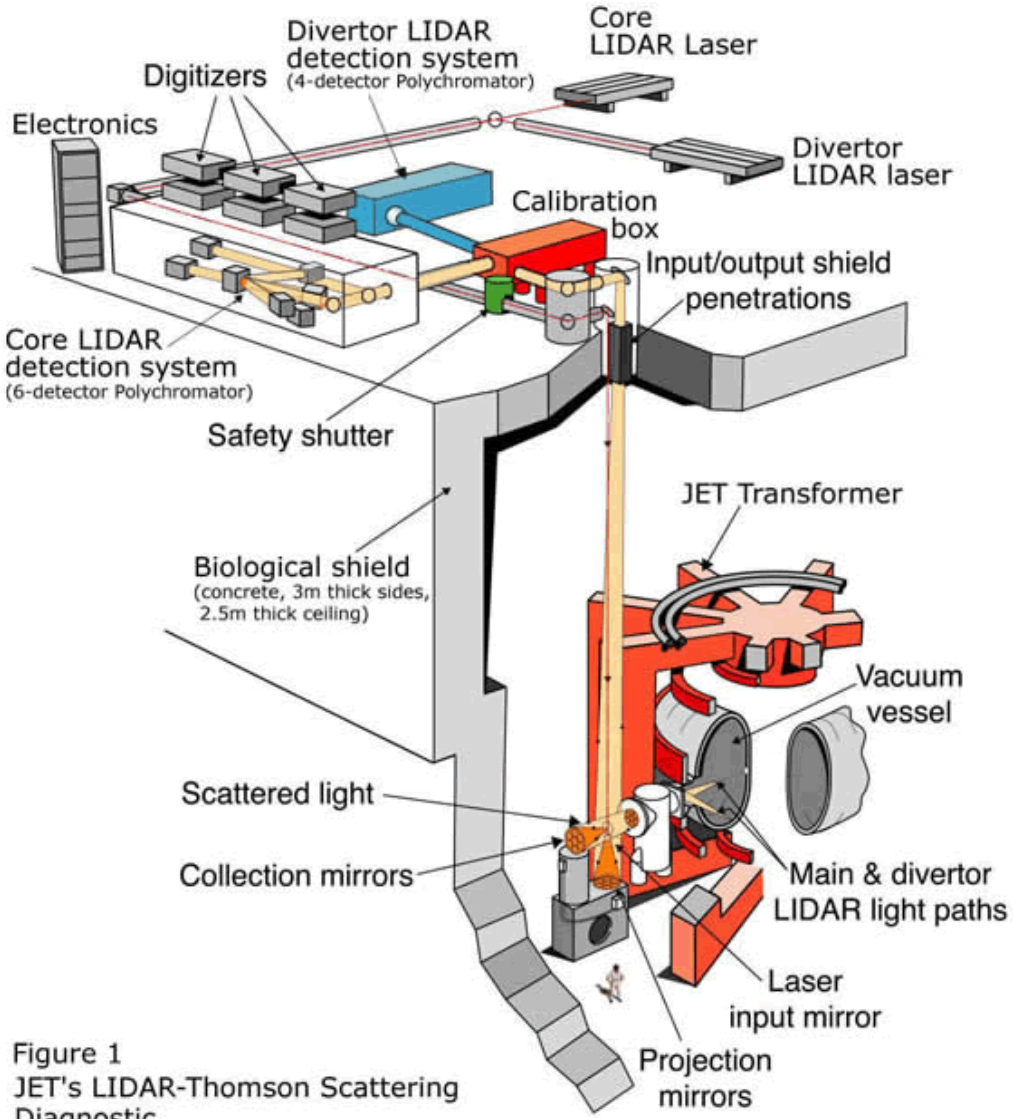

Figure 1
JET's LIDAR-Thomson Scattering Diagnostic

- **Electrons oscillate in light's electric field ⇒ emit photon of same wavelength**

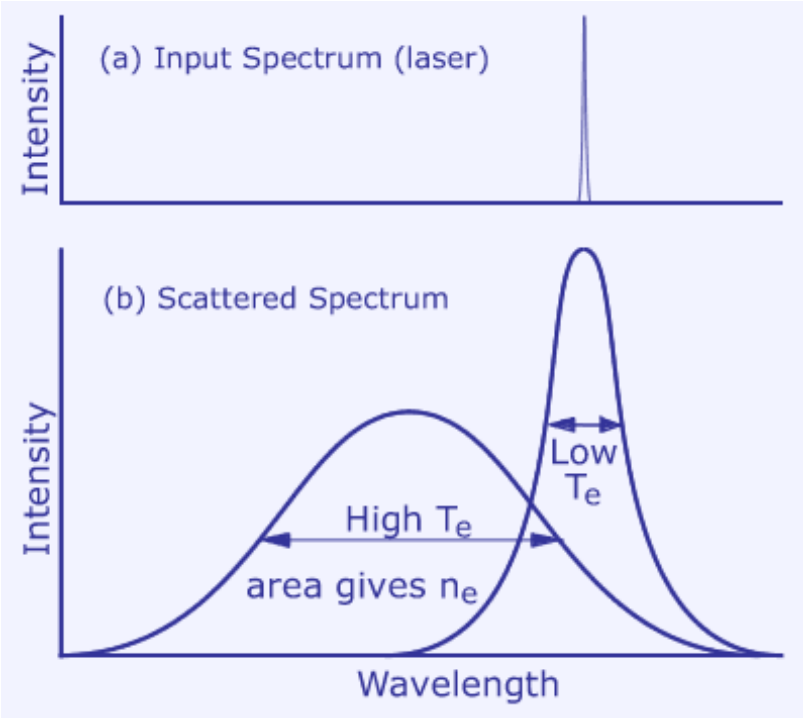

Imaging a laser beam path and spectrally resolving the scattered light yields the electron temperature and density

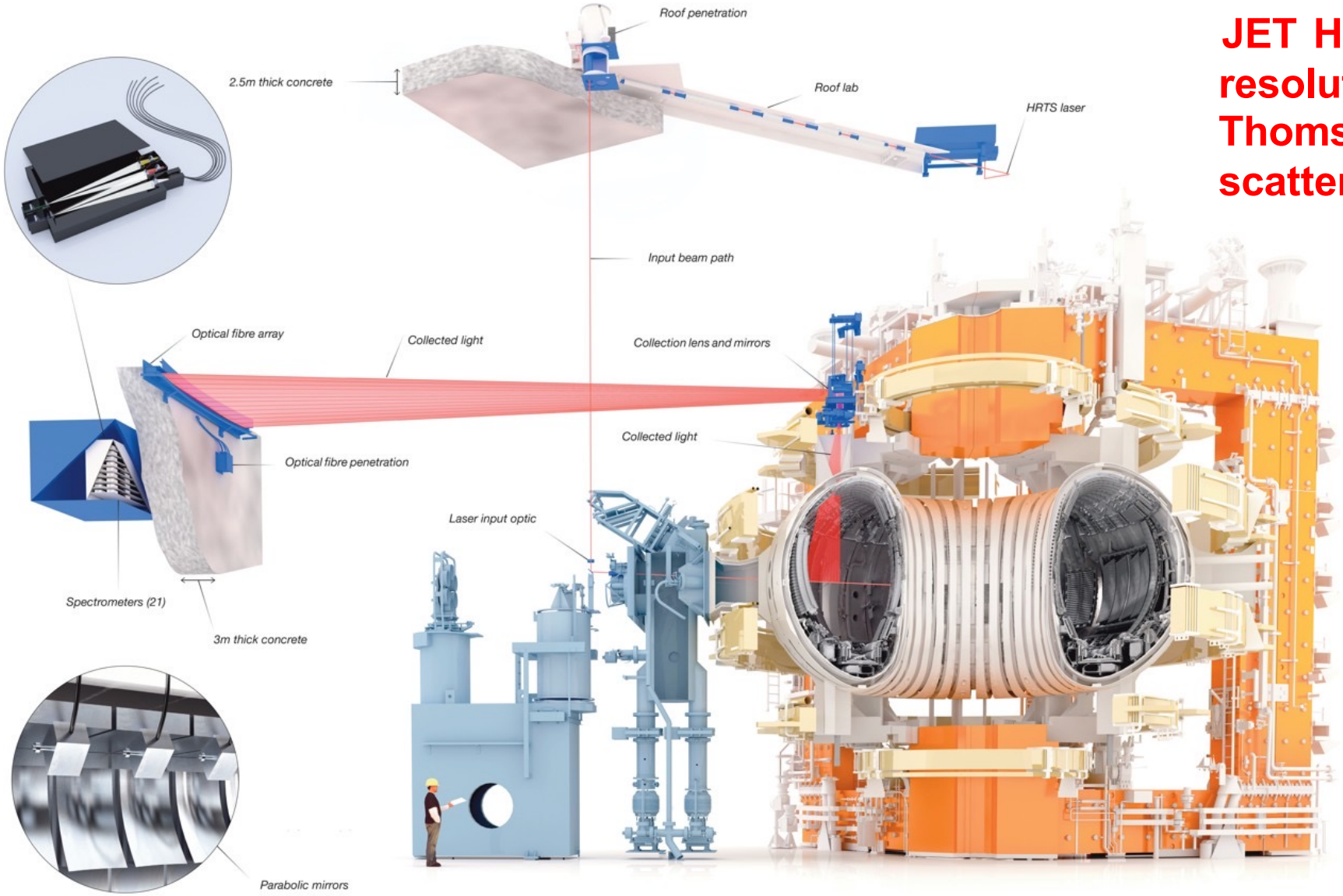

JET High-resolution Thomson scattering

The Light Detection and Ranging (LIDAR) system is a short-pulse system for electron density and temperature

- **Radar measurement:** pulse delay times are translated into position
- **High-power Ruby or NeYAG laser (10 GW during 300 ps), at 20 Hz**

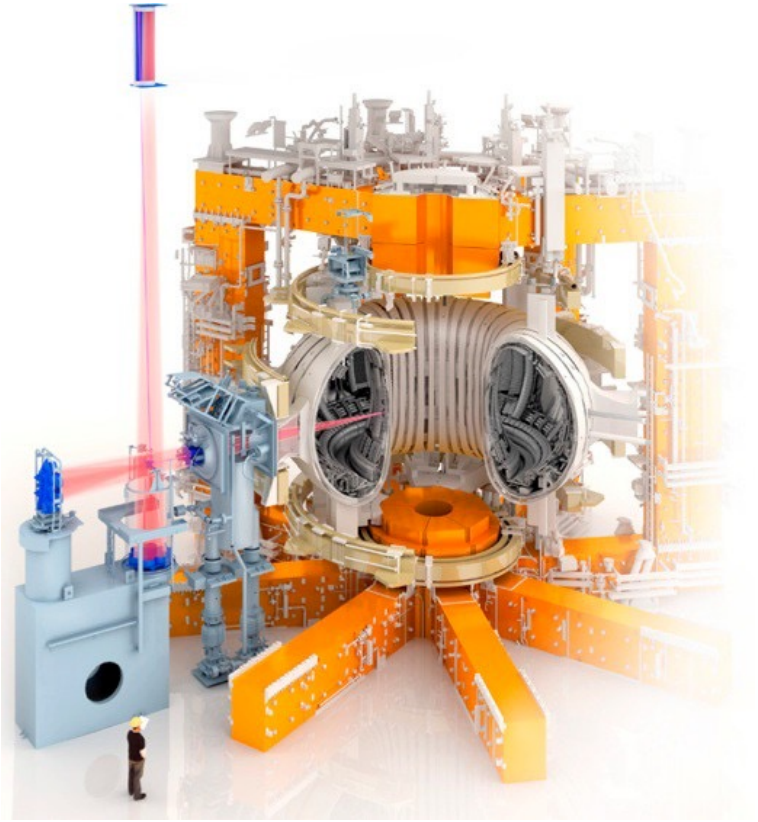

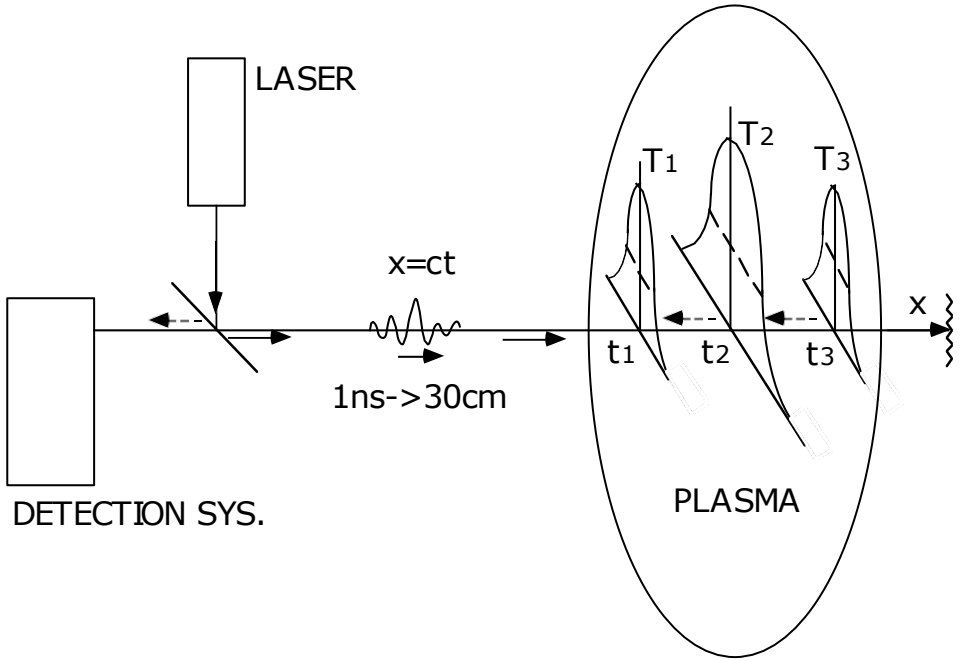

Microwave Doppler reflectometer systems measure density turbulence and the radial electric field

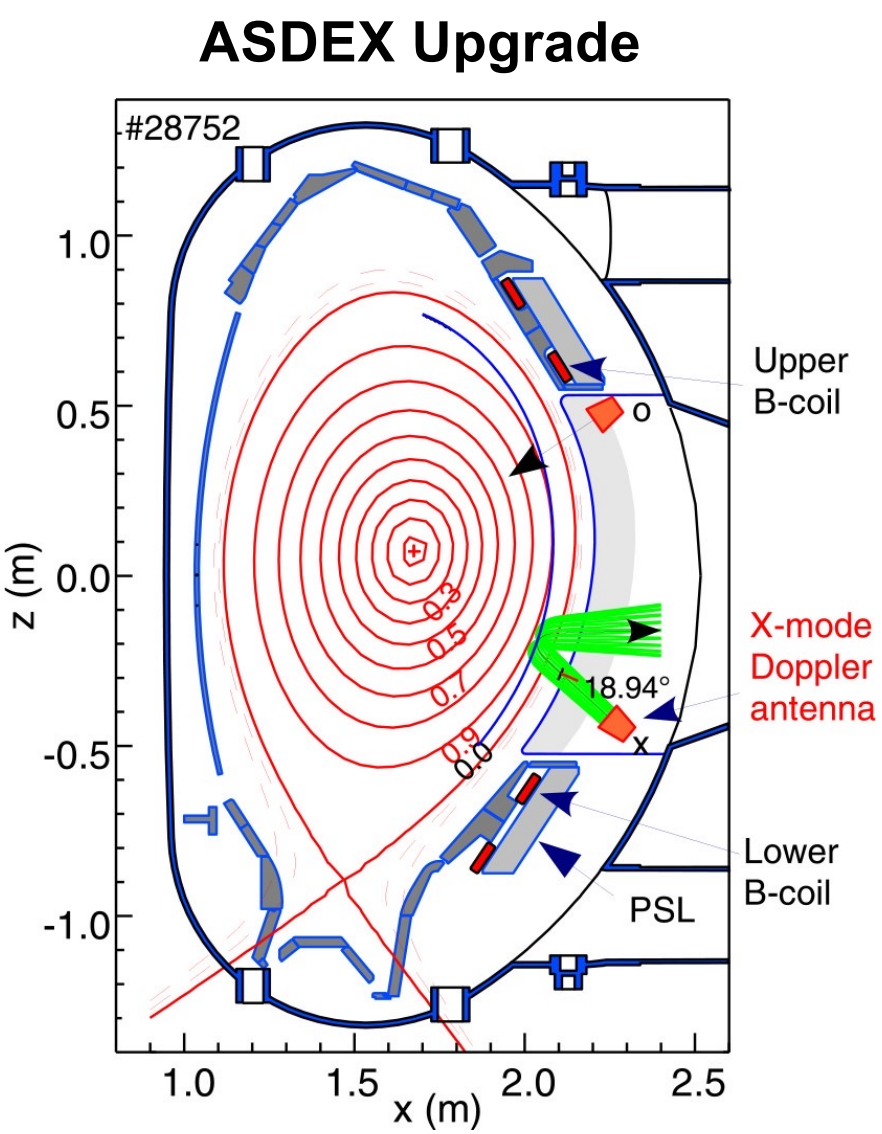

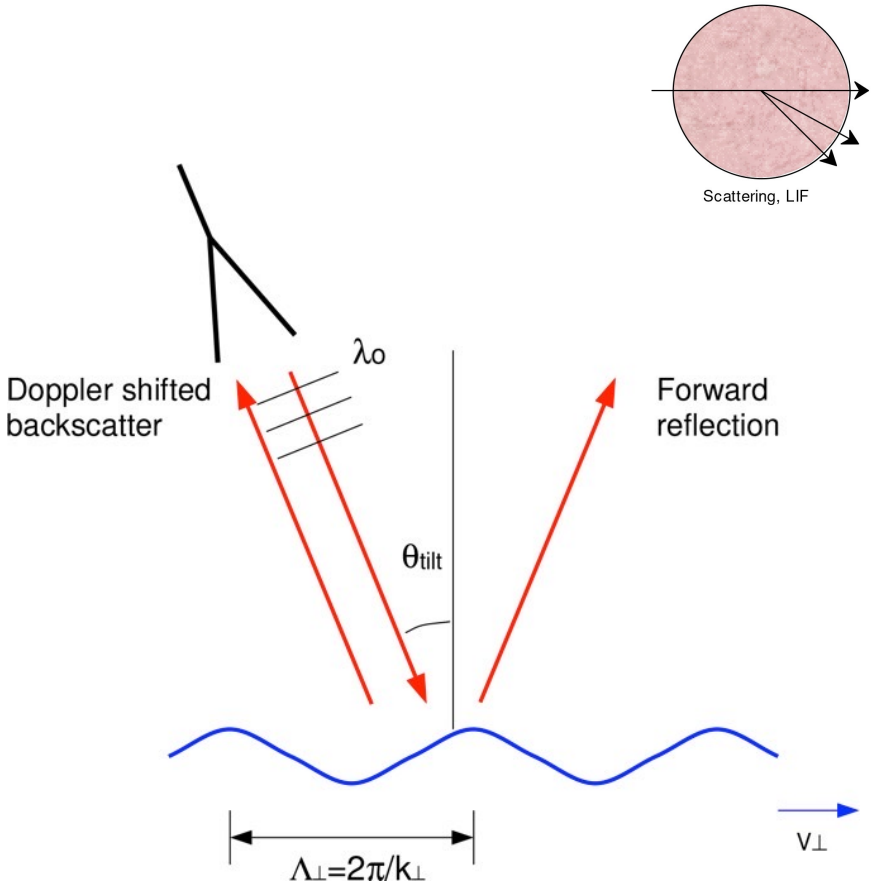

$$f_D = u_\perp \frac{2}{\lambda_0} \sin(\delta_{tilt})$$

Measuring the Zeeman-splitting components of line emission yields the internal magnetic field

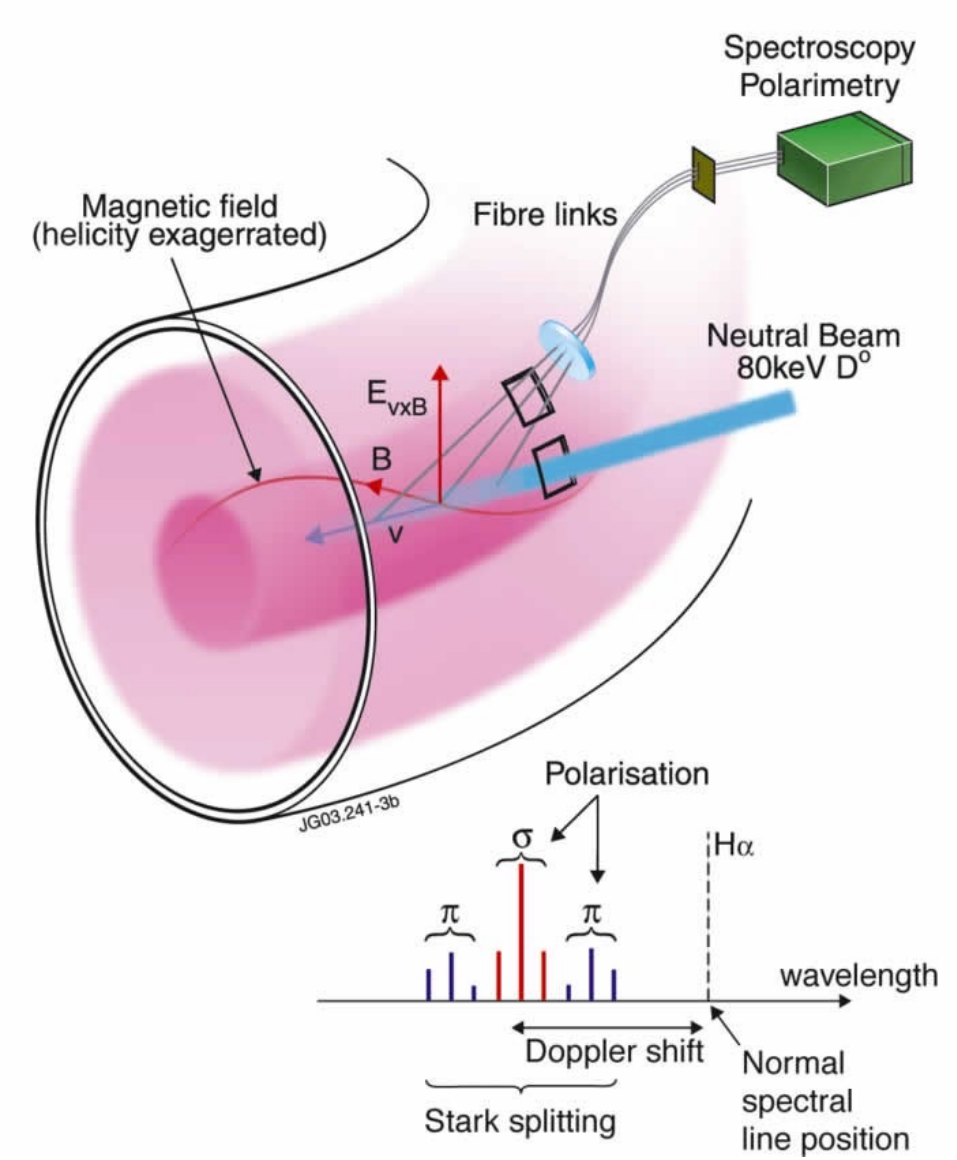

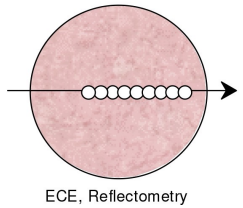

- **Motional Stark Effect (MSE) on (Doppler-shifted) Balmer-α line emission**
- **Polarization of light in linearized (σ) and circular (π) components + Doppler shift:**

$$tan(\gamma) = \frac{A_1 B_t + A_2 E_r}{A_3 B_p}$$

At ASDEX Upgrade, lithium and helium beam emission spectroscopy is used for ne and CXRS measurements

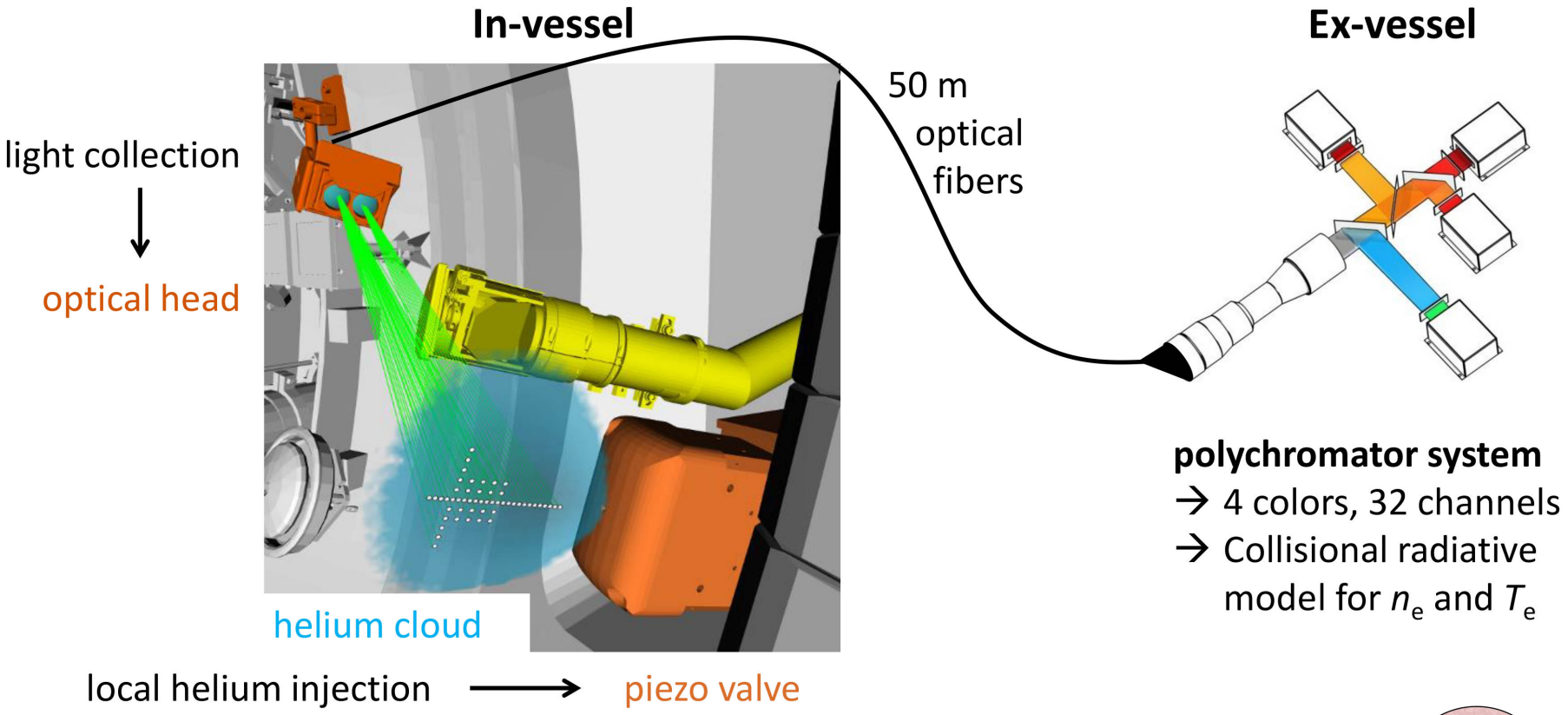

Griener et al. Review Scientific Instruments 2017

Using multiple diagnostics measuring the same plasma parameter yield highly resolved profiles

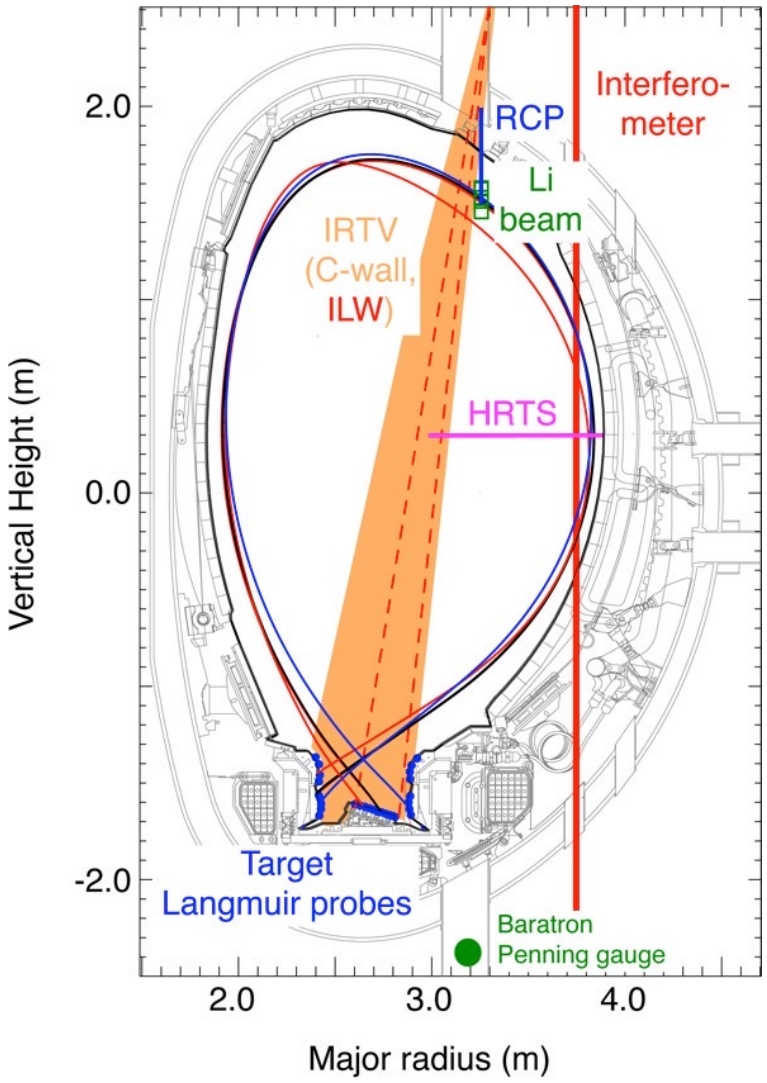

- **Region just inside separatrix and SOL are of particular interest ⇒ power exhaust**

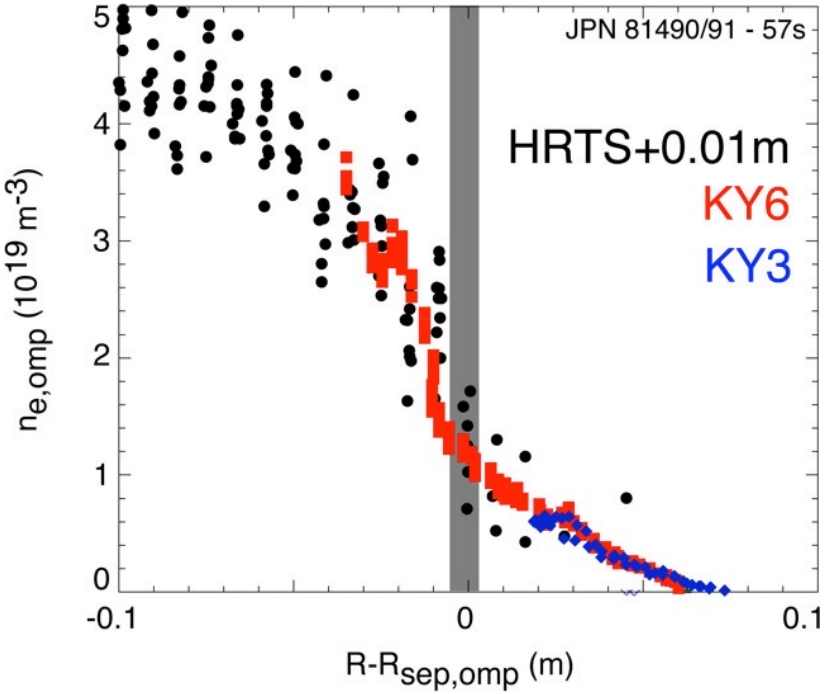

Loss of reciprocating Langmuir probe body in JET in October 2013 caused a two-month shutdown

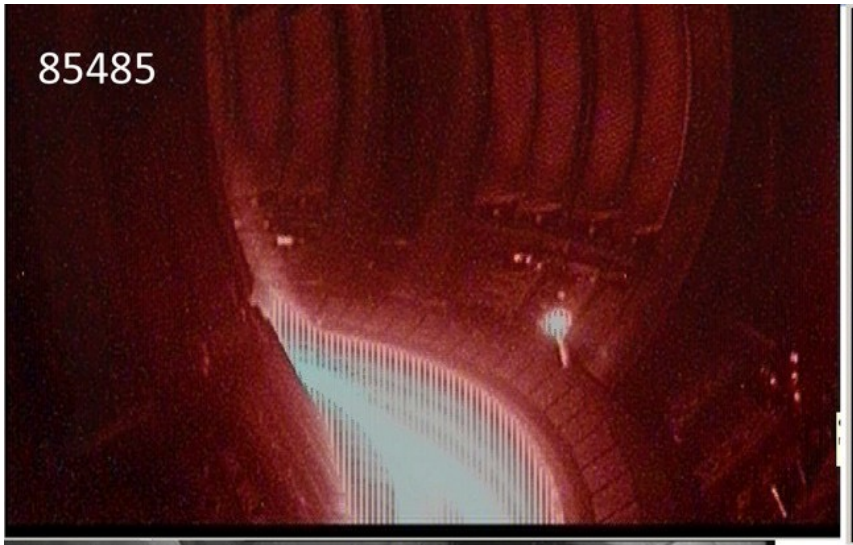

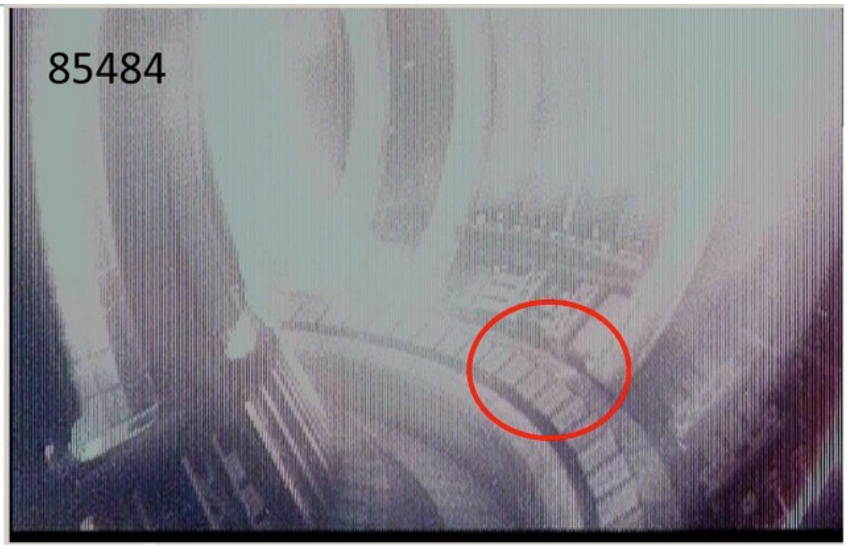

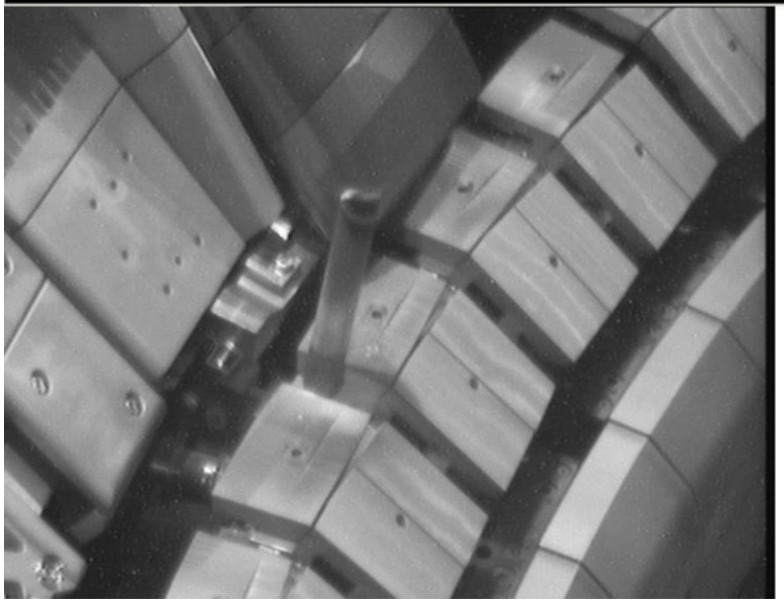

- Boron nitride probe body broke and fell during a disruption in B13-15
- Cause is still under investigation and a mystery:
  - no direct halo or EM force possible
  - no thermal stress fracture possible
  - mechanical shock via main tube?
- Since BN used for probes this is the first such event in ~ 20 years
  - disruptions different with ILW

Matthews et al. JET TFE1E2 2013

Requirements for divertor power / detachment control in ITER

- **Divertor specifically designed for high dissipation:**
  - Actively cooled
  - Easy to detach in early phases (PFPO-1, even without impurities)
- **Heat exhaust control only critical in full performance operation (Late PFPO-2) but:**
  - Controllers need to be designed and implemented
  - Diagnostic-PCS interfaces frozen early
  - Limited experimental time
  - Commissioning in preceding, low power regimes
  - Moderate changes already require formal re-commissioning

⇒ **Difficult on ITER to develop new control methods:**

- Demonstrated reliability ⇔ State-of-the-art
- Develop now, refine on ITER and advance the ITER Research Plan

Ravensbergen, Piits ITPA-DSOL Jan 2022

ITER is organized in measurement parameters with 4 different roles

- **4 roles are:**
  - Machine protection (1.a1)
  - Basic control (1.a2)
  - Advanced control (1.b)
  - Evaluation and physics studies (2)
- **Operation only possible when ALL measurements in 1a are online**
- **High-performance/advanced operation only when ALL 1.b measurements are online**
- **Different diagnostics have different contributions to measurements (PR2359):**
  - Primary (diagnostic is well suited)
  - Back-up (diagnostic provides similar data to primary, but has limitations)
  - Supplementary (diagnostic validates/calibrates the measurement but is not complete in itself)

Ravensbergen, Piits ITPA-DSOL Jan 2022

55.A0: Magnetic diagnostics

- **Large number of pick-up and Rogowski coils on the first wall and divertor cassettes.**
- **Primarily used for equilibrium reconstruction (and shape control)**
- **Of particular interest: Shunts (55.AM) mounted on divertor cassette**
  - Accurate measurement of total SOL current1
  - Total current monotonically decreases for detaching plasma

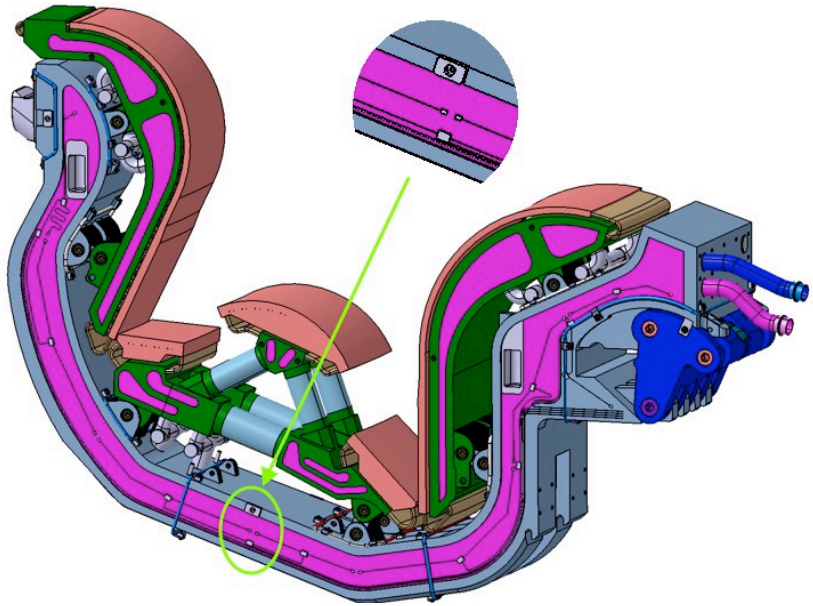

[1]C. Orrico *et al.* in prep.

Ravensbergen, Piits ITPA-DSOL Jan 2022

55.D1:Bolometry

- **Bolometer cameras in 2 Upper ports, 1 equatorial port, 5 divertor cassettes, and 22 in-vessel (in between HFS blanket modules), total ~500 LoS**
- **10 Hz (BC) – 100 Hz AC – 1 kHz (PH)**
- **Resolution ~ 5 cm in divertor and X-point area**

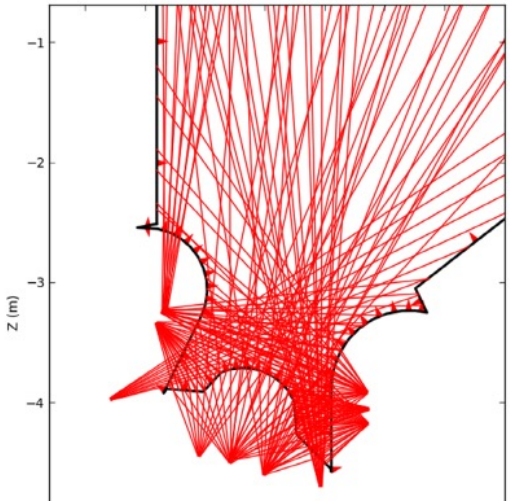

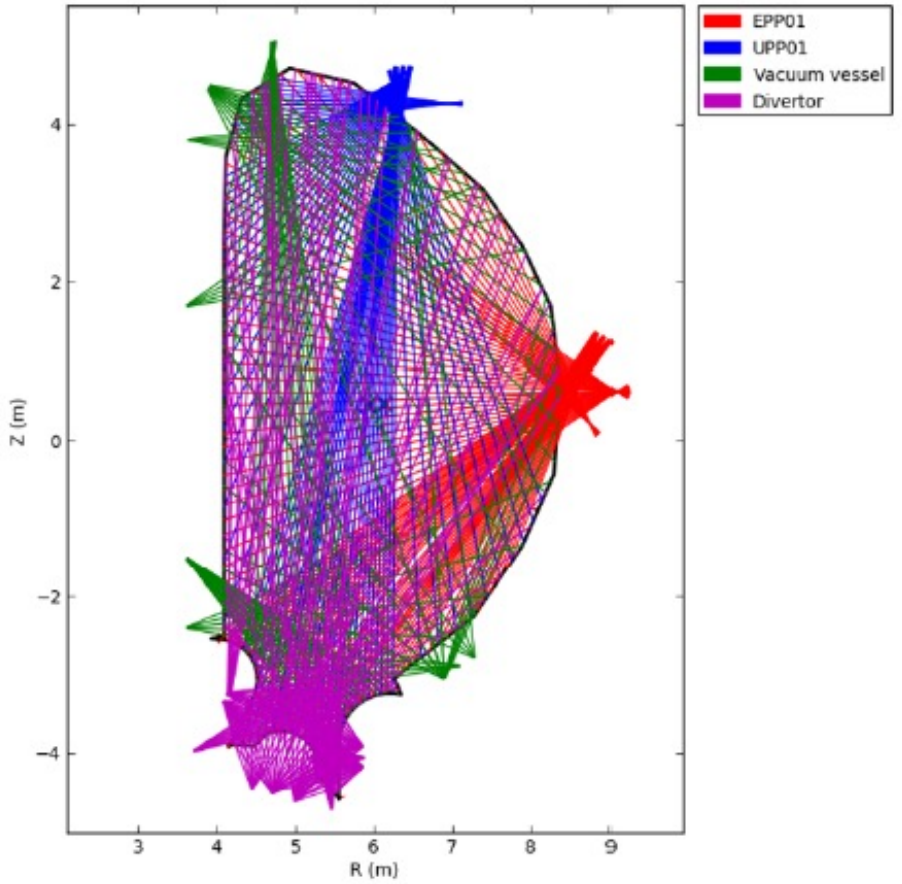

Ravensbergen, Piits ITPA-DSOL Jan 2022

55.EG VUV spectrometer

- **Measure impurity ion radiation (Be, W, C, O, Ne, N, Ar)**
- **Lyman-alpha (particularly relevant for detaching plasmas)**
- **10 ms time resolution**
- **Line-integrated measurement**

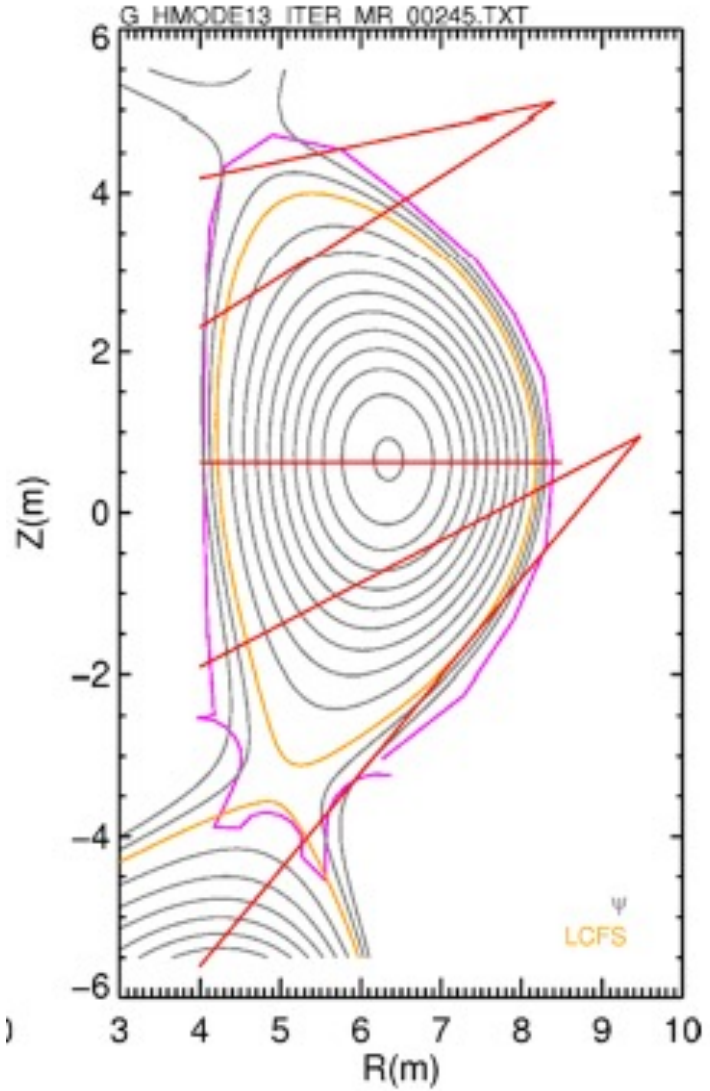

Ravensbergen, Piits ITPA-DSOL Jan 2022

55.E4 Divertor impurity Monitor

- **Measure line emission of H and impurities**
  - 4 views directly into divertor
  - ~250 LoS
  - Ionization front (based on Dα): 1 ms with 100 mm resolution
  - D,T, Be influx: 1 ms with 50 mm resolution

Optics arrangement
SU: single-outer
SL: side-lower
CO: Divertor central-outer
CI: Divertor central-inner

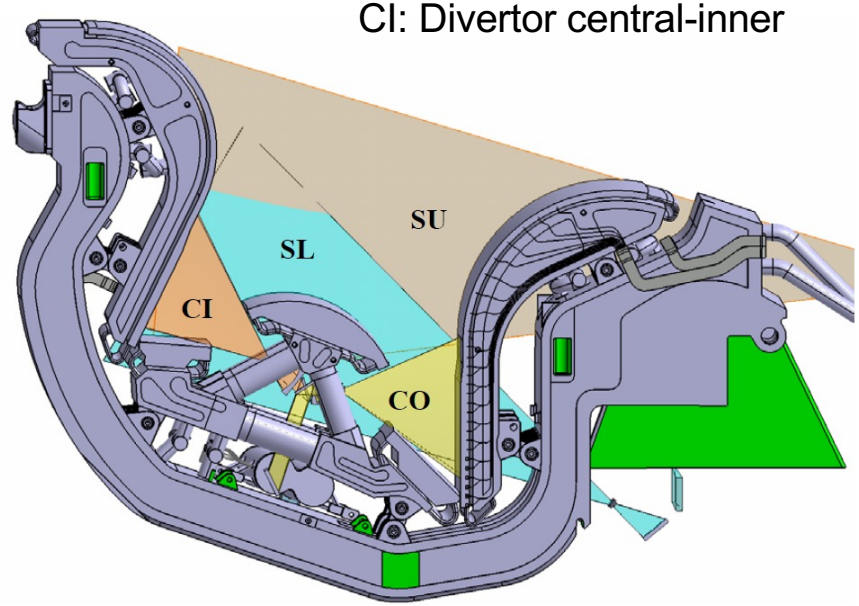

Ravensbergen, Piits ITPA-DSOL Jan 2022

55.G1/G6/GA VIS/IR

- **Interface with PCS and precise specs tbd**
- **Max surface temperature (BC), luminance (MP) and their profiles (AC)**
- **Power load and its profile for AC (inverse problem)**
  - 55.G1: 4 eq. ports. 15 views. ~6-12 mm VIS, ~8-24 mm IR
  - 55.GA: 5 upper ports, 5 views. 3 mm VIS, 5 mm IR
  - 55.G6: 1 eq. port and view, high res. 3 mm IR
- **Time resolution 2 ms, fast windowing mode at 0.02 ms**

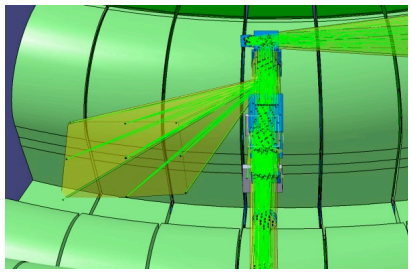

55.G6

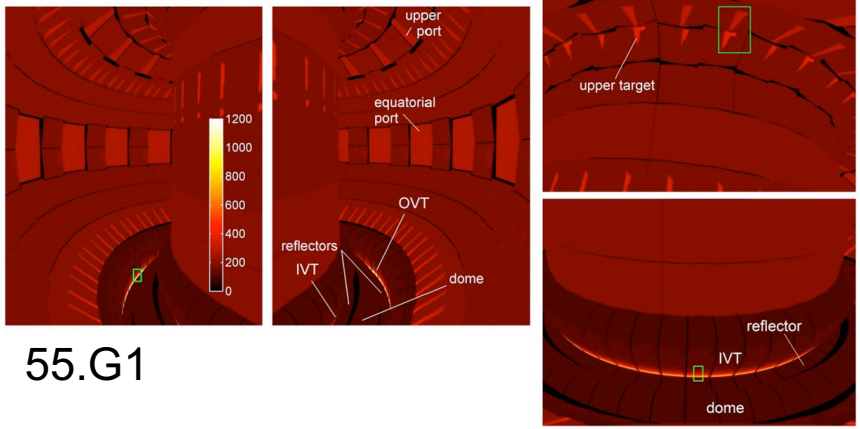

55.G1

55.GA

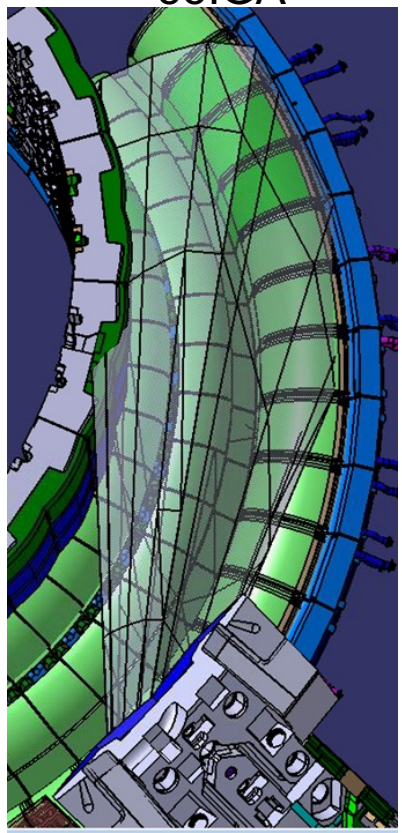

Ravensbergen, Piits ITPA-DSOL Jan 2022

55.G3 Pressure gauges

- **6 AUG-type fast pressure gauges per cassette, 4 equipped cassettes**
- **Divertor neutral pressure: 50 ms time resolution**
- **Key to start developing control on current machines**

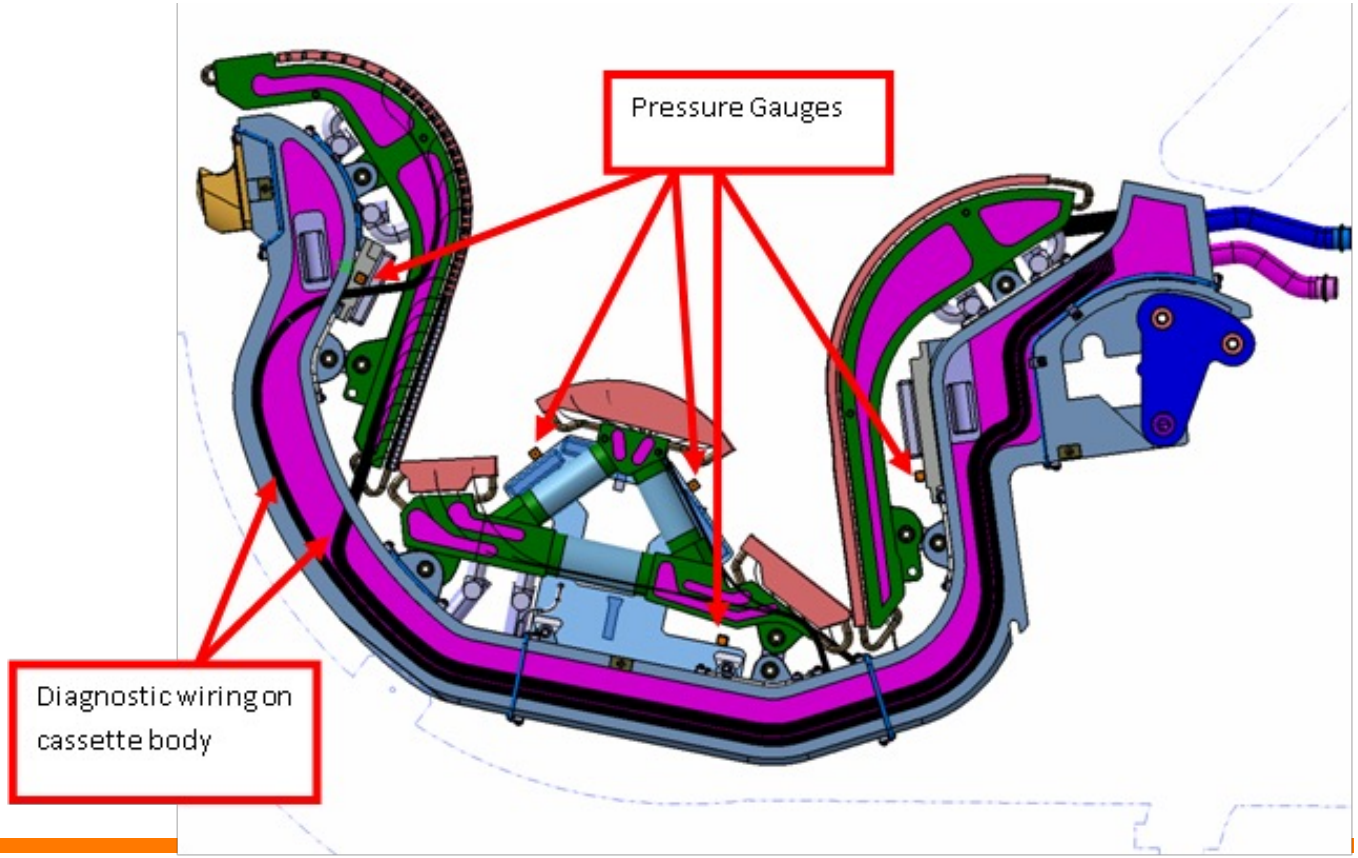

Ravensbergen, Piits ITPA-DSOL Jan 2022

55.G7 Langmuir Probes

- **400 probes to provide target plate measurements on 5 different cassettes of:**
- **ne and Te in double-probe configuration (PHY)**
- **Γion (BC) in DC-biased mode (BC)**
- **<10 ms time resolution with 12 mm spatial resolution on the targets**

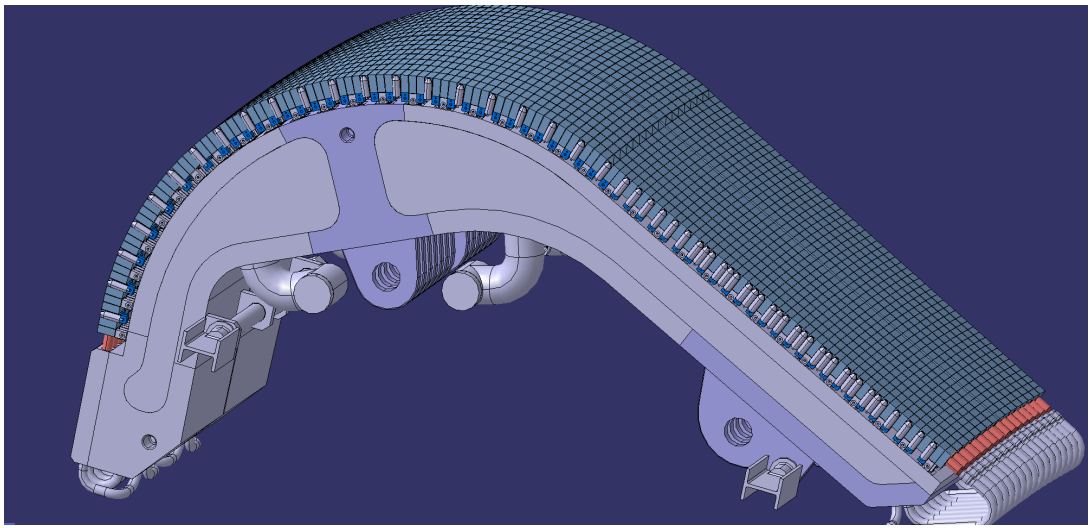

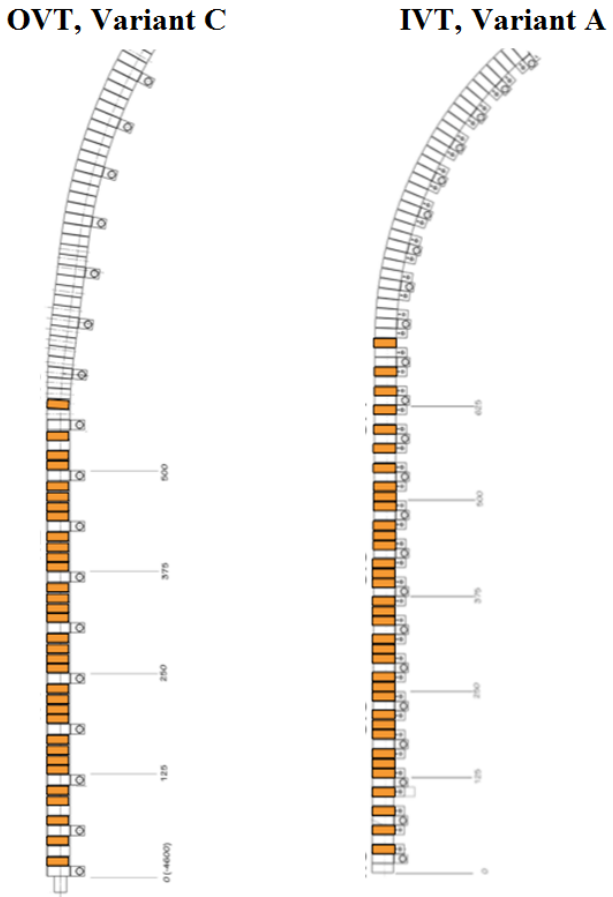

Ravensbergen, Piits ITPA-DSOL Jan 2022